LA-UR-14-29124
Approved for public release; distribution is unlimited.

Title: Determining the Pu Mass in LEU Spent Fuel Assemblies: Focus on Differential Die-Away Technique (Expanded Report)

Author(s): Henzl, Vladimir

Intended for: Report

Issued: 2014-11-25

Determining the Pu Mass in LEU Spent Fuel Assemblies: Focus on Differential Die-Away Technique (Expanded Report)

Prepared for:
Office of Dismantlement and Transparency (NA-241)
U. S. Department of Energy

Funded by:
Next Generation Safeguard Initiative
U. S. Department of Energy

Prepared by:
Vladimir Henzl
Nuclear Engineering and Nonproliferation Division

Los Alamos National Laboratory
Los Alamos, NM 87545

November 2012

LA-UR 14-xxxxx

Table of Contents

1. Executive Summary 3

1.1. Purpose 3

1.2. Method of Investigation 3

1.3. Conclusions 3

2. Introduction 5

3. Physics of the DDA Technique in Spent Fuel 6

3.1. Concept of a DDA Assay 6

3.2. DDA Instrument Requirements in the Context of Spent Nuclear Fuel 7

3.3. Contribution of the Burst Neutrons to the Total Response of the DDA Instrument 14

3.4. Spatial Sensitivity Analysis 17

3.5. Analysis of the Spent Fuel Signal 22

3.5.1. Concept of the Effective ^{239}Pu Mass ($^{239}Pu_{DDA_eff}$) 23

3.5.2. Concept of the First Generation 26

3.5.3. DDA Signal vs. $^{239}Pu_{DDA\_eff}$ Mass 29

3.5.4. Role of Neutron Absorbers in Determining the Effective Fissile Mass $^{239}Pu_{eff\_DDA}$ 31

3.5.5. Multiplication 33

3.5.6. Signal vs. Background 41

3.5.7. Variation in DDA Signal with IE, BU and CT 43

3.5.8. Systematic Uncertainty in the Count Rate of the DDA Instrument 45

4. Determination of the Elemental Plutonium Content in an Assayed SFA 47

4.1. ^{244}Cm Method 47

4.2. $^{239}Pu_{eff}$ Method 50

4.2.1. Determination of $^{239}Pu_{eff}$ if IE is Known 50

4.2.2. Determination of $^{239}Pu_{eff}$ by Evaluation of Neutron Absorber Effects 52

5. Detection of Diversion of the Nuclear Material from SFA 58

5.1. Comparative Diversion Detection 59

5.2. Self-Consistent Diversion Detection 65

6. Conclusions 68

References 69

1. Executive Summary

1.1. Purpose

This report quantifies the capability of a standalone differential die-away (DDA) instrument to measure the mass of elemental plutonium in a spent nuclear fuel assembly (SFA). It is part of a multi-instrument research effort, within the scope of the Next Generation Safeguards Initiative (NGSI), whose purpose is to evaluate the performance and feasibility of several nondestructive assay techniques, and their potential for integration into complex instruments with enhanced capabilities.

1.2. Method of Investigation

The performance of the DDA instrument has been evaluated based on a multitude of MCNPX simulations. Within this approach, various mechanical designs, measurement conditions and counting scenarios were most of the time tested against an ensemble of spent fuel assemblies of different degree of burn-up (BU), initial uranium enrichment (IE) and differing in cooling times (CT) as defined in the NGSI Spent Fuel Library 1 (SFL1).

1.3. Conclusions

Since the underlying physical processes of the DDA instrument (i.e. emission of prompt fission neutrons) and the delayed neutron (DN) instrument (i.e. emission of delayed neutrons by fission products) are complementary and because the technical requirements are essentially compatible, the mechanical design of the instrument has been envisioned since the beginning to be used as a possible integrated DDA+DN instrument as well, although the DN results are not considered further in this report.

The DDA instrument is expected to produce a signal as strong as, or stronger than, the background produced by the fuel for the wide range of spent fuel in SFL1 provided the driving deuterium-tritium fueled neutron generator can deliver $5x10^7$ n/s with a pulse rate of 100 Hz and pulse width of 10μs (i.e. instantaneous strength $5x10^{10}$ n/s). Such neutron generators are already available off-the-shelf.

Similar to all other techniques that measure fissile content ($^{239}Pu_{eff}$) in a given SFA, the correlation between the DDA signal and the $^{239}Pu_{eff}$ can be strongly influenced by the inventory of neutron absorbers. However the dynamic nature of the signal allows (under certain conditions) to either evaluate and correct for the effects of the absorbers directly or diminish their influence to a tolerable, correctable or negligible level. Within this report we explore several measurement and analytical scenarios leading either to the determination of the absolute amount of the fissile content in the terms of $^{239}Pu_{eff}$ or to the absolute amount of the elemental plutonium (^{tot}Pu) with the precision in order of a few %.

A fundamental design parameter of the DDA system is the time interval after the interrogating burst over which the neutrons are counted. The traditional approach in DDA technique calls for measurement in a constant time window typically after the thermalisation of the interrogating neutron field (after few hundreds of μs). In this report we present several novel approaches to the analysis of the DDA signal in various time intervals including times immediately after the interrogating burst and at different locations

across the SFA, and demonstrate how such additional information can lead to the direct measurement of the SFA multiplication, amount of neutron absorbers and the absolute amount of the $^{239}Pu_{eff}$ and/or ^{tot}Pu.

We conclude our study with investigation of 27 standardized diversion scenarios adopted by the NGSI study. We have evaluated the sensitivity of the instrument and have demonstrated that a diversion of ~5% of the fuel mass from any region of the assembly could be detected, provided a base measurement was available for comparison. Additionally, we introduce several novel analytical approaches which allow for self-consistent and independent detection of several diversion scenarios even if no base measurement is available.

2. Introduction

In order to provide regulators with an instrument capable of directly measuring Pu content in spent fuel assemblies, as well as detecting the diversion of pins from such assemblies, a five-year research effort sponsored by the Next Generation Safeguard Initiative (NGSI) of the U.S. Department of Energy was started in March of 2009 [1]. The initial two years of this five-year effort are focused primarily on Monte Carlo modeling, while the latter three years involve the fabrication of hardware and the measurement of spent fuel assemblies. The Monte Carlo effort has two main goals:

1) To quantify the expected capability of each technique as an independent instrument
2) To determine how to integrate various techniques together in order to determine elemental Pu mass and pin diversion.

This report is a part of the first goal and quantifies the capability of the differential die-away (DDA) technique. Since the general motivations and approaches being taken by the NGSI research effort have been provided in recent publications [2,3], they will not be repeated in detail in this paper. However, in order to provide context to the research of the DDA technique presented in this report, the other 13 techniques are listed below:

- Delayed neutrons (DN)
- Differential die-away self-interrogation (DDSI)
- Lead slowing-down spectrometer (LSDS)
- Neutron multiplicity counting (NMC)
- Passive neutron albedo reactivity (PNAR)
- Total (gross) neutron counting
- X-ray fluorescence (XRF)
- ^{252}Cf interrogation with prompt neutron detection
- Delayed gamma (DG)
- Nuclear resonance fluorescence (NRF)
- Passive prompt gamma (PPG)
- Self-interrogation neutron resonance densitometry
- Neutron resonance transmission analysis

A description of the basic physics of each of these techniques, along with more detailed references, are given in the publications of Tobin et al.[4], Menlove et al. [5], and Simpson et al. [6].

3. Physics of the DDA Technique in Spent Fuel

3.1. Concept of a DDA Assay

DDA is a neutron-generator-driven active neutron assay technique often used to assay the fissile content of radioactive waste drums [7] and cargo containers [8]. The fundamental characteristic of a DDA system is that only neutrons above a certain cutoff energy are detected. In the case of the most common safeguards systems, the cutoff energy is ~1 eV since the neutron detectors are wrapped in a layer of Cd that absorbs neutrons below this energy. Given such a detector, the neutron population ***detected*** in the detector can be divided into two basic parts that differ by how quickly they decay (i.e. die-away) in time.

The "***detected burst neutron population***" consists of detected neutrons which originate in the neutron generator or in any kind of inelastic reaction or reaction chain which does not involve fission. The neutron-generator burst is typically very short (~10 μs). The detected burst neutron population quickly propagates through the assayed system, reaches its maximum at the place of the detector after approximately 30μs and then dies-away very rapidly – in the case of our system $\tau_{1/2}$ ~30 μs. The word "***detected***" is being emphasized since the undetected neutrons that come from the neutron generator can still live on in the interrogated sample long after they are no longer detectable because their energy is too low to penetrate through the Cd layer. In our case, these burst neutrons have a significant population in the sample for several thousands of microseconds rattling around as thermal neutrons.

If there is any fissile material in the item, the thermalised neutrons from the neutron generator burst will give rise to the second detected population of neutrons. This "***detected fission neutron population***" consists of neutrons which were directly produced in an induced fission or are a product of an inelastic collision initiated by some other fission neutron. Due to the average neutron energy of ~2 MeV dictated by the Watt fission spectrum, these fission neutrons can easily penetrate through the Cd layer and be detected. As a consequence the typical die-away time of this fission neutron population is significantly longer than that of the detected burst neutron population. In the case of the system within this study the die-away times of fission neutron populations vary between 100-200 μs depending primarily on the composition of the SFA. The difference in the die-away time of these two populations provides for the name of this particular assay technique. On the other hand, although the detected fission neutron population is indeed predominantly created by thermalised neutrons from the burst inducing fission, we will shown later, that fast and epithermal neutrons also play a significant role and can provide qualitatively different yet complementary information about the assayed sample.

The signal from a DDA instrument is the total number of neutrons detected within a certain time window. Traditionally, the time window is opened late enough after the interrogating burst so essentially no burst neutrons are detected. However, we will demonstrate that within the scope of the SFLI the population of the detected burst neutrons effectively does not depend on the parameters of the assayed SFA. It can be then treated as a constant contribution to the measured DDA signal which depends only on the counting time window itself, and is thus easily correctable for. This finding will allow us to extend our measurements into very early times after the initial neutron burst and provide information about the composition of the SFA otherwise inaccessible with the traditional measurement scheme.

3.2. DDA Instrument Requirements in the Context of Spent Nuclear Fuel

The ultimate requirement of the DDA instrument is to measure the total mass of the elemental plutonium in a spent nuclear fuel assembly with a ***sufficient precision***, and to recognize when a ***significant amount*** of fissile material from the assembly got diverted. The numerical definition of "sufficient precision" and "significant amount" are arbitrary decisions made by the regulators taking into account practical as well as political circumstances. It is beyond the scope of this report to argue in favor or against any particular value of these requirements, and we will therefore restrict ourselves to simply exploring and presenting the limits of the DDA technique given by the proposed physical design of the instrument. We are also aware of the possibility that under certain conditions the DDA instrument alone may not be able to provide sufficient information to determine the mass of the elemental plutonium present or recognize certain types of diversion at all. We therefore intend to design the instrument in such a way, that a subsequent integration with other NDA techniques is possible. For the DDA technique the natural candidate complementary technique is DN which can take profit both from the driving neutron generator as well as the individual detectors. Essentially the only difference in the DN and the DDA instrument would then be the interrogation mode (neutron pulse length and frequency) and the measurement time window. More details about the DN technique can be found in a separate report [9].

Focusing now on the specific design requirements of the DDA instrument, we have to take into account that the target material of the DDA technique in this study is spent nuclear fuel, which will respond to active interrogation in a very different way than a "typical" waste drum. The various isotopes present in the spent nuclear fuel can be categorized into four general groups:

- Fissile isotopes
- Fertile isotopes
- Fission products
- Oxygen

Considering the possible interactions with neutrons, the isotopes in the spent fuel can be categorized in a different way as:

- Fissile isotopes
- Fertile isotopes
- Neutron absorbing fission fragments (aka "poisons")
- Others

Among the fissile isotopes contained in the spent fuel only three contribute in any significant way to the DDA signal: ^{235}U, ^{239}Pu and ^{241}Pu [10]. The range of neutron absorbers is much broader and greatly varies with burnup (BU), initial enrichment (IE) and cooling time (CT). Some of the major neutron absorbers among the fission fragments are ^{99}Tc, ^{131}Xe, ^{133}Cs, ^{143}Nd, ^{145}Nd, ^{149}Sm, ^{150}Sm, ^{151}Sm, ^{151}Eu, ^{154}Eu, ^{155}Gd, and ^{157}Gd. The major absorbers from the group of actinides are ^{238}U, ^{240}Pu, ^{241}Am, ^{237}Np and ^{236}U.

Fig.1 displays the geometry of the DDA instrument used in our Monte Carlo simulations. The DDA instrument consists of one 14-MeV deuterium-tritium (DT) neutron generator and eight ^{3}He detectors that are ¾" in diameter and 2'' in length. The detectors are embedded in high-density polyethylene and six of

them are covered by 0.1cm thick Cd liner. These detectors are foreseen to be used both for measurement of both prompt and delayed neutrons in integrated DDA+DN instrument, while the two remaining detectors without any Cd liner are considered to be used exclusively for measurement of the delayed neutrons.

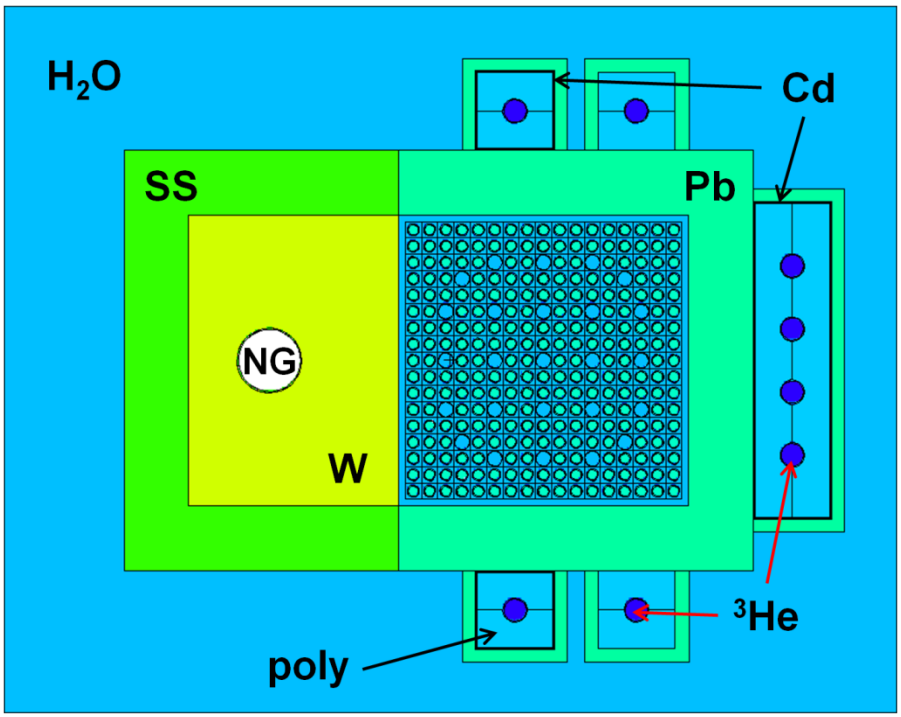

Fig.1 Schematic cross-sectional view of the DDA instrument used in the Monte Carlo simulations

We chose a DT neutron generator as the interrogating source of the DDA instrument over deuterium-deuterium (DD) neutron generator. The primary reason is the achievable strength of the neutron source which is 50-100 times higher in case of the DT neutron generator. However the DT reaction yields neutrons with rather high energy of 14.1 MeV, which will require a substantial spectrum tailoring in order to provide sensitivity to fissile material and at the same time have suppressed sensitivity to fertile ^{238}U the mass of which exceeds by far that of all fissile isotopes combined.

Fig.2 shows the fission cross section of the fissile isotopes ^{235}U, ^{239}Pu and ^{241}Pu and the fertile isotope ^{238}U. Even though the thermal fission cross section of ^{238}U is more than seven orders of magnitude smaller than those of the major fissile isotopes, the fission events induced on ^{238}U can be significant since ^{238}U makes up about 95% of the total actinide mass. Moreover the neutron generator and induced fission events both produce neutrons with energies above 1 MeV where the cross sections of ^{238}U and the fissile isotopes differ by less than an order of magnitude.

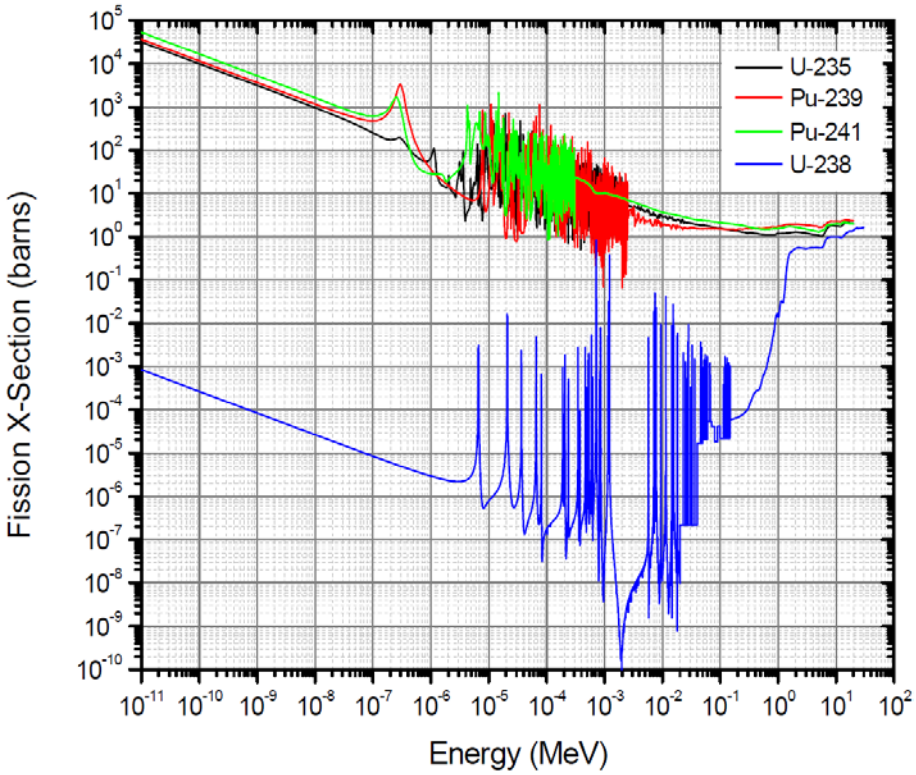

Fig.2 Fission cross-sections for ^{235}U, ^{239}Pu, ^{241}Pu and ^{238}U as a function of incident neutron energy.

Considering the different nature of the cross sections of the fissile isotopes and the fertile ^{238}U it becomes apparent that the 14.1 MeV energy of neutrons from the DT generator ideally needs to be reduced below 1 MeV. The need for a rather soft interrogation neutron spectrum is even more desirable in case of the DN technique, since on a per fission basis ^{238}U produces approximately seven times more delayed neutrons than ^{239}Pu. On the other hand the faster the neutrons the better their penetrability of a thick and dense sample such as SFA. In the earlier iterations of this research effort [11] and particularly in the work of Blanc et al. [9] various spectrum tailoring materials and designs were investigated. In this report we will limit ourselves to the final design choice which has also been used for vast majority of results presented in this work. Thus looking back at Fig.1 we can observe that the DT neutron generator (NG) is positioned in the centre of a thick tungsten block (W) surrounded by a stainless steel sleeve (SS) which serves as a reflector of neutrons emitted in backward direction. The neutron energy spectrum at the entry to the fuel assembly, before the neutrons enter the water surrounding the array of fuel pins, is displayed in **Fig.3**, which is reprinted from [9]. It shows that in case of our design (labeled "design #2") the majority (95%) of the neutrons entering the SFA have energy below 1 MeV.

Since spent fuel is an intensive gamma-ray source itself, the lead blocks around the SFA are used to prevent gamma events in the ^{3}He gas. The small size of the ^{3}He gas tubes has been also chosen in order to reduce the gamma effects. The positions of the ^{3}He detectors on the outer surface of the SFA were optimized to have a uniform DDA response across the SFA in a horizontal direction, while the prospect of using the instrument for DN technique has also been taken into account.

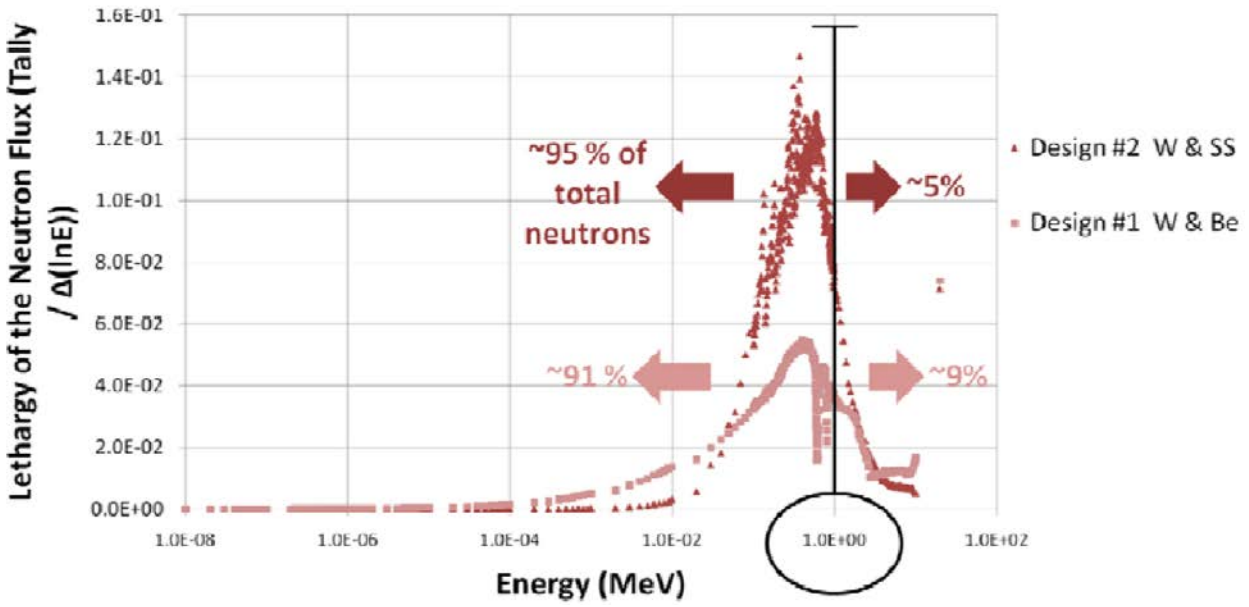

Fig.3 The lethargy of the neutron flux at the entry of the fuel assembly at the surface of the SFA for two different tailoring concepts [Pauline]. The results do not include any returning neutrons.

The time response of the DDA system defined as the sum of detected neutrons on all ^{3}He detectors with Cd liners (i.e. DDA detectors only) for several fresh fuel assemblies with different initial enrichment is shown in **Fig.4**. The interrogating neutron pulse, or burst, is of constant intensity generated between 0 to 10 µs. The neutron population registered by the detectors after the neutron pulse quickly reaches its maximum between 15-80 µs but then decreases with a die-away time specific for each individual fuel assembly. The higher the initial enrichment (i.e. higher fissile content), the longer the die-away time. The neutron die-away time of a pure $^{238}UO_2$ assembly (no fissile material) is much shorter than that of the other fuel assemblies. This is because the detected neutrons come predominantly directly from the neutron source or from fast fissions in ^{238}U. The probability of a thermal neutron inducing fission in ^{238}U is too low to be a significant source of neutrons. Contrary to that the fuel assemblies with significant amount of fissile material can to a much greater degree support a fission chain reaction due to the high cross-section for fission induced by thermal neutrons. **Fig.5** then displays how the time response of the DDA system changes with increasing degree of burn-up of the nuclear fuel. With higher burn-up less fissile ^{235}U remains in the fuel to support the fission chain reaction. To a certain degree, the decrease in the amount of ^{235}U is compensated by the increase of mass of fissile plutonium isotopes ^{239}Pu and ^{241}Pu; this however is still not enough to offset the influence of the increasing mass of fission products and other actinides, which being mostly strong neutron absorbers lead to a significant suppression of fission chain reactions resulting in faster die-away times.

It is also worth pointing out that even after the intensity of the detected neutrons reaches their maximum for any particular fuel assembly, the die-away time does not appear to stay constant. One of the reasons is that the simulated data presented in Fig.4 and Fig.5 consider all detected neutrons, that means also neutrons coming directly from the neutron generator, which behave (i.e. die-away) differently than “true” fission neutrons. Additionally the integral results from Fig.4 and Fig.5 are sums of neutrons

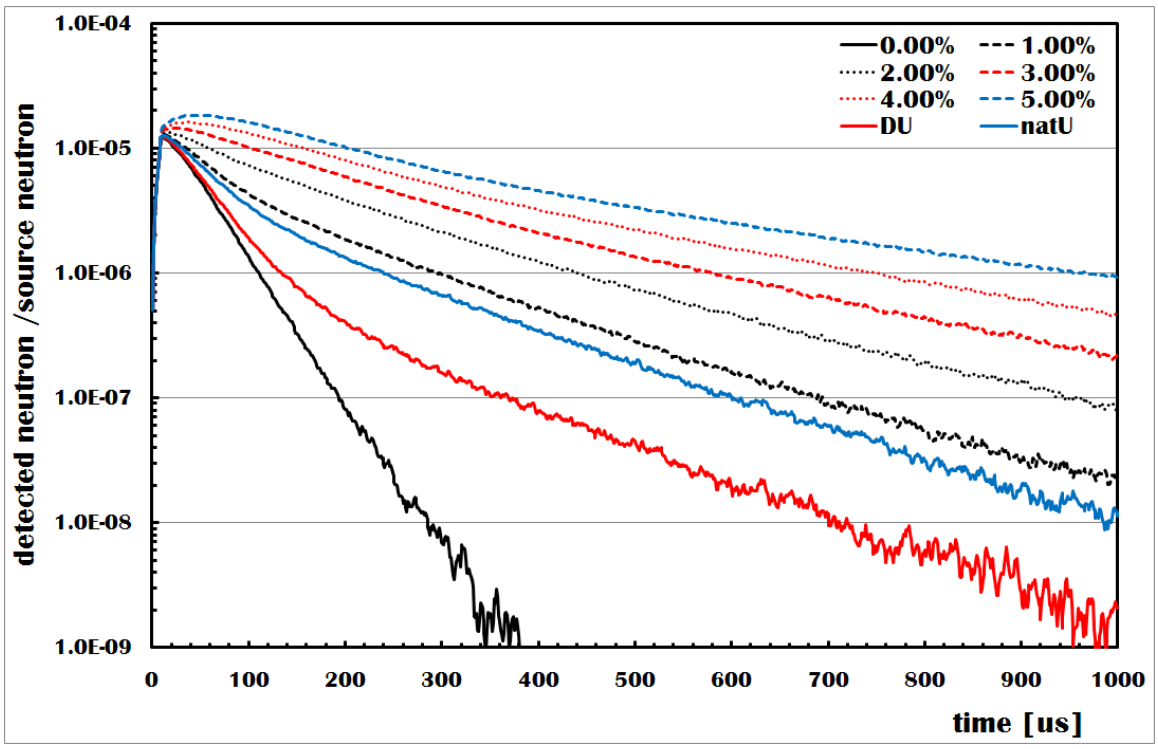

Fig.4 Time response of DDA system for several fresh fuel assembly cases with 0-10 μs interrogation neutron pulse.

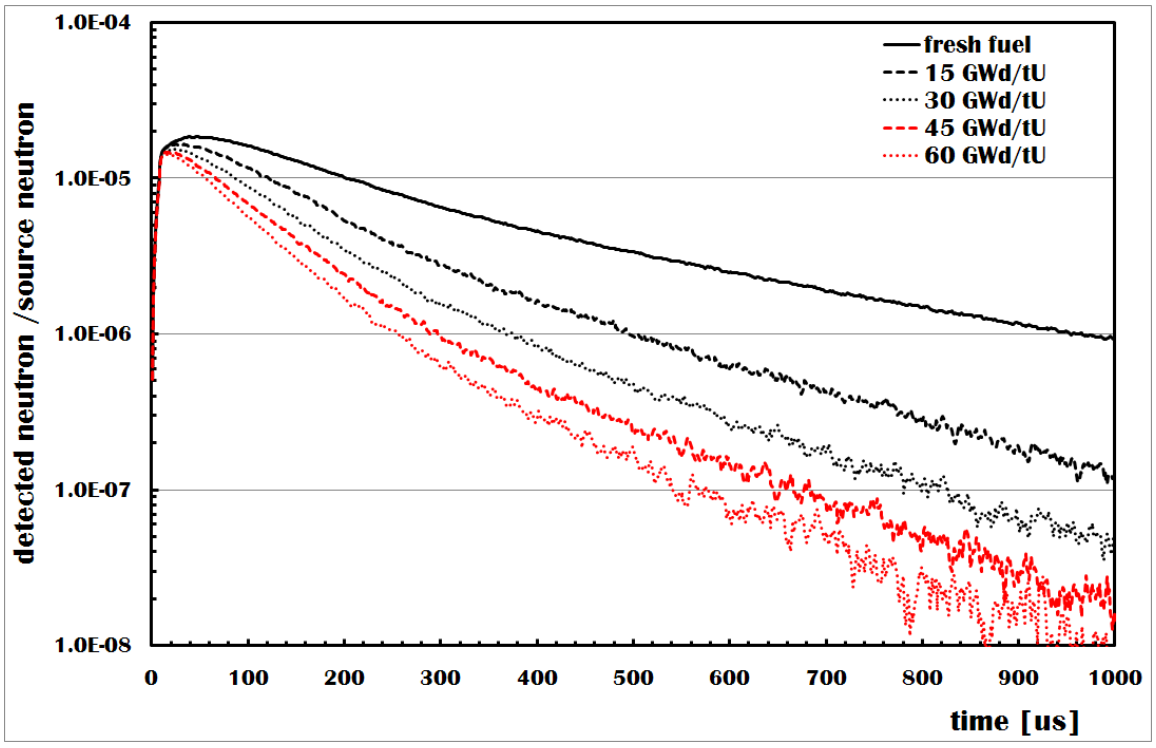

Fig.5 Time response of DDA system for several spent fuel assembly cases of original 5% initial enrichment and with 0-10 μs interrogation neutron pulse.

detected in all ^{3}He detectors, even though each of them is at a different position with respect to the neutron generator and fuel assembly. It is easy to imagine that the dynamic evolution of the neutron flux will be different across the fuel assembly until the neutrons get fully thermalized. **Fig.6** demonstrates exactly that fact on the example of one particular SFA (4% IE, 45 GWd/tU, 5y CT) where contributions of both neutron populations (burst neutrons and fission neutrons) on individual detectors are compared to the time response of the whole DDA system. The individual ^{3}He detectors are labeled according to the schematic display of the DDA instrument in **Fig.7**. (*Note: here we are taking the advantage of the symmetry of the DDA instrument and essentially of all SFA's in SFLI, meaning that the neutron flux in*

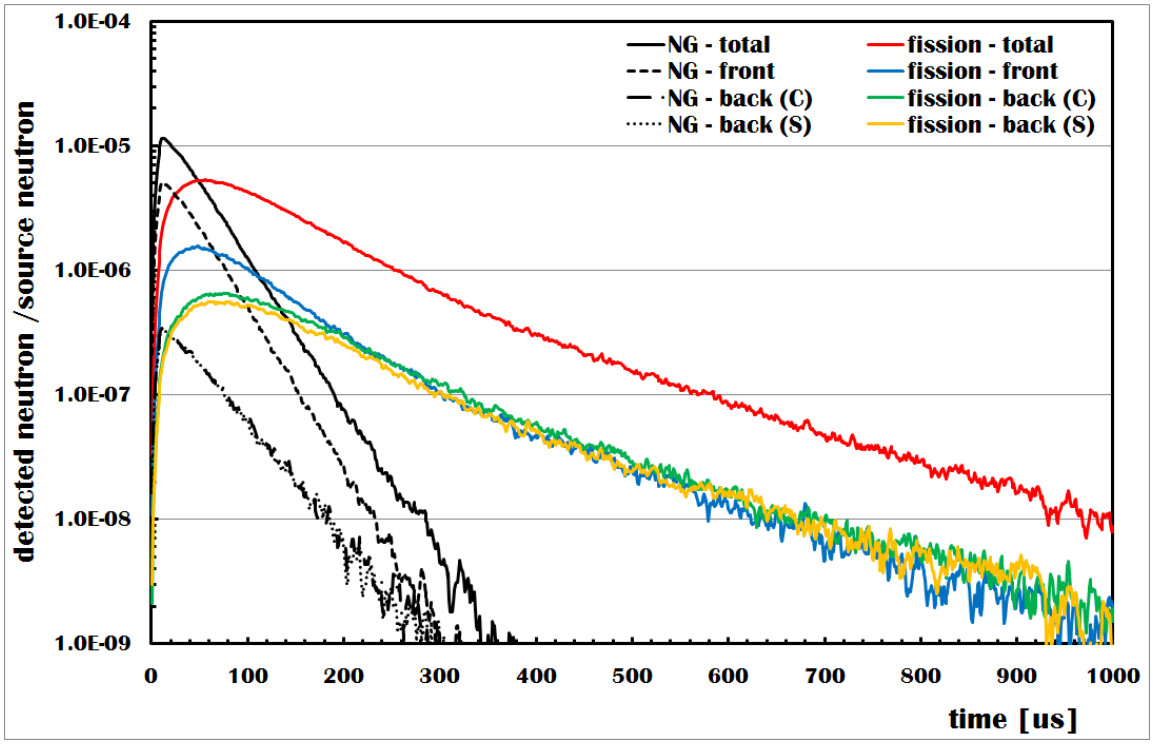

Fig.6 Time response of the DDA system in terms of the origin of the detected neutron (neutron generator or from fission) and the place of the detection (individual front or back detectors,)

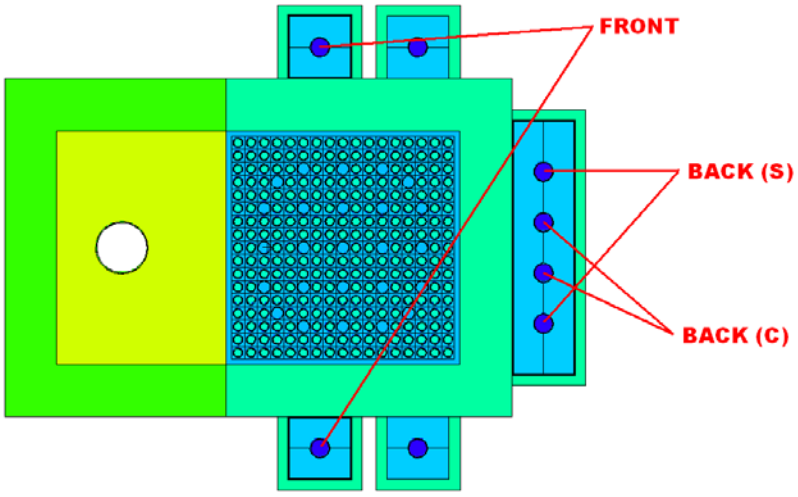

Fig. 7 Schematic view of the DDA instrument with designated naming convention for the six ^{3}He detectors as used within this report *(the two unmarked detectors are dedicated to the DN instrument and are thus not considered for DDA analysis).*

positions symmetric with respect to the horizontal axis (in Fig.7) will be statistically the same. Thus instead of distinguishing between "Front-top" and "Front-bottom" detectors, we will simply use "front" or "F" meaning the sum of the detected neutrons on both "front" detectors. Similarly, we will denote the sum of the center two of the back detectors as "back-C" or "BC" and of the two back detectors on the side of the detector quadruplet as "back-S" or "BS".)

The data in Fig.7 reveal that the position of the detector across the SFA plays a very significant role particularly during the first 250 μs after the interrogating burst. The front detectors "see" many more burst neutrons than the back detectors and more importantly they also register additional fission neutrons while simultaneously the die-away times of both neutron populations evolve differently depending on the detector positions. Only after ~250 μs the neutron field seems to be equilibrated across the whole apparatus and detection rates become almost identical across all six ^{3}He detectors dedicated to the DDA technique. This observation leads to the conclusion that one universal counting window for the whole instrument may be too limiting and perhaps several counting gates for each individual detector should be implemented. The straight forward consequence for the design of the DDA instrument is that a shift register based data acquisition system (DAQ) may not be appropriate but rather list-mode data DAQ should be our choice. Within this opening chapter we will restrain ourselves from debating detailed physical explanations behind the above intriguing observation, but will do so in subsequent chapters when appropriate.

For the purpose of the thorough analysis and motivated by the results presented in Fig.7 we have decided to explore the capabilities of the DDA instrument in six different time windows spanning across the first millisecond following the start of the interrogating burst, and, when advantageous, then also sorted by the detector position. The time windows used across this report (denoted "A" to "F") are the following (where time 0 μs is considered to be the beginning of the interrogating neutron pulse):

A) 0 - 50 μs
B) 50 - 100 μs
C) 100 – 200 μs
D) 200 – 500 μs
E) 500 – 1000 μs
F) 50 – 1000 μs

While suggesting to measure DDA signals in times immediately after the interrogating neutron pulse may sound impractical if not unrealistic, the additional information gained from such approach more than justifies consideration of this measurement scheme. We, as authors, are well aware of possible technical difficulties trying to measure such high rate DDA signals with state of the art ^{3}He detectors and electronics. However, rather than providing mere exact engineering solutions for the proposed DDA instrument we decided to also explore several novel approaches from a conceptual perspective, hoping that the revelation of potential gains will spur tackling otherwise uncontested technical challenges as well.

The ending point of 1ms for the latest counting window was selected because the signal is becoming small relative to the background (more about signal-to-background ratios and neutron generator strength requirement in chapter 3.5.6.).

3.3. Contribution of the Burst Neutrons to the Total Response of the DDA Instrument

By the definition, the detected burst neutrons were not involved in any fission reaction nor are they product of any inelastic collision initiated by a neutron produced in fission. Therefore the burst neutrons are considered not to carry any information on the fissile content of the assayed fuel assembly. While the burst neutrons may have been involved in inelastic collision with nuclei of fissile isotopes, the differences in cross sections of inelastic collisions on fertile or fissile isotopes are rather limited and relevant only for the fast neutrons before they get thermalized. This again provides negligible amount of information in terms of the true fissile content of the assayed fuel assembly, and further underscores that burst neutrons can be considered noise accompanying the true signal in form of fission neutrons.

Fig.6 reveals that the total population of burst neutrons is different and dies-away at a different rate depending on the position of the detector. However, for a given detector position the absolute number of detected burst neutrons per one source neutron is nearly constant regardless of the parameters (IE, BU, CT) of the assayed fuel assembly. The **Fig.8** displays the yield of detected burst neutrons per one source neutron in the F detectors (*left*) and the B detectors (*right*) as the function of the fuel assembly number. FA's numbered 1-64 are spent FA's from SFLI differing by their IE,BU and CT. FA's numbered 70-75 are special case FA's used in the study of the uniformity of the DDA instrument response detailed in chapter 3.4. FA's with numbers 80-92 represent fresh fuel (FF) FA's with IE 0-5% and special cases of FF FA loaded with DU or ^{nat}U only. FA's with numbers 100-128 represent diversion scenarios studied in detail in chapter 5. The Fig.8 thus represents all FA's studied within this report. Considering the statistical uncertainty of the simulated contribution of the burst neutrons (~0.2% in F detectors and ~0.7% in B detectors) and especially when focusing on the front detectors in FA's #80-92 we may conclude that the IE does indeed have an effect on the number of detected burst neutrons. However, this effect seems to be of the order of ~0.5% and thus provides a valid argument for considering the absolute contribution of burst neutrons to response of the DDA instrument as constant, allowing to be treated in any further analysis as simply ever-present background.

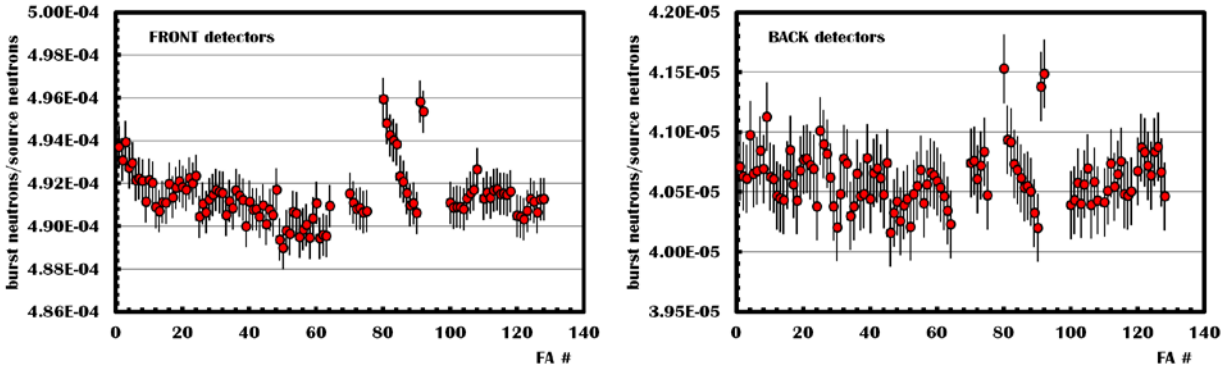

Fig.8 The yield of detected burst neutrons per one source neutron in the F detectors (*left*) and the B detectors (*right*) as the function of the fuel assembly number (*see text for details*).

On the other hand, the relative contribution of the burst neutrons to the total number of detected neutrons varies with parameters of the FA as well as the position of the detector, and most importantly the time of the counting window. The **Fig.9** displays relative contribution of burst neutrons to the overall detected signal in F detectors during time windows A-D. The relative contribution of the burst neutrons in

the times later than 500 μs (time window E) are negligibly small, thus not displayed. The **Fig.10** displays the similar information for the B detectors. The FA numbering convention remains the same as in the Fig.8.

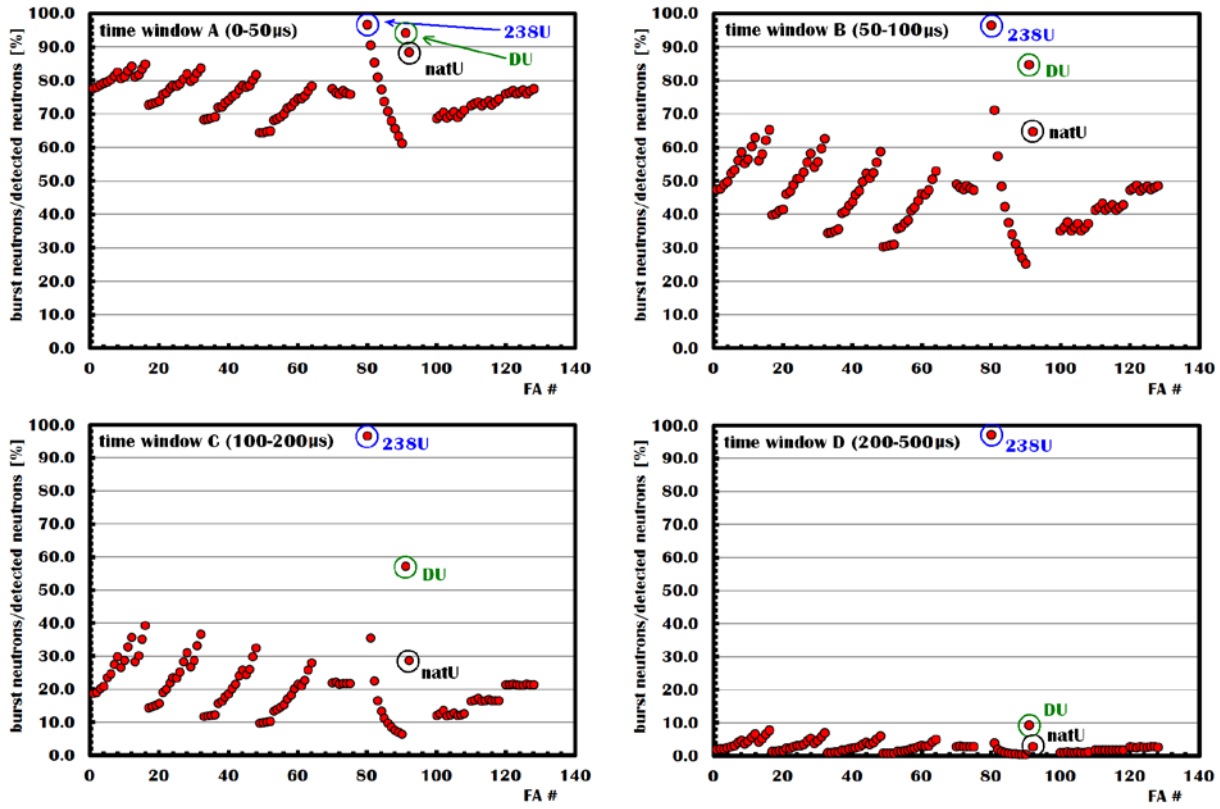

Fig.9 Relative contribution of burst neutrons to the overall detected signal in F detectors during time windows A-D.

Not surprisingly, the biggest relative contribution of the burst neutrons to the DDA signal is at the front detectors during the earliest times after the interrogation pulse where it can reach up to 85% depending on the isotopic composition of the assayed FA. The systematic uncertainty of ~0.5% in the total number of detected burst neutrons can thus easily translate into a systematic error of ~4% on the number of true fission neutrons, should the detected burst neutron contribution be subtracted in case of an assay of a FA for which IE is not known. However, in any later time window and in case of all time windows for the B detectors, the relative contribution of the burst neutrons is less than ~50-60% thus resulting in a manageable additional systematic error typically <1%. The only exceptions are then FF assemblies with extremely low enrichment, from which the most interesting seems to be FA #80 which "fuel" is 100% ^{238}U and FA #92 that is composed of DU. The significance of the earlier case is that the relative contribution of the burst neutrons is constant in all 4 different time windows. It is ~97% in F detectors and ~86% in the B detectors suggesting, that such a fuel assembly could be used for calibration, i.e. direct measurement of the yield of the burst neutrons detectable by the DDA instrument. Based on the conclusions from Fig.8, one could use results of such measurement to correct any DDA measurement of any spent fuel assembly for the contribution of the burst neutrons.

However since the fabrication of FA consisting of pure ^{238}U is hardly realistic, we have considered another similar yet more practical scenario – FA with fuel pins filled with DU. But looking at Fig.9 and 10 we can observe that the relative contribution is not constant anymore and significantly decreases in later times. Comparing the die-away curves displayed already in Fig.4 we can clearly see how big of a difference already a small fraction of fissile material makes, especially in later times after the interrogation pulse. Alternatively, inspired by the results for pure ^{238}U FA we may consider to use some other non-fissile material such as tungsten or lead in a mock-up FA to measure propagation of the burst neutrons through the assembly as well as for the evaluation of the DDA system efficiency. Exploration of such idea unfortunately exceeds the scope of this report and will not be elaborated any further. The main point of the above paragraphs and figures was just to demonstrate that the contribution of the burst neutrons to the response of the DDA system can be for the most of the practical applications considered constant and as a part of the background. With that being said, we will restrict all of our subsequent analysis (unless specifically stated) ***only*** to the detected fission neutrons, i.e. part of the detected signal that does depend on the properties of the assayed FA.

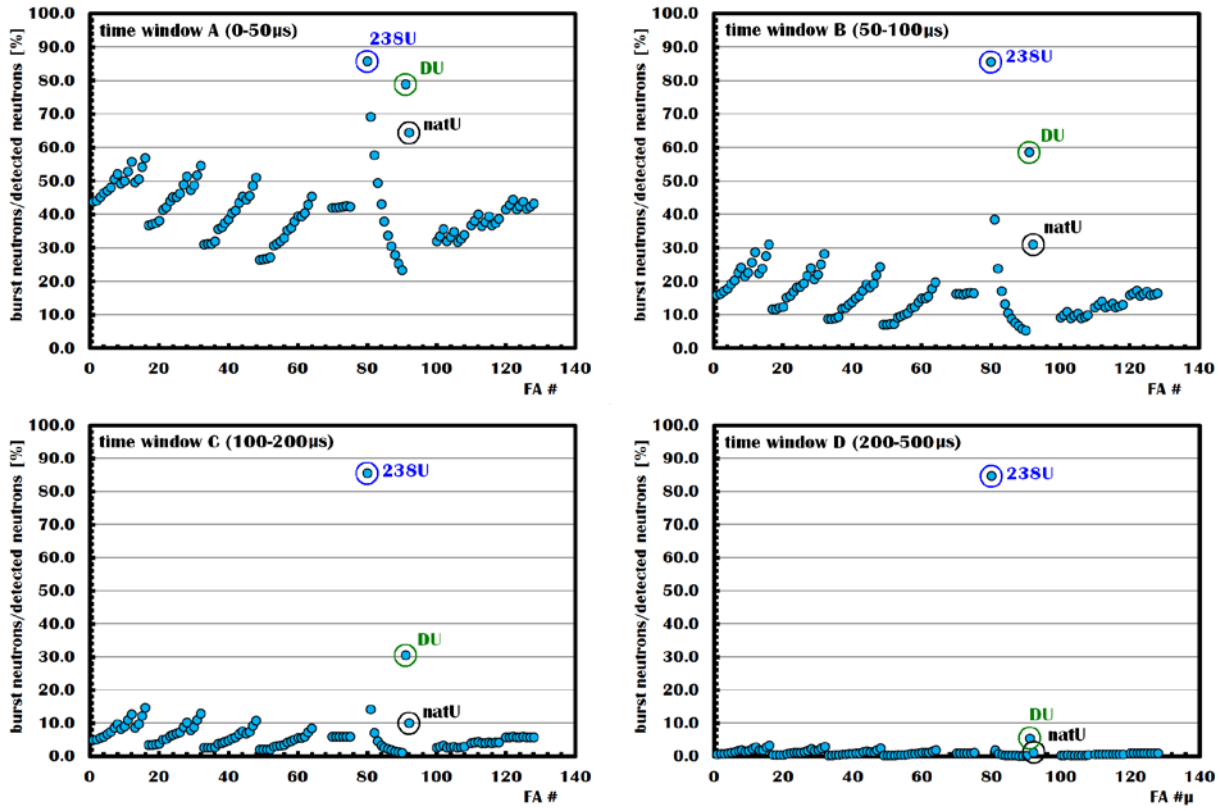

Fig.10 Relative contribution of the burst neutrons to the overall detected signal in B detectors during time windows A-D.

3.4. Spatial Sensitivity Analysis

Ideally any NDA instrument should have equal sensitivity to a unit mass of the material of interest, independent of the location of the mass in the assayed object. In order to produce a relatively uniform spatial response of the DDA instrument the number of ^{3}He tubes and their locations and the structure of the neutron generator were considered. In order to quantify the variation in the spatial sensitivity, 12 pins were replaced with depleted uranium from 6 different regions of the assembly as illustrated in **Fig.11**, and marked as SV1 - SV6.

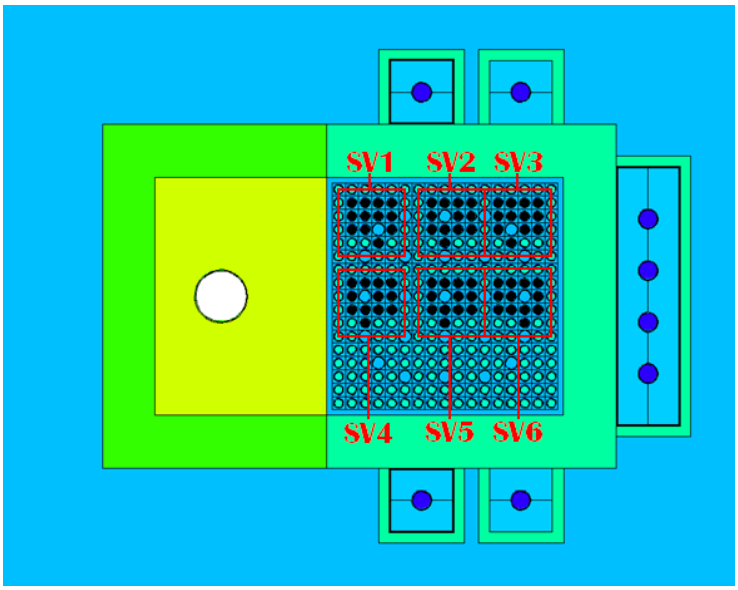

Fig.11 Replacement pattern of 12 pins for each of six sections of the spent fuel assembly.

In the previous version of the report on the performance of the DDA technique 2 different SFA's were investigated still using original design of the DDA instrument with only four ^{3}He tubes and additional Cd liners on the inner wall of the instrument. First, the authors analyzed the spatial sensitivity for fresh fuel assembly with 2% IE with the DDA signal defined as sum of all counts on all ^{3}He detectors in the time 200-1000μs after the interrogating pulse. The results are reprinted in **Fig.12** ***(left)*** and resulted in a conclusion that the detection efficiency at the back of the assembly (with respect to the position of the neutron generator) needs to be increased and ultimately led to the removal of the Cd liners on the inner walls of the instrument and incorporation of additional two ^{3}He detectors at the back side of the assembly. However, the subsequent analysis of various diversion scenarios revealed a suspicion that instrument may be inherently blind to the center of the assembly. This suspicion was considered confirmed with the spatial analysis of the spent fuel assembly with a significant burnup (4% IE, 45GWd/tU BU and 5y CT). The results are reprinted in **Fig.12** ***(right)***. Consequentially, it has been suggested, and later demonstrated, that the sensitivity of the instrument to the removal from the center of the assembly is restored provided the counting window is shifted into earlier times after the interrogation pulse, namely 100-150 μs. This finding has been one of the main motivations behind more rigorous investigation of how the DDA signal evolves in time as is presented within the current version of the report.

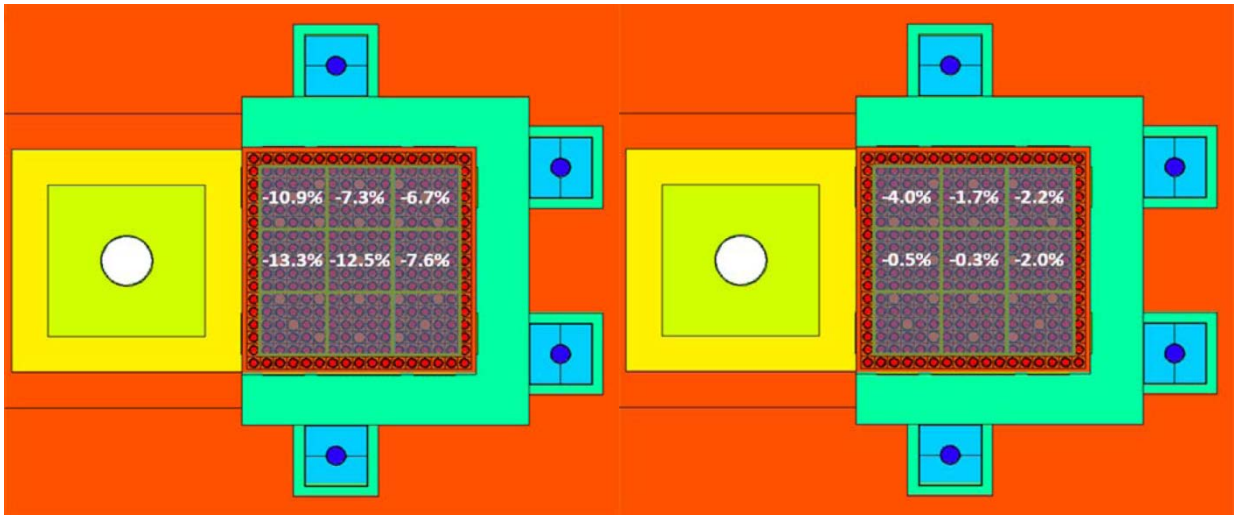

Fig.12 DDA signal change for each section in a fresh fuel assembly with 2% IE (left) and burned up fuel assembly with 4% IE, 45 GWd/tU and 5 y CT (right) after 12 pins were replaced with depleted uranium pins. Each substitution of 12 pins was simulated separately (reprinted from [11]).

In order to investigate the spatial sensitivity of the instrument we adopt similar approach as performed previously for the DDA technique and as has been adopted by other NDA techniques investigated within the current NGSI effort. We simulate substitution of 12 fuel pins by DU in 6 different regions of the SFA with 4% IE, 45 GWd/tU BU and 5y CT as depicted in Fig.11 using the newest design of the DDA instrument. However, instead of a single integral number we analyze the difference between modified and unmodified FA for 6 different time windows (A-F) as defined in chapter 3.2. The results of the simulations are displayed in **Fig.13**. The statistical errors associated with the results and displayed in the individual panels of Fig. 13 are almost independent of the position of the fuel pin substitution since the count rates are very similar in all six substitution scenarios. On the other hand the DDA signal count rate significantly varies in time (see Fig.6) and thus the associated statistical errors vary for different time windows. Therefore only one value for all six scenarios and a given time window is displayed.

Close inspection of the results in Fig.13 reveals that the substitution of 12 pins results in significant drop of the number of detected neutrons in rather early times, but seems to have little if any effect on the relative count rate in later time windows such as D and E. The results also point to the fact that in very early times after the interrogation pulse the DDA signal is indeed sensitive to the place of the fuel pins substitution as can be seen on panel with results for the time window A (0-50μs), but at times of window C (100-200μs) the overall number of detected neutrons is statistically independent of the place where the real spent nuclear fuel was substituted with depleted uranium. It is also worth pointing out that the relative change of the DDA signal in the later times is somewhat ambiguous and even results in statistically significant enhancement of the signal in times 200-500μs (window D) for spatial variation scenarios SV4-6. Results for window E unfortunately suffer from a statistical error comparable to the observed effect and are thus not really conclusive, although the average values seem to indicate that the DDA signal of modified FA is very similar to that of the unmodified FA. Such result seems to be rather counterintuitive since the amount of fissile mass removed by substitution of 12 pins with DU is ~4.5%, thus one would expect the DDA signal to drop by ~4.5% as well. On the other hand if we consider the most generous

counting window F (50-1000μs) we can see that the DDA signal decreases in a statistically significant manner for all 6 fuel pin substitution scenarios allowing us to conclude that the overall response of the DDA instrument is generally quite uniformly sensitive to a unit mass of the material of interest, independent of the location of the mass in the assayed object.

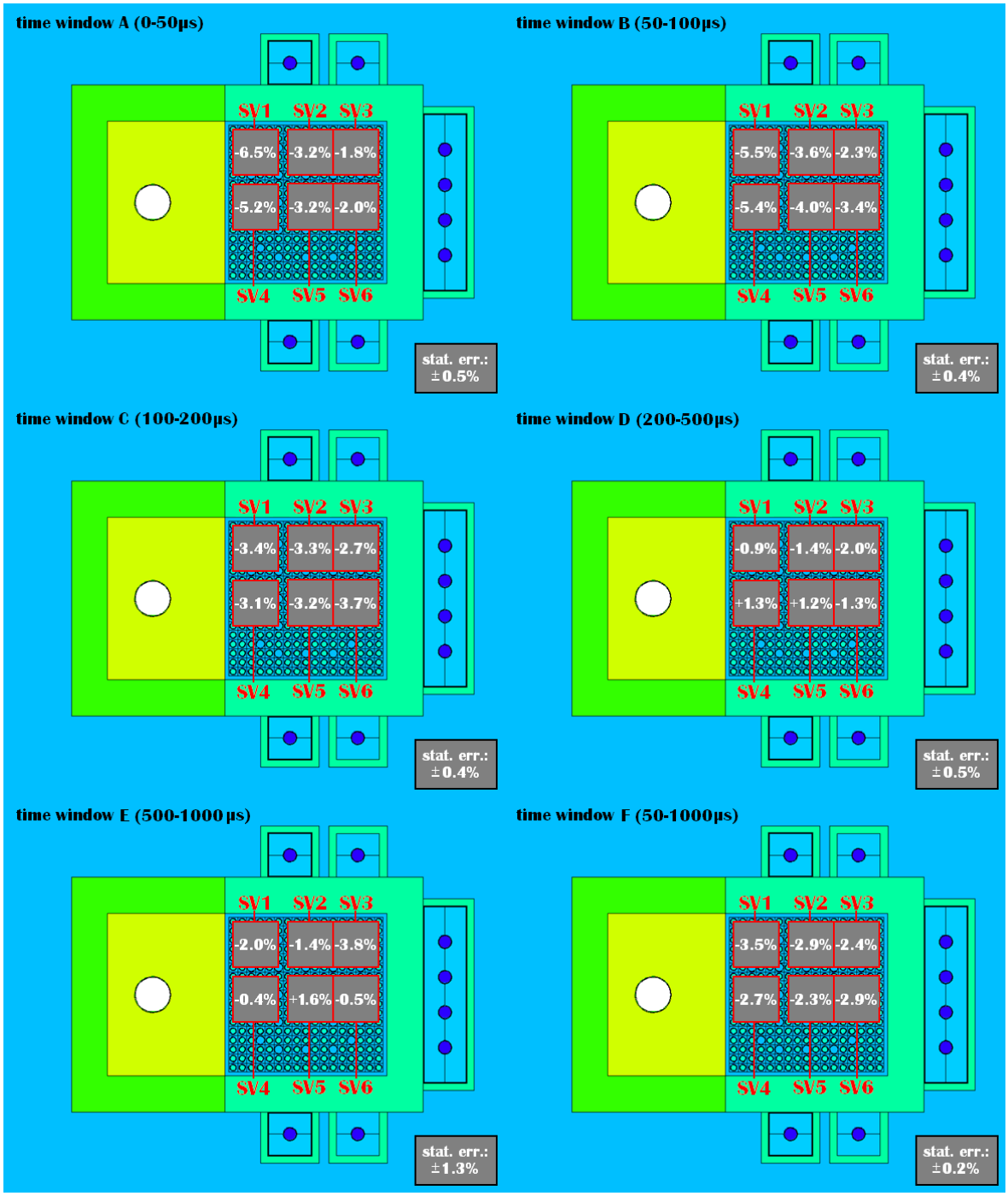

Fig.13 DDA signal change for each section of the FA (4% IE, 45 GWd/tU BU and 5 y CT) for six different counting time windows.

However, motivated by the differential nonuniformity of the DDA instrument response we decided to explore its response in time based on the location of the ^{3}He detectors. The **Fig. 14 a-c)** displays evolution of the relative response of the front (a), back (b), and all detectors combined (c) separately in time for all six fuel pin substitution scenarios SV1 to SV6. As discussed above, the statistical errors are almost independent of the substitution scenario, thus are for simplicity of Fig.14 displayed only for SV1, but still provide a clear indication of statistical uncertainty associated with SV2-6 as well.

The general feature of the displayed results is the relative decrease of the detector count rate in early times (0-200us) and its recovery in later time possibly reaching even higher count rate with implanted DU compared to unmodified FA. But more detailed comparison of the results for front and back detectors reveal also a significant difference in how the detector position matters with respect to the position of the fuel pin substitution. The Fig.14 a) shows that the front detectors are by far the most sensitive to the exchange of the fuel pins closest to their position, i.e. SV1 but seem to be rather insensitive to exchange of fuel pins far away from the front detectors such as SV6. On the other hand the bigger the drop in count rate during the early times (0-200us) the bigger seems to be the relative count rate recovery later, such as clearly profound for SV4, while results for SV3 remain quite flat for the full first millisecond after the interrogating pulse. The results for back detectors displayed in Fig.14 b) are in stark contrast to their front counter parts. All fuel pin substitution scenarios result in an initial count rate drop of very similar magnitude and difference between SV1 (farthest from the back detectors) and SV6 (closest to the back detectors) is only ~2.5% compared to ~8.5% difference seen by the front detectors.

While the exact reason for the different sensitivity of front and back detectors to the removal of fissile material from a FA is not yet understood, we can easily imagine that the group of fuel pins made of DU provides for a localized opacity for thermal neutrons propagating through the system. Should such neutron opaque object stand directly between the neutron source (neutron generator) and the detector the rate of detected neutrons may get disrupted in a similar way as any material object may disrupt propagation of sound waves. The thermalized neutrons will essentially reach the detector by scattering around the opaque object but with a slight delay compared to a scenario where they can propagate via the shortest possible path. Such hypothesis could explain why the front detectors observe the largest drop in detected count rate in case of SV1 and SV4 and while the count rate remains almost unaltered in case of SV3 and SV6. On the other hand any of the fuel pin exchange scenarios SV1- SV6 results in a neutron opaque object between the neutron generator and the back detectors, with alternate paths around the group of DU pins being essentially very similar no matter of the position where the fissile material was removed. In short, we believe that further more detailed investigation of the neutron propagation through the FA may provide the needed insight, and moreover that the differential nonuniformity of the DDA instrument may even prove to be an advantage. After all, SV1 to SV6 can be considered as just another possible fissile material diversion scenarios (additional to diversion scenarios discussed in detail in chapter 5.) and as such their detection being possible by the inherent differential nonuniformity of the instrument would be of the utmost interest for the NGSI effort.

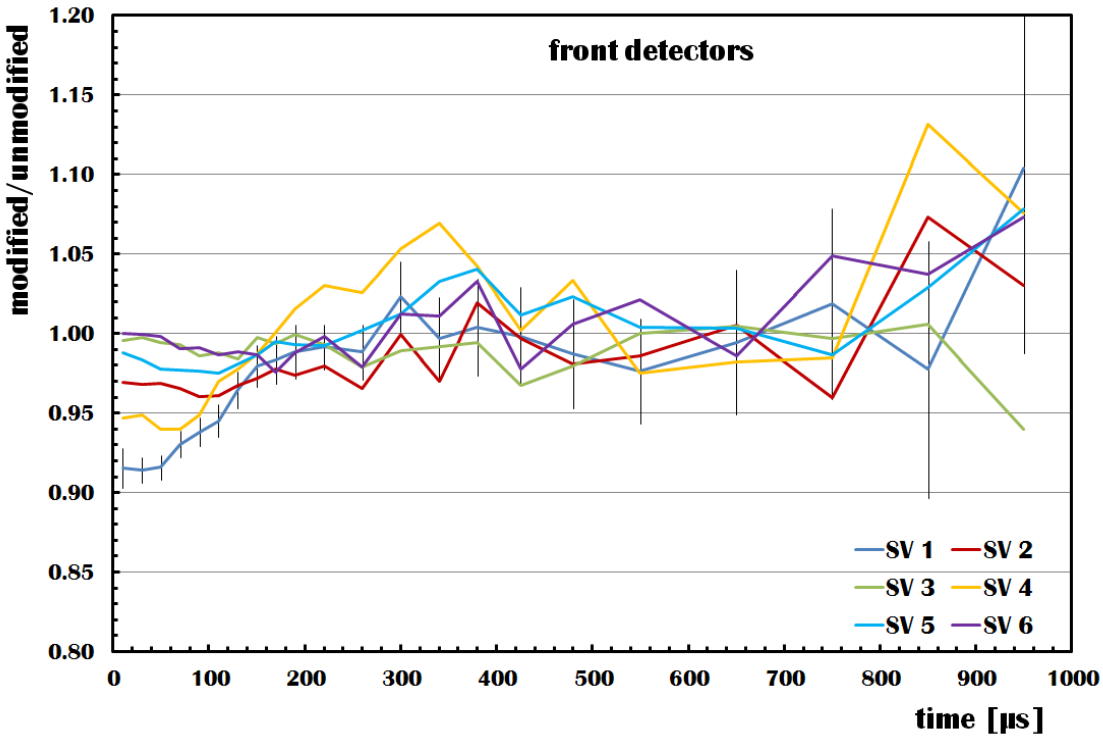

Fig.14 a) Time evolution of the relative change of the DDA signal from the front detectors for six different fuel pin substitution scenarios in the FA with 4% IE, 45 GWd/tU BU and 5y CT.

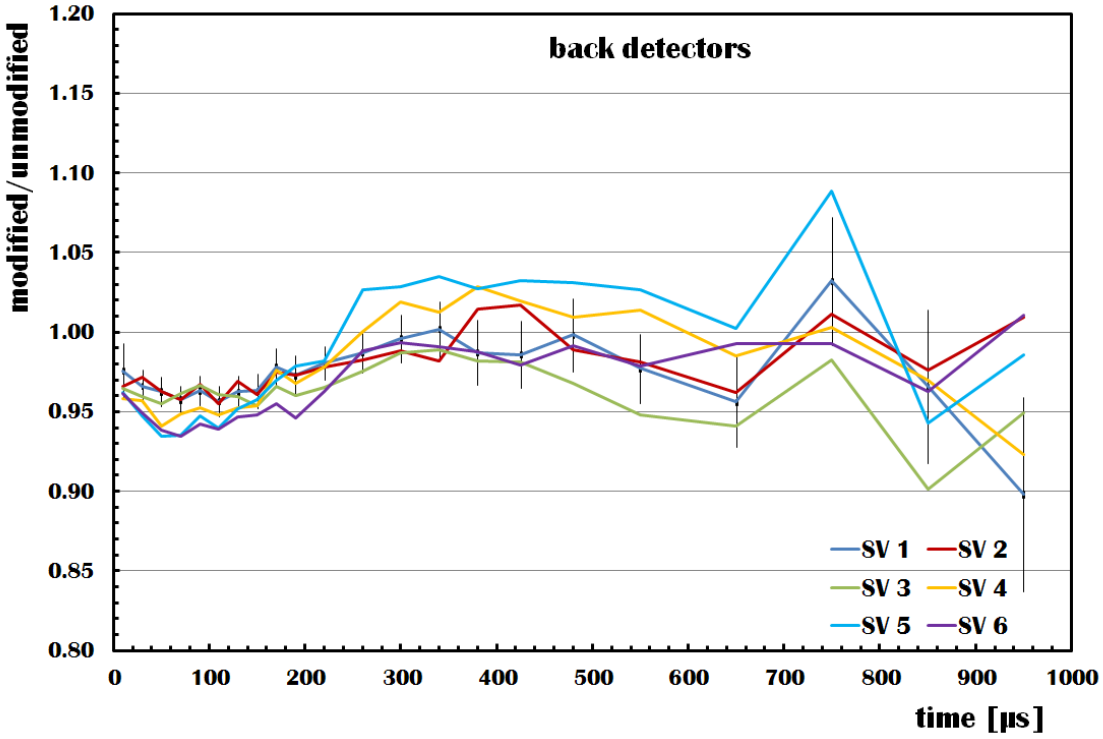

Fig.14 b) Time evolution of the relative change of the DDA signal from the back detectors for six different fuel pin substitution scenarios in the FA with 4% IE, 45 GWd/tU BU and 5y CT.

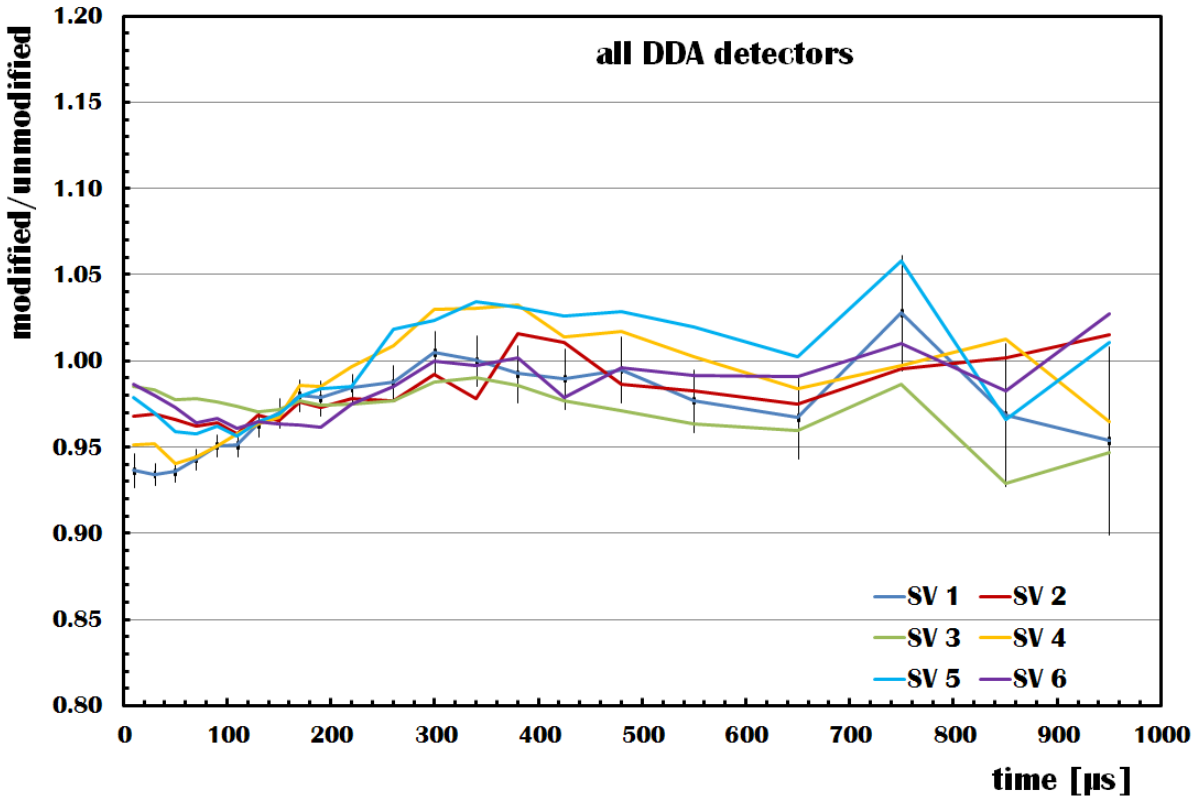

Fig.14 c) Time evolution of the relative change of the total DDA signal for six different fuel pin substitution scenarios in the FA with 4% IE, 45 GWd/tU BU and 5y CT.

3.5. Analysis of the Spent Fuel Signal

The fission neutrons detected during the DDA data acquisition time are the fast prompt neutrons from induced fission events occurring mainly in the fission isotopes of ^{235}U, ^{239}Pu and ^{241}Pu. Neutrons from the induced fission events of ^{238}U also contribute to the DDA signal, however depending on the measurement time and the definition of the signal neutrons coming from ^{238}U may be considered rather as a signature of the fissile isotopes ^{235}U, ^{239}Pu and/or ^{241}Pu. For example, in later times (such as 200-1000us) the interrogation source neutrons are already thermal, hence having only extremely low probability of causing fission in ^{238}U. But a chain reaction that starts with a thermal neutron inducing fission in ^{235}U, ^{239}Pu or ^{241}Pu produces neutrons with energies of several MeV for which the cross section for fission of ^{238}U is several orders of magnitude higher than for thermal neutrons. Considering the high abundance of ^{238}U in the FA (95-98%), its contribution to the detected DDA signal may thus be already quite significant. On the other hand since such fission of ^{238}U would not be possible without the initial fission induced by thermal neutron on some fissile isotope it perhaps may be more appropriate to consider the detected neutron as a signature of the initial fissile isotope rather than of the ^{238}U. This of course raises a more general concern in terms of how to properly account for contribution of various fissile isotopes to the DDA instrument response. Not only that the individual neutrons (despite their possibly different origin) appear identical when detected by ^{3}He detectors, but to make matters more complicated they are typically

a byproduct of a chain reaction involving several different fissile isotopes. In order to properly evaluate the contribution of various isotopes tot the overall DDA signal two ground braking concepts were developed – the ***effective ^{239}Pu mass*** ($^{239}Pu_{DDA_eff}$) allows to properly weight contributions of various isotopes to the signal while the ***first generation concept*** defines how individual neutrons are associated with a particular fissile isotope.

3.5.1. Concept of the Effective ^{239}Pu Mass ($^{239}Pu_{DDA_eff}$)

In order to define a term which represents the weighted sum of the three main fissile isotopes (considering contributions of other fissile isotopes and ^{238}U for now negligible) we utilize as our model the well developed safeguards concept of $^{240}Pu_{eff}$ used by passive Pu coincidence counting technique [12]. In this chapter we will also mainly follow the argumentation already laid out in the previous version of the DDA report [11]. We will show that the determination of $^{239}Pu_{eff}$ is instrument dependent and will strictly adhere to using subscript "DDA" to distinguish it ^{239}Pu effective masses determined by other instruments. It is also important to stress out that the general $^{239}Pu_{eff}$ mass concept fundamentally different from $^{240}Pu_{eff}$ which involves only combination of spontaneously fissioning isotopes that unlike induced fission driven $^{239}Pu_{eff}$ are not impacted by the energy spectrum of the interrogating neutrons in the sample. Furthermore in $^{239}Pu_{eff}$ concept, each of the dominant fissile isotopes that contribute to the $^{239}Pu_{eff}$ is in competition for neutrons with each other and possibly also with other neutron absorbers present in burned nuclear fuel. The challenge heading forward is to understand the variability of the $^{239}Pu_{eff}$ concept and finding ways to minimize the resulting uncertainty.

Following the discussion above, the weighted sum of the three fissile isotopes contributing to the DDA signal and defining thus the ^{239}Pu effective mass can be written as:

$$^{239}Pu_{eff\_DDA} = C_1\ ^{235}U + {}^{239}Pu + C_2\ ^{241}Pu \tag{1}$$

where $^{239}Pu_{eff\_DDA}$ is the effective ^{239}Pu mass of the DDA instrument, ^{235}U, ^{239}Pu, and ^{241}Pu are the respective masses of each fissile isotope contained in the fuel assembly, and C_1 and C_2 are the coefficients that weight the contribution of the unit mass of ^{235}U and ^{241}Pu to the DDA signal relative to the mass of the ^{239}Pu. However, since each of the fissile isotopes have different energy-dependent fission cross section, the C_1 and C_2 coefficients are expected to be FA dependent as the energy spectrum in each assembly may slightly differ as well. Moreover, if we extend our analysis into more than a single counting window (as in previous report) we may expect an additional dependence of C_1's and C_2's on time too.

A considerable amount of effort was spent determining the weighting factors C_1 and C_2 and the DDA technique was among the first to do so. In particular, the implications of using "*net neutron profit*" or "*net neutron contribution*" concept and their implications were debated. The main difference being that the net neutron profit considers only neutrons being produced by a given fissile isotopes, while the net neutron contribution concept in addition considered the neutrons which were being absorbed by the fissile isotopes without resulting in any fission.

Let's assume that a neutron collides with a nucleus of the atom of ^{235}U, ^{239}Pu or ^{241}Pu. As a result of an average collision several (=x) neutrons are produced. The "x" can be expressed as:

$$x = C_0 \cdot (\bar{\nu} \cdot \bar{\sigma}_f - \bar{\sigma}_f - \bar{\sigma}_a) \quad (2)$$

$$x = C_0 \cdot ((\bar{\nu} - 1)\bar{\sigma}_f - \bar{\sigma}_a) \quad (3)$$

Where σ_a is the sum of cross-sections of all reactions leading to the absorption of the incident neutron such as (n,γ), (n,α) and etc, and C_0 is a constant for unit conversion. The eq.3 reflects the main idea of the "*net neutron contribution*" concept. When the absorption term is dropped as in eq.4:

$$x = C_0 \cdot ((\bar{\nu} - 1)\bar{\sigma}_f) \quad (4)$$

we end up with a formula representing the "*net neutron profit*" concept, which has been later adopted as the appropriate approach for evaluation of the C_1 and C_2 coefficients. In reality, σ_f and ν both depend on the incident neutron energy, and the neutron flux Φ is a function of both energy and space. Thus eq.4 is a rather brute and simplified mathematical representation of the applied concept, and more precise description of the number of neutrons increased by fission of an isotope i is given by eq.5:

$$wt_i = \int_V \int_E \sigma_f(E)_i(\nu(E) - 1)\Phi(E, V)dEdV \quad (5)$$

The impact of each fissile isotope atom on the neutron balance is quantified as wt_i, and is implemented in MCNPX calculations by using the tally multiplier card (FM) and referred to as "*tally in the fuel*" method.

The **Tab. 2** lists cross sections for fission of the fissile isotopes of interest by thermal neutrons and the corresponding nubar. Considering these values, value of C_1 can be estimated to be ~0.60. Hence it should take almost twice as much ^{235}U mass to give the same signal as ^{239}Pu inside a typical spent fuel assembly. Similarly the C_2 values can be estimated to be ~1.40 meaning that ^{241}Pu provides for ~40% more signal than the same mass of ^{239}Pu.

Tab. 2 Thermal Cross sections [13] and Nubars [14] of three major fissile isotopes

	^{235}U	^{239}Pu	^{241}Pu
σ_f (barns)	585	748	1012
ν	2.438	2.874	2.946

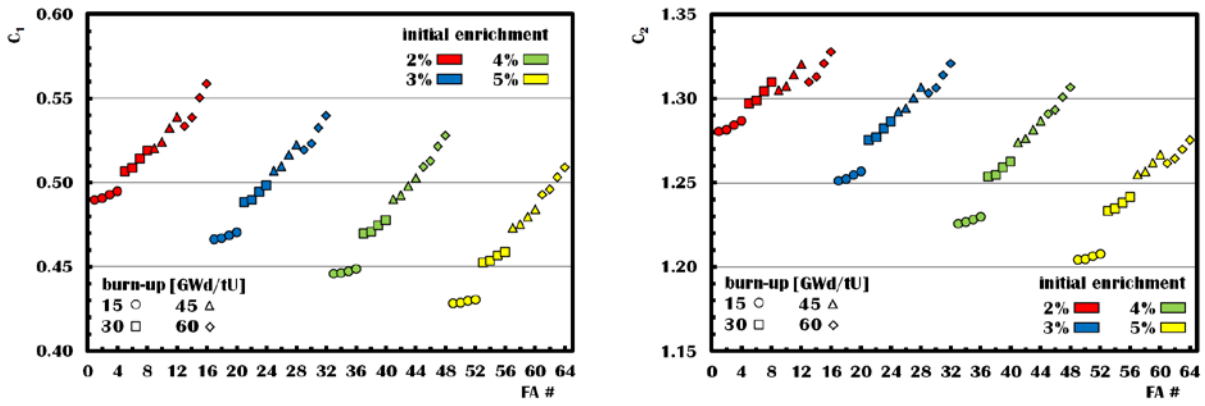

Fig.15 C_1 (*left*) and C_2 (*right*) weighting coefficients of eq.(1) for 64 SFA of the NGSI spent fuel library SFLI. Among the four points with the same burn-up and initial enrichment, the cooling time increases from left to right.

The value of C_1, which is depicted in Fig.15 (left) varies between ~0.42 and ~0.56 and is thus a little lower than the estimate based solely on the ratios of thermal neutron fission cross sections and nubars, and is simply a reflection of the fact that not all fission in the assayed FA is caused by thermal neutrons. Moreover, the structure in the figure clearly indicates that properties of the fuel, such as fissile material and neutron poisons content due to various BU, IE and CT may influence the interrogating neutron flux enough to alter the relative contribution of various fissile isotopes to the detectable signal, i.e. weighting coefficient C_1. The Fig.15 (*right*) depicts values of C_2 coefficient for the same 64 SFA's from SFLI. Also in this case the values of C_2 are somewhat lower (~1.20-1.33) than the estimate based purely on fission by thermal neutrons (~1.40).

Such a dependence of the weighting coefficients on the properties of the assayed FA seems to require more detailed knowledge of at least some of the key parameters such as BU, IE and CT otherwise an exact appropriation of the measured signal among the contributing isotopes may result in too high uncertainties. Should all three of these parameters be known, the uncertainty of individual weighting coefficients can be then narrowed down to a ~1-2% level. That however still excludes the systematic uncertainty which is given by the nature of the "tally in the fuel method". As can be understood from eq.(5) and the implementation in the MCNPX code, this method "measures" relative contributions to the ***detectable*** rather than the ***detected*** signal. In the discussion of chap. 3.4., we have learned that each individual ^{3}He detector has different sensitivity to various places inside the FA. Moreover this sensitivity is time dependent, and generally varies for each possible counting window of the DDA instrument. The values of C_1 and C_2 coefficients depicted in Fig.15 were "determined" by the tally in the fuel method with equal statistical weight across the whole FA in time window 200-1000us after the interrogating neutron pulse. It does not factor in whether the produced neutron was subsequently detected or not, nor whether the neutron was coming from the first or last event of a more complicated fission chain which may influence whether we (for example) consider fission of ^{238}U as background or amplification of the "good" signal from some fissile isotope. Thus not unexpectedly, wary of the inconsistency between the definition and the use of the C_1's and C_2's from the tally in the fuel method, a novel *concept of the first generation* aiming to overcome these shortcomings was developed.

3.5.2. Concept of the First Generation

The first generation concept was developed to address shortcomings of the tally in the fuel method. While tally in the fuel method calculates relative contributions of various fissile isotopes to the total number of neutrons produced via fission, it does not provide any direct link between created neutrons and their detection in a ^{3}He tube, nor does it provide information about the kind of reaction in which any particular neutron was produced. Therefore an individual ^{3}He detector with time and position dependent sensitivity as well as due to the potential non-uniform burnup of the fuel in the assembly may perceive reality differently then we may expect based on the tally in the fuel method. On the other hand, the first generation concept deals only with detected neutrons and unambiguously assigns what particular isotope is a given neutron signature of. The main idea of the concept is that the quality of the signal is defined by the first generation fission and that any subsequent fission or inelastic reactions are only due to the multiplicative property of the environment. While the results of the first generation fission depend on the fissioning nucleus, the subsequent chain reaction is in a given FA statistically identical no matter what kind of nucleus fissioned first. The **Fig.16** is a schematic and simplified drawing of two possible fission chains, starting with fission of ^{235}U and ^{239}Pu. The products of the first generation fission will differ in terms of the average number of prompt and delayed neutrons. However the remains of the chains (2nd and any higher order generation) will be in both cases statistically identical, since the products of the 1st generation interact in the same environment with the same amount of fissile material as well as neutron poisons.

In MCNPX the 1st generation concept was implemented in such a way, that each neutron "carries" a tag with the information what was the original fissioning nucleus which started the chain reaction of which that particular neutron is part of. The neutron interacting (i.e. being registered) in the ^{3}He tube thus carries information on its origin and the time of detection. In post-processing analysis we may utilize this information and evaluate a contribution of any fissile isotope to the truly detected signal as function of time, as well as the detector position. Based on the concept of the 1st generation, the **Fig.17** displays relative contributions of the three fissile isotopes and ^{238}U to the signal detected by all detectors combined in three different time windows A,C and E for all 64 fuel assemblies of SFLI.

The range of relative contributions and its dependence on detector position, time, IE, BU and CT of ^{235}U, ^{239}Pu and ^{241}Pu is hardly surprising considering the amounts of individual isotopes in a particular FA and only documents how wide of a parameter space is being investigated. However, the magnitude of the relative contribution of ^{238}U is somewhat striking. The fact that it peaks at ~25% in the earliest time windows is certainly due to the not yet fully equilibrated neutron field, which apparently does not happen before 200us after the interrogating pulse. But even after that the relative contribution of the ^{238}U hovers around 5%. Having in mind that different time windows may provide qualitatively different but complementary information about the assayed FA, and that our ultimate goal is to estimate amount of present elemental plutonium with high precision, we are forced to rethink our definition of $^{239}Pu_{eff\_DDA}$ and include term accounting for the ^{238}U as well. Should it turn out that the overall most effective DDA measurements are only in the late times after the interrogating pulse when contribution of ^{238}U is rather small (~5%) and almost independent of the assayed FA, we may easily drop or neglect the ^{238}U term. However in order to provide a complete and most accurate evaluation of the instrument we decide to proceed with inclusion of the ^{238}U term in eq.(1) turning it into eq.(6) defined as follows:

$$^{239}Pu_{eff\_DDA\_1st} = C_1\ ^{235}U + ^{239}Pu + C_2\ ^{241}Pu + C_3\ ^{238}U \quad (6)$$

The evaluation of the C coefficients within the 1st generation concept is straight forward and is a ratio of the number of detected counts per gram of the isotope of interest over the number of detected counts per gram of ^{239}Pu, as described by the following eq.(7):

$$C_i = (N_{det}(i)/m(i))/(N_{det}(^{239}\text{Pu})/m(^{239}\text{Pu})) \quad (7)$$

On the other hand the above prescription does not provide any help as how to determine C_1 and C_3 coefficients for cases of fresh fuel. That however can be considered a limit case when BU=0 and CT=0 and thus can be extrapolated from the calculations of true spent fuel assemblies.

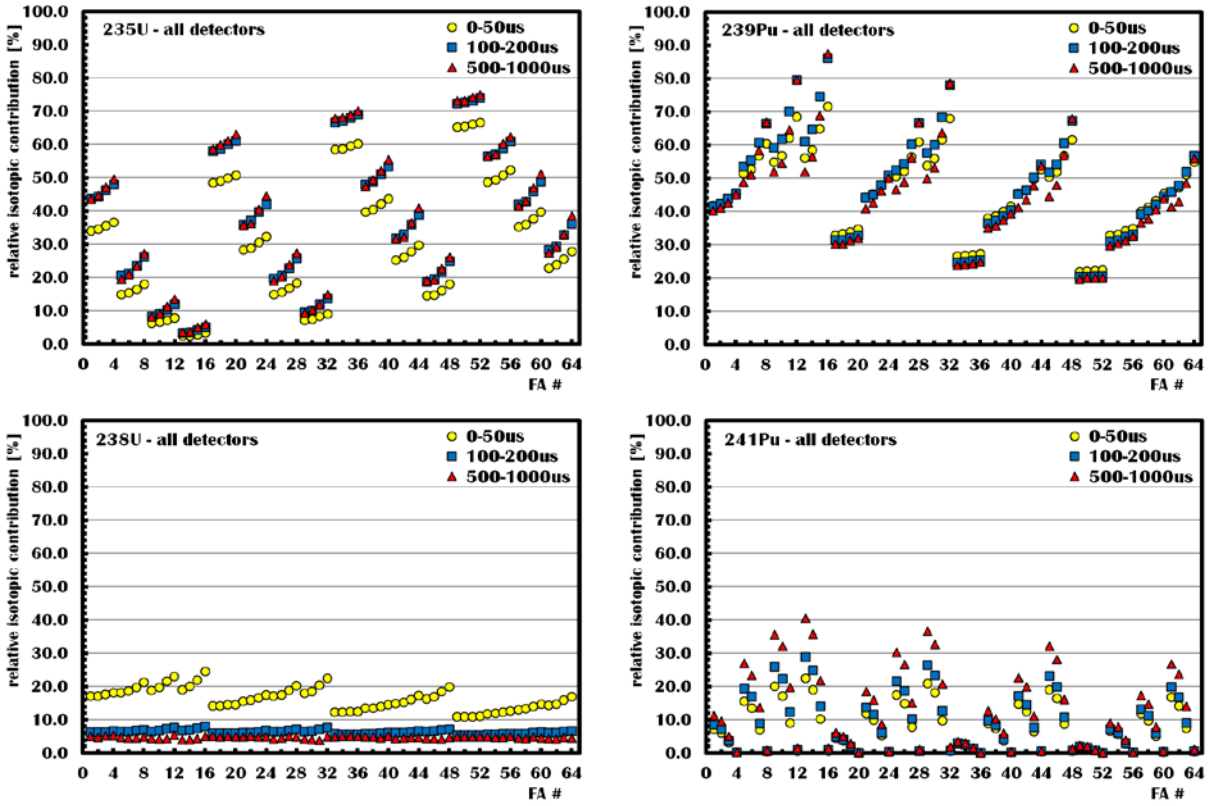

Fig.17 Relative contributions of various isotopes to the total DDA signal in three different time windows for 64 basic SFA's from SFLI.

The values of weighting coefficients C_1, C_2 and C_3 determined with the 1st generation method are displayed in Fig.18. For simplicity we limit ourselves to 3 different time windows and the total DDA signal in left panels, while the right panels demonstrate how C coefficients may vary with the detector position even if a generous time window is used (50-1000μs). The grey dots in plots with C_1 and C_2 represent the values of these coefficients calculated by the tally in the fuel, which was performed during a time window between 200 and 1000 μs after the interrogating neutron pulse.

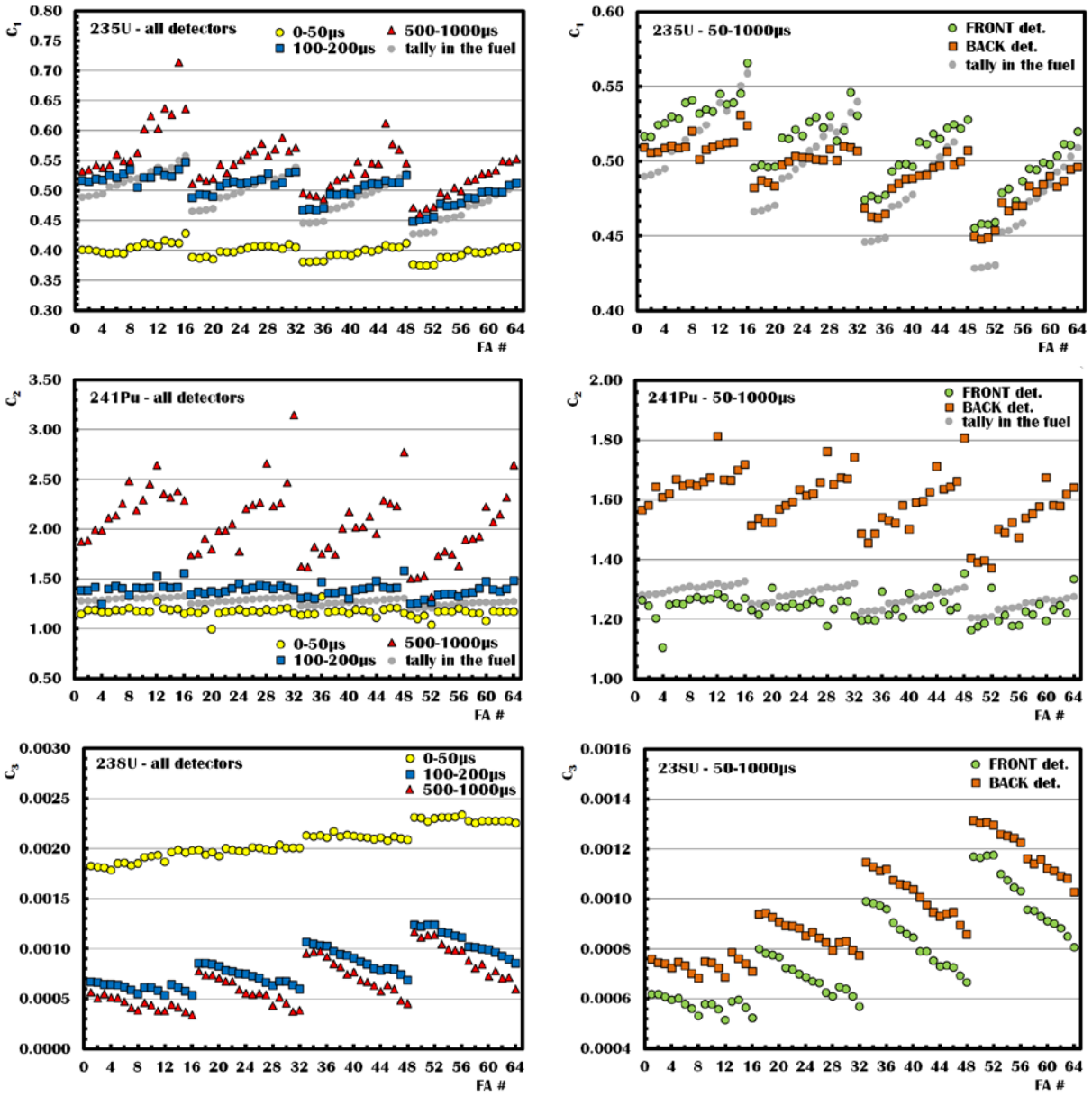

Fig 18 *Left panels* - Weighting coefficients C_1, C_2 and C_3 evaluated using 1st generation concept in three separate time windows for the total DDA signal defined as sum of the signals detected on individual ^{3}He detectors. *Right panels* – weighting coefficients C_1, C_2 and C_3 evaluated using 1st generation concept for front and back detectors separately in a time window from 50 to 1000μs. The grey dots in upper two rows represent values of C_1 and C_2 coefficients determined by the tally in the fuel method.

The data in Fig.18 generally follow already a well established pattern. Due to the dynamic evolution of the interrogating neutron field the *C* coefficients values differ depending on the time window as well as the position of detector, not to mention the ever present dependency on the "quality" of the SFA represented by its IE, BU and CT. But also the pace of evolution of *C* coefficients for different isotopes is quite intriguing. In case of C_1, the values rise quickly from ~0.40 to 0.50 within first 200 μs, only to add mere 10% in next 800μs. Meanwhile the C_2 representing ^{241}Pu rises about 15% from ~1.2 to 1.4 to

skyrocket to even up to ~2.5-3.0 within the first millisecond after the interrogating pulse exhibiting the strongest dependence on BU and CT among the three contributing isotopes. The drop of the weight of the contribution by ^{238}U in time is hardly surprising. As the interrogating neutron flux softens, the C_3 quickly drops from ~0.002 to ~0.0007 and keeps slowly sliding to ~0.0005 for the latest of utilized time windows.

The comparison to the values retrieved by the tally in the fuel method reveals a good deal of similarity, however, considering that the tally in the fuel was performed for time window of 200-1000μs the values of the *C* coefficients appear to come a little too low, and seem to be comparable rather to values of 1st generation method at times around 100μs. Yet it is worth pointing out that for a comparable computational time the statistical uncertainty of the results achieved by the tally in the fuel are by far superior to the results achieved by the 1st generation method, as can be seen from the general scatter of the points. The reason is of course easily understood, since it is the fundamental principle of the 1st generation concept to separate and count only neutrons which ultimately reach the detectors, statistically thus suffering from generally low efficiency of detection (~1‰) in the present design of the DDA instrument.

For the practical considerations, the dynamic nature of *C* coefficients as demonstrated in Fig.18 may look disappointing. Any hope that some sort of average or universal values of C_1, C_2 and possibly C_3's could be used seem to be rather fading. Unless BU, CT and IE are known, our selection of weighting coefficients could be off by tens of percents. On the other hand, their dynamic nature provides for multitude of opportunities starting with consistency cross-checks and systematic error evaluations due to the possibilities to measure $^{239}Pu_{eff}$ at different time windows as well as from the perspective of different detector position. While the introduction of the 1st generation concept led to the revelation of an unanticipated complexity, it also significantly expanded our tool pool. In the following chapters we will try to outline various approaches which with sufficiently reasonable assumptions may lead to a reduction of the complexity of the problem, or at special cases even to its direct solution.

3.5.3. DDA Signal vs. $^{239}Pu_{DDA\_eff}$ Mass

In **Fig.19**, the DDA signal for 64 fuel assemblies from SFLI is illustrated as a function of $^{239}Pu_{DDA\text{-}eff}$ determined by the 1st generation method based on eq.(6) and considering contribution of ^{238}U to the detected signal. The individual panels display the total DDA signal as defined by the sum over all ^{3}He detectors in different time windows. For the comparison the gray points represent the DDA signal as presented in previous report [11] with $^{239}Pu_{DDA\_eff}$ determined by the tally in the fuel method based on eq.(1) (i.e. not considering ^{238}U). The **Fig.20** also displays the DDA signal for 64 SFA's from SFLI as the function of the $^{239}Pu_{DDA\_eff}$, yet in this case the DDA signal is calculated for front and back detectors separately and for simplicity displayed only in two panels representing time windows A (*left*) and D (*right*).

The Fig.19 allows us to track the evolution of the DDA response in time as the function of the property of an assayed FA. In very early times the data yield rather subtle sensitivity to the IE of the fuel assembly. Moreover for a given IE, the magnitude of the detected signal is directly proportional to the amount of fissile material (represented by $^{239}Pu_{DDA\_eff}$) regardless of the CT or BU. However, as the time after the interrogating neutron pulse progresses, the IE starts to play more important role, and the DDA response starts to depend exponentially on the mass of the fissile content, resulting in a complex pattern

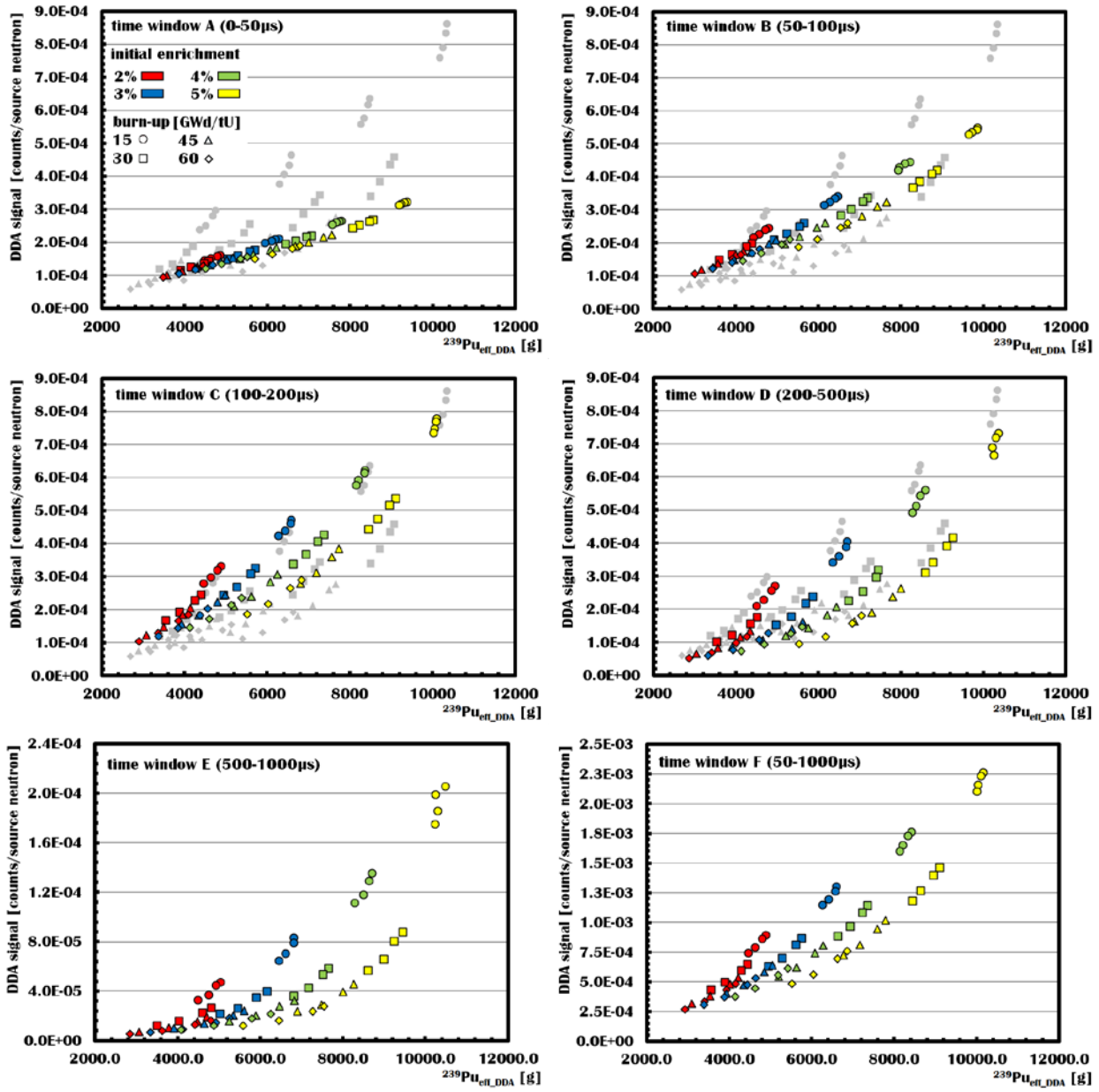

Fig. 19 The total DDA response per source neutron for 64 SFA's from SFLI as a function of $^{239}Pu_{eff\_DDA}$ for various counting time windows. Colored symbols represent values determined by 1st generation method; gray symbols represent values determined by the tally in the fuel method in a universal time window 200-1000μs.

such as in the panel dedicated to the counting time window D. The similarity with the pattern observed in earlier studies when tally in the fuel method was used (gray points) is quite remarkable. On the other hand the two panels in Fig. 20 show how the DDA response differs based on the position of the detector. It seems that only the relative magnitude of the signal changes in time. While in early time window the front detectors contribute the most to the overall detected signal, in later times it is at the back of the FA where most of the neutrons is detected. The data in Fig. 20 are not normalized to the number of detectors in front (two) and back (four) positions, but should that be taken into account the back detectors would still see a

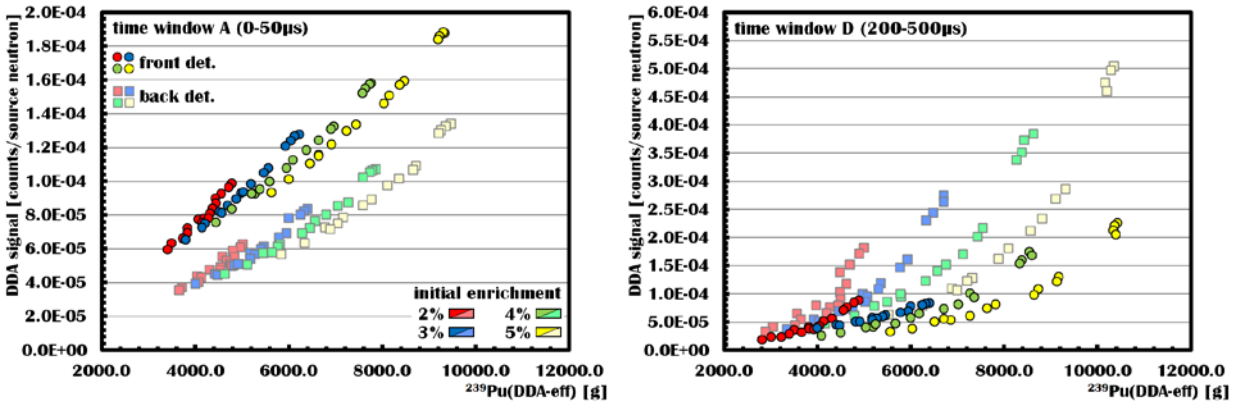

Fig. 20 DDA response per source neutron in front and back detectors for 64 SFA's from SFLI as a function of $^{239}Pu_{eff\_DDA}$ in time window A (left) and D (right).

little bit more than the front ones in the late time windows, as can be deduced already from Fig. 6. We attribute this difference in late times to the different material in the close proximity of the detectors (tungsten block near front detectors, back detectors surrounded by water).

Since all of the considered fuel assemblies have identical geometry, one may expect a smooth curve of DDA signal vs. the effective fissile mass. While we do observe a general trend that the DDA signal increases with effective fissile mass, the structure of the points is a function of the time, IE, BU and CT. Considering the principle of operation of the DDA instrument and how isotopic content of FA evolves in a reactor and while it cools, it seems likely that the structure is due to the buildup of neutron absorbers.

3.5.4. Role of Neutron Absorbers in Determining the Effective Fissile Mass $^{239}Pu_{eff\_DDA}$

To illustrate and quantify the role of neutron absorbers we adopt results of the analysis performed with the previous version of the DDA design with strong conviction, that conclusions drawn by [11] are still valid and applicable for the current version of the DDA instrument design.

In the above mentioned work the DDA response (based on a tally in the fuel method and 200-1000us counting window) for the 64 SFA's of SFLI was simulated with exclusion of all isotopes in the FA except ^{238}U, ^{235}U, ^{239}Pu, ^{241}Pu, ^{16}O and ^{17}O while adjusting the density of the fuel to maintain the proper mass of each of these isotopes. The DDA response for these "simplified" assemblies is displayed in **Fig.21** along with the 64 "real" assemblies.

In Fig.21 a smooth dependence of the DDA signal on the effective fissile mass has been obtained, confirming the expectation that it is the presence of neutron absorbers that causes complex structure of the DDA response in the real fuel assemblies. This figure thus demonstrates one of the key challenges of the current as well as possible future integration effort: to quantify and make corrections for the impact of neutron absorbers on the instrument that aims to measure the fissile content in a spent fuel assembly.

To further illustrate how influential the amount of the neutron absorbers can be the overall DDA response we compare the neutron flux for two assemblies with nearly identical $^{239}Pu_{eff\_DDA}$ as illustrated in

Fig.22. Both SFA's were cooled for 1 year, but they differ in IE (3% vs. 4%) and BU (15 GWd/tU vs 45 GWd/tU). Although the difference in $^{239}Pu_{eff\_DDA}$ is only ~7.6% the difference in the produced signal is ~53%. In both cases the thermal neutrons dominate the flux. The shapes of the neutron spectra are nearly identical, and the difference in the magnitude of the thermal neutron flux is ~49%. The challenge to future analysis is to determine a correction factor or analytical approach that will either account for or bypass the effect of neutron absorbers which cause the suppression in the overall neutron flux.

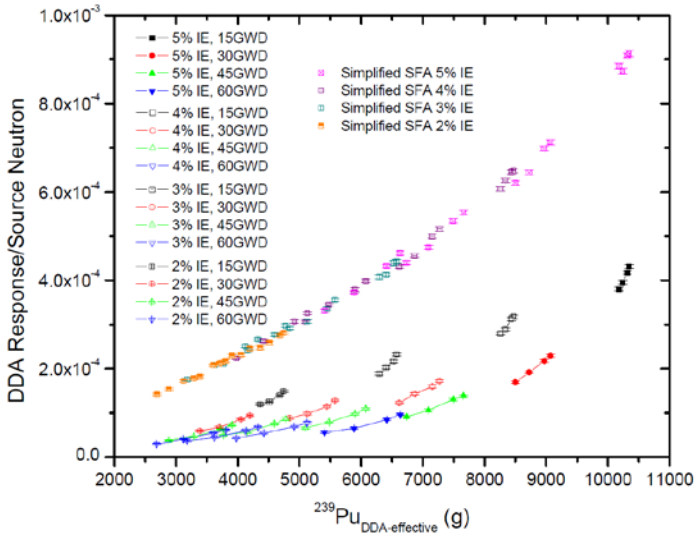

Fig.21 DDA response per source neutron for 64 "real" and "simplified" spent fuel assemblies as a function of $^{239}Pu_{DDA\_eff}$. (reprinted from [11])

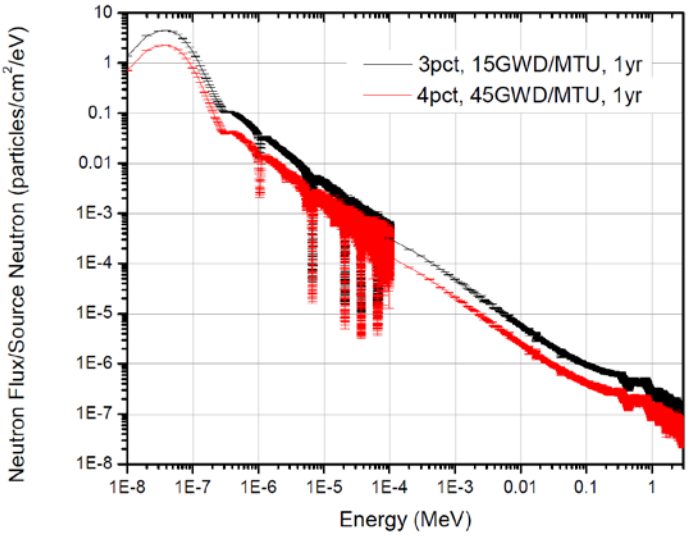

Fig. 22 The Neutron fluxes for two FA's with nearly identical $^{239}Pu_{eff\_DDA}$ but different IE (3%, resp. 4%) and BU (15 GWd/tU, resp. 45GWd/tU). (reprinted from [11])

3.5.5. Multiplication

Within the context of this report, the *net multiplication M* is defined as the average number of neutrons produced in the system per one neutron delivered into it by the source. The multiplication thus can be a quantity characterizing the property of the environment in terms of the amount and quality of the fissile material and neutron absorbers, their spatial distribution, the geometry of the system and properties of the neutron source.

It is currently beyond our capabilities to determine *M* for every single FA analytically. Therefore we will consider values of net multiplication provided by MCNPX. However, in such case we have to consider how the multiplication in the system develops and what does it exactly characterizes. If we need to limit ourselves to the property of the fuel assembly alone, with help of MCNPX we can allow ^{242}Cm and ^{244}Cm spontaneously fission in the SFA and then count how many neutrons are produced per a single neutron from Cm fission. Such "*passive*" multiplication will be labeled M_{pass}. This should not be confused with the "*active*" multiplication M_{act} which is calculated in simulations of active interrogation of a fuel assembly and reflects how many neutrons are produced per neutron of the neutron generator. In principle the main difference is that M_{pass} describes the multiplicative property of the fuel assembly itself, while M_{act} characterizes the multiplicative property of the instrument with the assayed fuel assembly as a whole. Since during the active interrogation the components of the DDA instrument remain the same and only the FA changes, one could expect a direct relation between M_{pass} and M_{act} such as in the following equation:

$$M_{act} = a_{inst} \cdot M_{pass} + b_{inst} \tag{8}$$

where a_{inst} and b_{inst} are constants characterizing the specific instrument design. The **Fig. 23** displays that in case of 64 SFA's from the SFLI the eq.(8) indeed describes the relationship between passive and active multiplication well. In other words, knowing, or having the ability to measure one kind of multiplication means direct knowledge of the other one as well. The **Fig.24** displays the deviation of the actual values of M_{act} (*left*) and M_{pass} (*right*) from the calculated values using the fit displayed in Fig.23. Indeed, the correlation between M_{act} and M_{pass} is not perfect and exhibits dependence on BU and CT, on the other hand these perturbations typically do not exceed 1-2%, and for our needs can be neglected. More important issue is whether we can, in some way, measure any actual multiplication, passive or active.

In the previous chapters we have documented the dynamic evolution of the neutron flux across the fuel assembly during the first millisecond after the interrogating neutron pulse. The Fig.6 demonstrates that the neutron flux reaches its maximum in the front detectors earlier, than in the back detectors. The concept of the first generation describes the quality and magnitude of the DDA signal as being determined by the first generation fission and multiplicative property of the environment, where fissile material competes for neutrons with the neutron absorbers. Thus by definition, the multiplication is generally being realized in the later times as the neutrons traverse through the fuel assembly. Should that be true, the relation between the signal detected on the front and the back detectors should be a measure of the active multiplication M_{act}. The **Fig.25** displays the ratio of the number of neutrons detected in the back and the front detectors as the function of the active multiplication M_{act} determined by the MCNPX for all six different counting windows A-F. Tracking the dependence of the B/F ratio in various time windows, we can observe that especially in the early times, the back detectors see relatively more neutrons when

SFA with higher multiplication is assayed. We can also observe in which time windows the most of the multiplication occurs by comparing the B/F ratios of SFA's with the lowest and the highest multiplication M_{act}. In window A, the difference is ~18%, in window B it is already ~38% and reaches its maximum in time window C where the difference is ~52%, while in window D it drops back to ~30%. Window E, which lasts from 500-1000us even provides for quite ambiguous results, where B/F ratio stays on average constant but for M_{act}<2.25 (typically very high BU) seems to heavily depend on the CT, moreover, with many assemblies exhibiting higher B/F ratio than the SFA's with M_{act}>2.25.

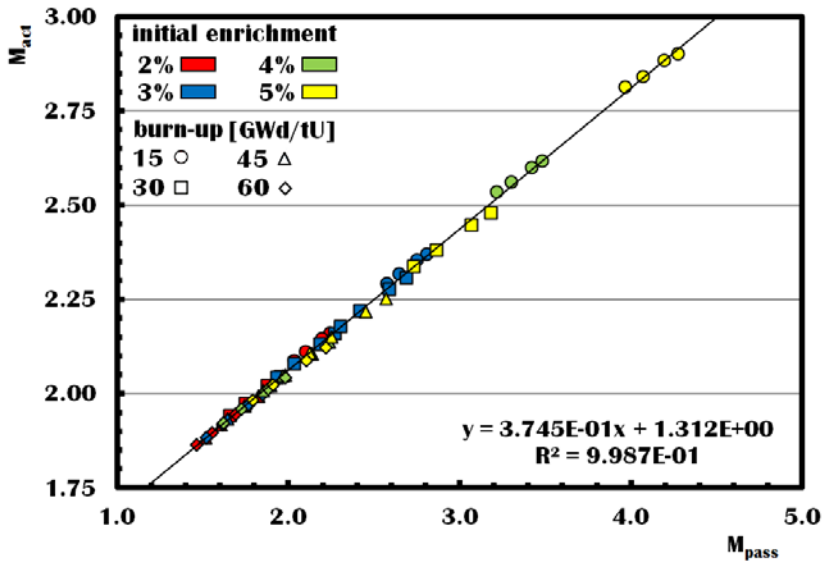

Fig.23 Active (M_{act}) and passive (M_{pass}) multiplications of 64 SFA's from SFLI are directly related.

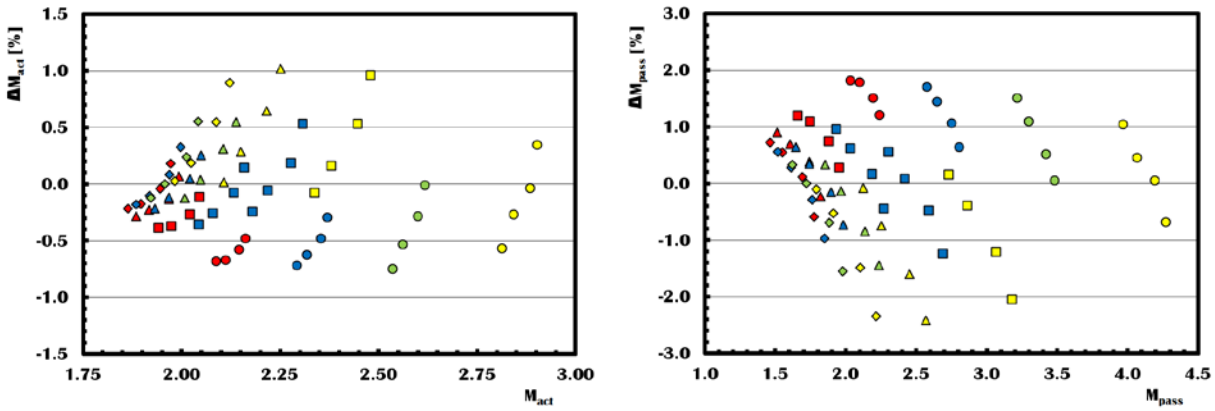

Fig.24 Deviation of actual M_{act} (*left*) and M_{pass} (*right*) from a fitted linear relationship between active and passive multiplication for 64 SFA's from SFLI (see Fig.23).

In our interpretation, the individual panels of Fig.25 simply demonstrate that the evolution of the interrogating neutron field progresses at a pace which depends on the properties of the assayed fuel assembly. It also illustrates how and when the core of multiplication of the interrogating neutron flux is realized and when the effect of neutron poisons starts to dominate. In other words, it takes some time before the initial wave of neutrons from neutron generator gets multiplied in the FA, as is seen from the weak dependence of B/F ratio on M_{act} in window A, but a stronger dependence in window B. Most of the

multiplication seems to happen in the window C, i.e. 100-200μs after the interrogating pulse. The window D seems to indicate the onset of dominating effects of the neutron poisons in the most burned FA's. Results in window E on the other hand seem to suggest that the neutron population already is, or is close to, its relative dynamic equilibrium as indicated by on average a constant B/F ratio regardless of the M_{act}. This dynamic interpretation is further supported by remarkable splitting of B/F ratio dependence on M_{act} with BU particularly visible during the time window C. On the other hand, this BU dependence seems to disappear and over B/F ratio dependence on M_{act} smoothes out when a very general time window F (50-1000μs) is considered.

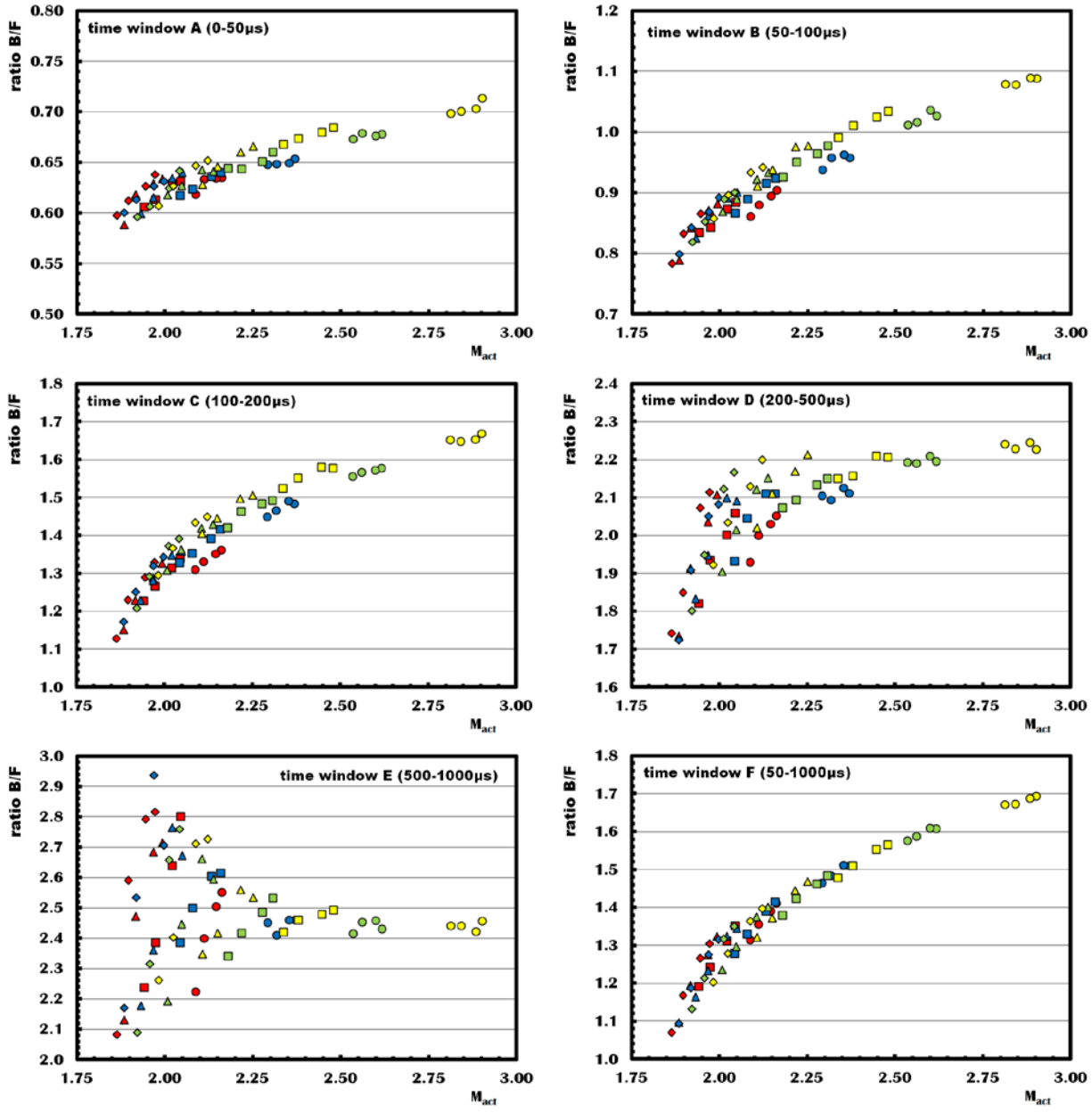

Fig. 25 The ratio of the number of neutrons detected in the back and the front detectors in six different counting windows A-F as the function of the active multiplication M_{act} determined by the MCNPX.

In general, results from Fig.25 indicate that multiplication cannot be reliably measured in a narrow time window, since for two different FA's the multiplication of the neutron flux progresses differently in time. In order to strip the B/F ratio of its inherent dependence on the parameters of the FA other than multiplication, we need to utilize a more integral measurement, such as suggested by the smooth dependence in Fig.25 (F). But since the time window F (50-1000μs) originally intended exactly for such kind of integral measurements also includes times when effects of poisons become dominant, we are forced to move such window forwards in time, and shorten it appropriately. The **Fig.26** (left) displays simulated results of B/F ratio in a time window from 0-200μs, with a 3rd degree polynomial fit to capture the dependence of B/F ratio on actual M_{act}. The right panel of Fig.26 then displays the deviation of the actual M_{act} from the value determined solely based on the B/F ratio and the polynomial fit. In other words, the ***B/F ratio is indeed a measure of multiplication*** with a precision typically better than 2%.

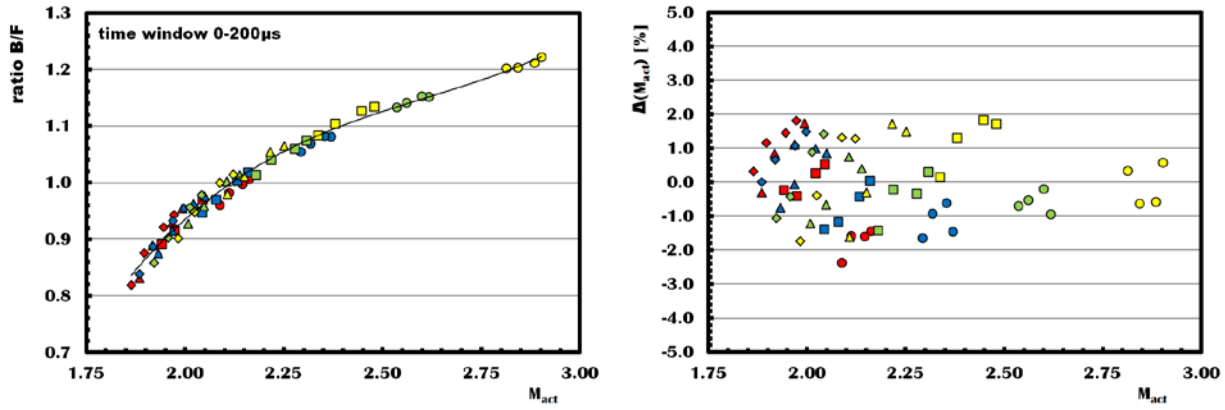

Fig.26 *Left* - The ratio of the number of neutrons detected in the back and the front detectors in a time window 0-200μs as the function of the active multiplication M_{act} determined by the MCNPX; *right* – relative deviation of actual M_{act} from values determined from a 3rd degree polynomial fit and B/F ratio.

Alternatively, we may follow the lead from the previous version of the report which indicated a strong correlation between the passive multiplication and the die-away time constant τ_{DDA} [11, Fig.19, p. 24]. However, as with all other observables, the die-away time was determined for a time window between 200-1000μs for the total DDA signal defined as the sum of all detected neutrons on all ^{3}He detectors. Within the current approach we will investigate the die-away time within several counting time windows and compare the results for front and back detectors separately, since already Fig.6 indicates that the die-away time-constants must be different for front and back detectors in the first 200μs after the interrogating neutron pulse. For obvious reasons it is virtually impossible to define die-away time constant for times before 100μs, and we will limit ourselves thus only to the time windows C,D and E. The **Fig.27** displays the die-away time constant as the function of active multiplication M_{act} for 64 SFA's from SFLI as determined for front and back detectors separately in time windows C and D and for total DDA signal (front and back detectors combined) in time window E. Same as the B/F ratio also τ_{DDA} undergoes a dramatic dynamic evolution during the first millisecond after the interrogating neutron pulse. In the earliest time window when τ_{DDA} is measurable (window C – 100-200μs) the die-away time constant is very different for front and for the back detectors. Moreover, while it is directly proportional to the

active multiplication M_{act}, the constant of proportionality is very strongly correlated with IE. The situation changes dramatically in a later time window D (200-500μs) where values of the time constant on the front and back detectors seem to be already very close and more importantly the IE dependent effects seem to almost completely vanish. In the latest time window E (500-1000μs) the τ_{DDA} values are virtually identical for front and back detectors allowing us to determine a single value for the whole DDA instru-

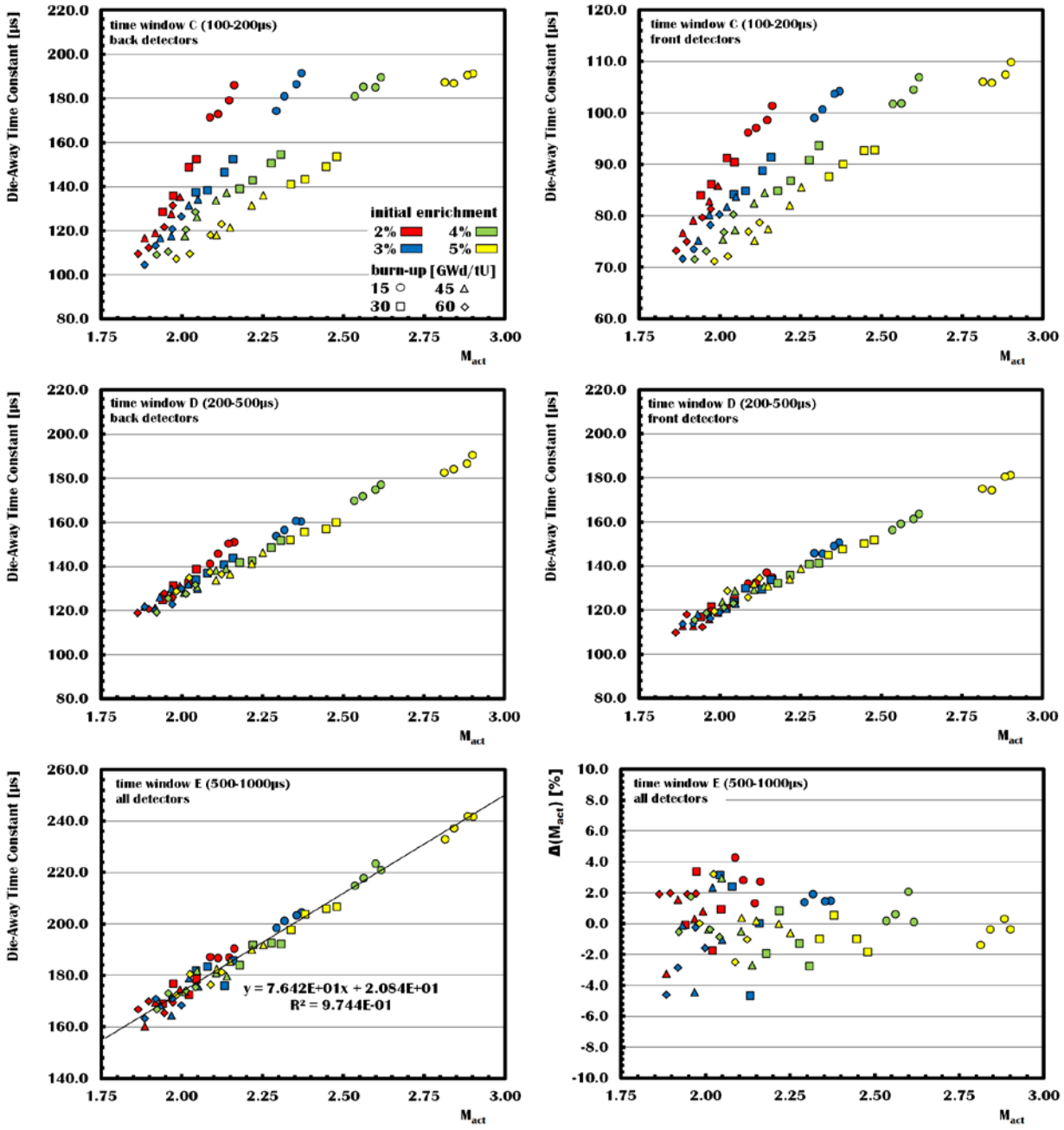

Fig.27 Die-away time constant as the function of the active multiplication M_{act} for 64 SFA's from SFLI as determined for front and back detectors separately in time windows C and D and for total DDA signal (front and back detectors combined) in time window E. Lower right panel displays the relative deviation of M_{act} determined from the linear fit of data in lower left panel with respect to the actual values of M_{act}.

ment. In this latest time window the τ_{DDA} scales with the multiplication M_{act} without any apparent dependency on IE, BU or CT. The lower right panel in Fig.27 further displays how good of a predictor of the M_{act} the τ_{DDA} provided the calculated data from window E are fitted with a simple linear dependence. Neglecting of course any possible systematic errors, we can learn that with the help of τ_{DDA} we can determine M_{act} within +/- 4%, i.e. approximately factor of two less accurate than when using the B/F ratio.

Another possible approach stems simply from the very definition of the multiplication. In other words, the number of detected neutrons per neutron injected to the environment from the neutron generator should reflect the multiplicative property of that environment. The question is, when exactly should such measurement take place, since Fig. 25 and Fig. 27 implicate vastly different dynamic evolution of the neutron flux depending on the actual properties of an assayed FA. In six separate panels the **Fig. 28** then displays how the total number of neutrons detected by all ^{3}He detectors in a given time interval depends on the active multiplication of an individual fuel assembly.

Starting from the earliest time window A (0-50μs) we can yet again observe a typical structure of 64 data points corresponding to the DDA response plotted versus the active multiplication of the FA. In the early times after the interrogating neutron pulse (window A and B), among the SFA's with similar M_{act}, the ones with higher BU and IE provide for higher DDA response than the SFA's with lower BU and IE. However, as we move further in time, the structure of the data almost completely disappears in time window C (100-200μs) only to be fully restored again in later times as can be seen in time window E (500-1000μs). It is certainly worth pointing out, that the "polarity" (i.e. orientation) of the data structure in the plot gets inverted in later times compared to times right after the interrogating neutron pulse. Now it is the lightly burned and lightly initially enriched SFA's which DDA response is larger than that of the SFA's with identical M_{act} but higher BU and IE. The most intriguing observation is then that the cross-over of these trends seem to happen simultaneously at the same time for all different SFA's, leading to the alignment of the data where DDA response is almost directly proportional to the M_{act}. Additionally, similarly as in the time window C, also the data in lower right panel (0-1000μs) display almost perfect linear correlation between the DDA response and the multiplication of the FA.

The results displayed in the lower right panel should perhaps not be really that surprising. Considering that the die-away time constants of the individual SFA's in any of the considered time domains range from 70-240μs, the intensity of the induced neutron flux 1000μs after the interrogating pulse should be rather negligible. This means that the longest time window from 0 to 1000μs should basically cover full evolution of the induced neutron population from its inception by the interrogating neutron pulse until its near full extinction at times corresponding to approximately 5-8 die-away time constants. The number of detected neutrons is then proportional to the number of neutrons created in the assembly, i.e. to the multiplication. The **Fig. 29** displays how the DDA response for various SFA's measured from 0-1000 μs after the interrogating pulse differs from a linear fit based on the results for all 64 SFA's from SFLI (as shown in lower right panel of Fig. 28).

The left panel of Fig.29 shows that the actual simulated data differ from a perfect linear fit mostly by +/- 2%, although several highly burned cases with long cooling times can be as far as 7% off. More interesting is the parabolic dependence of the deviation on the M_{act} suggesting that rather than liner, perhaps quadratic fit may be more appropriate. The right panel of Fig.29 then shows that indeed a

quadratic fit of the data from time window F* leads to a great description of the observed trend with DDA responses of individual SFA's differing from the fit typically by less than 1%.

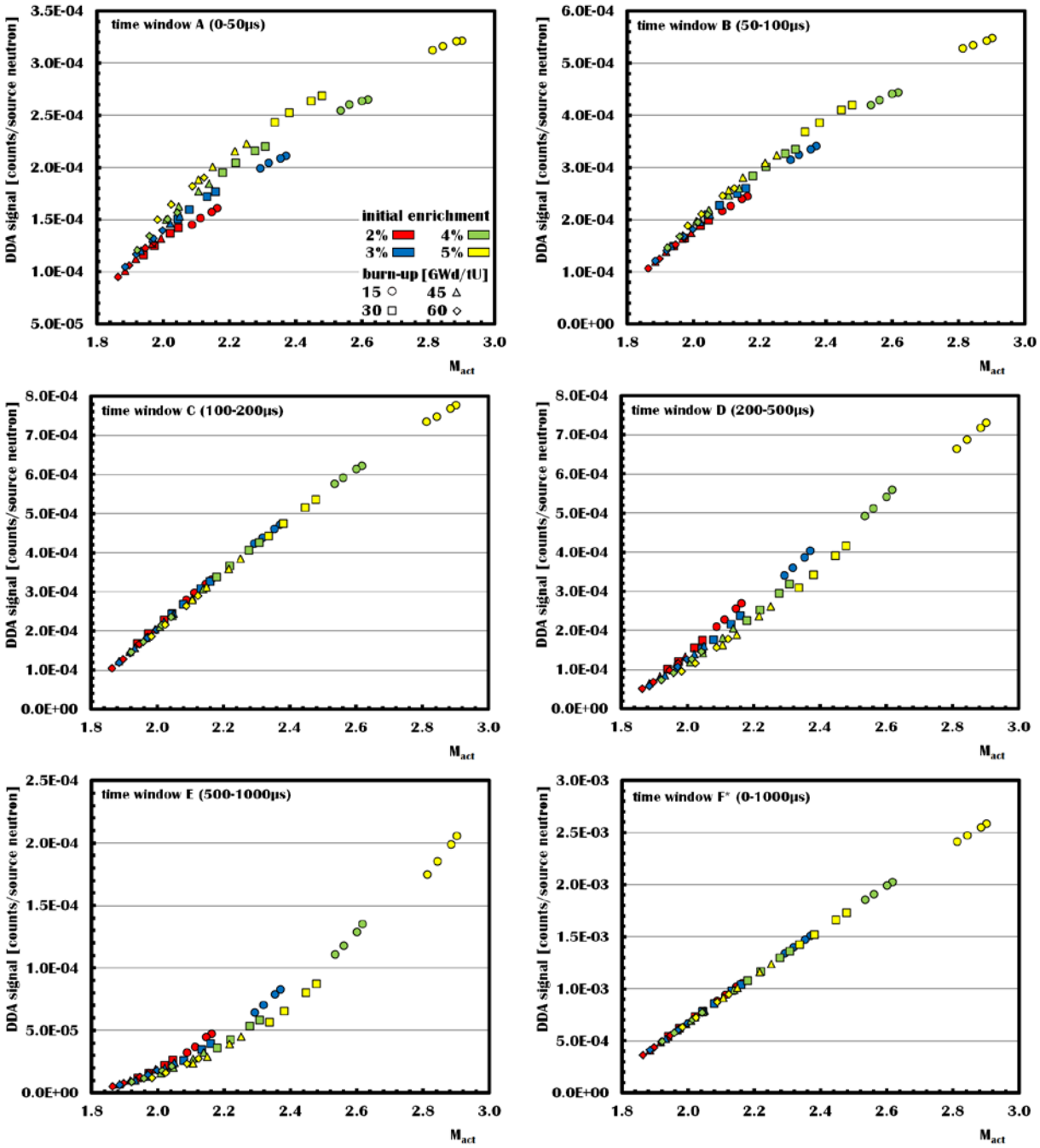

Fig.28 DDA response defined as the sum of neutrons detected on all ^{3}He detectors in different time domains as a function of the active multiplication M_{act} for 64 SFA's from SFLI.

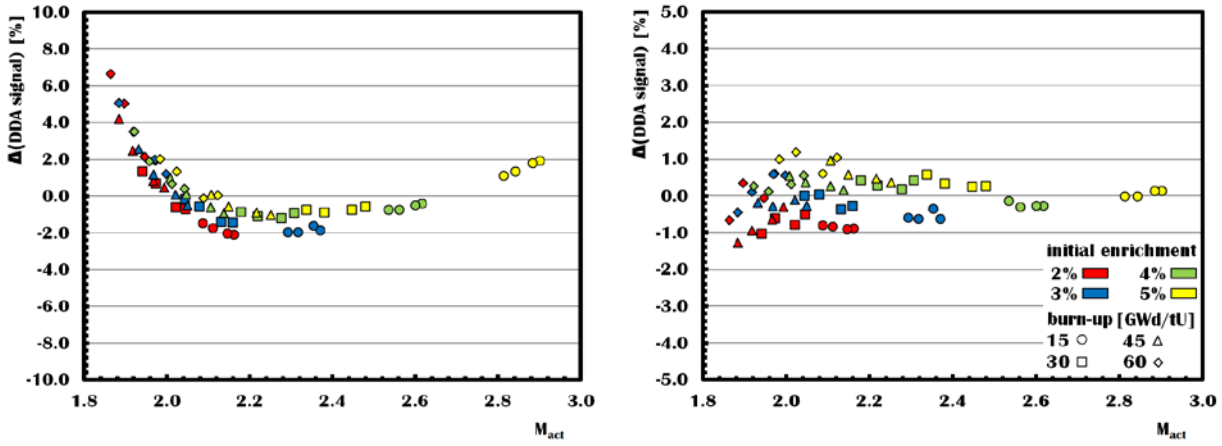

Fig. 29 Relative deviation of the actual DDA response from values predicted by a liner (*left*) and quadratic (*right*) fit of the data in Fig. 28 (time window F*).

While the difference between linear and quadratic fit seems rather miniscule, the fact that quadratic fit better describes the simulated results raises an interesting question. The issue is that the M_{act} in MCNPX is based on the number of neutrons created in the FA during the simulated time interval. Since the simulated time interval has been in all of the cases described within this report full 1000μs since the beginning of the interrogating neutron pulse, one could expect that M_{act} should be exactly linearly correlated with the total number of neutrons detected by ^{3}He detectors during this time interval. The fact that the correlation is indeed not linear suggests that ^{3}He detectors detect relatively less neutrons than is during an identical time interval produced. This apparent "neutron detection deficiency" increases with the overall multiplication of the system and in our opinion is a result of the delay between the "realization of multiplication" (i.e. neutron is created and immediately accounted for by MCNPX) and its real time detection (i.e. neutron is detected and accounted for by the DDA instrument). In general, one could diminish the effect of this neutron detection deficiency by allowing for detection of neutrons for a longer time interval (e.g. 0-2000μs), however, due to possibility of too low signal-to-background ratio (see chapter 3.5.6) for certain SFA's such measurement scheme may be ultimately counterproductive. Overall, we see the total number of detected neutrons as a potentially high precision measure of the active multiplication M_{act} of assayed SFA's, but due to necessity to cover very early (too high neutron counting rates) as well as very late (potentially too high background counting rates) time interval with respect to the interrogating neutron pulse may cause severe practical difficulties.

On the other hand, the results displayed in the panel corresponding to the time window C seem rather promising although counter intuitive. Apparently, during this limited time interval the difference in the DDA response caused by various amount of neutron absorbers ruled by different IE, BU and CT do not seem to matter, and only the overall multiplication of the SFA determines the DDA response measured by the instrument. Thus time window C provides us qualitatively with a similar information as the measurement of the DDA response in the full time range from 0 to 1000μs after the interrogating neutron pulse allowing us to avoid the most difficult to measure time domains right after the pulse as well as late time domains when background neutron count rate may bury the real signal. While the shifting of the structure of the data in time can be clearly attributed to different dynamic evolution of the neutron flux within a given SFA, as of now, we do not have any explanation why the data align so well regardless of

the SFA's parameters (IE, BU, and CT) during this special time interval. The correlation of DDA response measured during the time window C is not as perfect as in the case of time window F*. We attribute this simply by a somewhat arbitrary choice of the investigated time domains, and believe that following a dedicated study a better optimized time window could lead to a better alignment of the simulated data along a simple (probably quadratic) dependence as observed for data from time window F*.

Thus we may conclude this chapter that same as the B/F ratio also the die-away time constant τ_{DDA} and the total number of detected neutrons DDA_{tot} can in general be used as a measure of the multiplication of the assayed fuel assembly. But while the B/F can measure M_{act} in rather early times after the interrogating neutron pulse, the τ_{DDA} gains its predictive power only in the later times. DDA_{tot} on the other hand offers two vastly different time domains which however seem to lead to qualitatively same results. Interestingly enough, the time when B/F ratio loses its capability to measure M_{act} is almost exactly the same time when τ_{DDA} gains it. It also should not be left unnoticed, that in the early times when B/F measures M_{act} and is insensitive to the IE, BU and CT, the τ_{DDA} as a function of the very same M_{act} yields a very strong dependence on the IE. In other words, the τ_{DDA} measured in the early time window could be used to a self-consistent determination of IE of the assayed FA.

3.5.6. Signal vs. Background

Signal to background ratios (S/B ratio) and the following requirements concerning the strength of the driving neutron source have been well studied within the last edition of the DDA report [11, p.24]. Even though the design of DDA instrument has been revised and updated, we are convinced that the previously reported data are still relevant (see Fig.19 for comparison of DDA signal for new and previous design version of the instrument). We will therefore restrict ourselves to a mere reproduction of the results and figures from the previous report with only minor, predominantly stylistic alterations, complemented by several additional figures and expanded discussion and conclusions.

In case of the spent fuel assemblies from SFLI virtually all neutron background is composed of neutrons from a spontaneous fission of ^{244}Cm ($T_{1/2}$=18.11 y) and the subsequent decay chain. The **Fig.28** (*left*) shows a total amount of ^{244}Cm in each fuel assembly from the regular set of 64 SFA's from SFLI. The right panel of Fig.28 then displays the background count rate as detected by the DDA instrument (using previous design – as in fig.12) using 200-1000 μs counting window with frequency of 100 Hz (i.e. 8% duty cycle). It is easy to spot that the amount of ^{244}Cm in a FA does not directly translate into the background counting rate. The reason is again the amount of fissile material and poisons present in a given fuel assembly. This on the other hand can be characterized by the passive multiplication unique to the composition of each fuel assembly, which reaches values from 1.45 to 4.35. Schematically we can write:

$$B \sim M_{pass} \cdot m(^{244}Cm) \qquad \textit{eq.(9)}$$

where B is the background count rate, $m(^{244}Cm)$ the mass of the ^{244}Cm in the FA and M_{pass} its passive multiplication (to be distinguished from the active multiplication M_{act} as discussed in chapter 3.5.5).

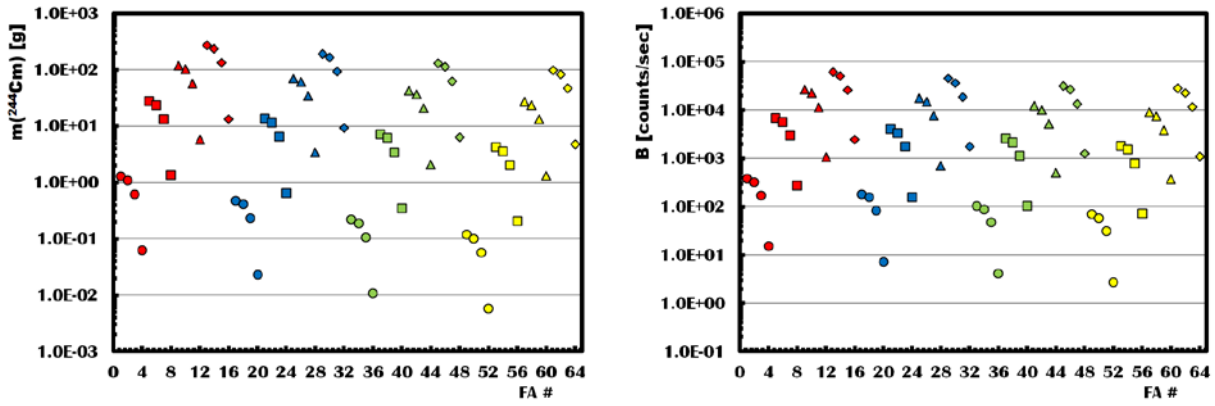

Fig.28 Total content of ^{244}Cm (*left*), and the background count rate as detected by the DDA instrument with 8% duty cycle (*right*) for each fuel assembly from the regular set of 64 SFA's from SFLI

During the active interrogation of a fuel assembly, the product of the DDA response or signal per source neutron and the strength of the neutron generator give the DDA instrument signal count rate. In **Fig.29**, a neutron generator with the *average* strength of $1x10^9$ neutrons per second was selected to compare the DDA count rate to that of the background as the function of the $^{239}Pu_{eff\_DDA}$. The data in Fig.29 use the sum of the detected neutrons from all ^{3}He detectors (as in design according to Fig.12) during the time window 200-1000μs as the definition of the signal. And the effective fissile mass $^{239}Pu_{eff\_DDA}$ is based on C_1 and C_2 coefficients determined by the tally in the fuel method. The data yet again exhibit a complex pattern based on the IE, BU and CT. While (based on the Fig.19) the dynamic range of the signal for 64SFA's from SFLI spans only across 1-2 orders of magnitude, the S/B ratio in Fig.29 covers full 5 orders of magnitude. The data thus demonstrate not only how significantly the background can vary, but also how important of a role it can play.

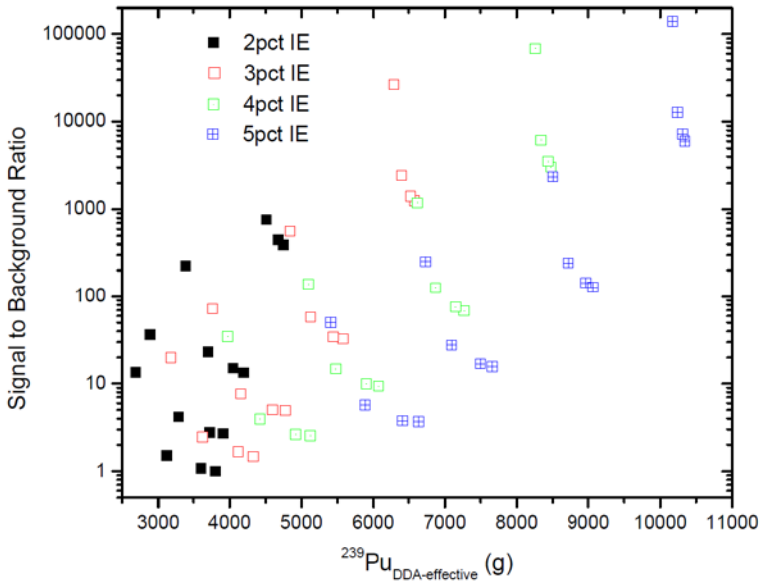

Fig.29 The signal-to-background ratios for 64 SFA cases from SFLI as a function of $^{239}Pu_{eff\_DDA}$ (reprinted from [11]).

According to the data in Fig.29 the S/B ratio can vary from ~1 to ~100000. However we have to keep in mind that with used 100 Hz repetition rate, 10 μs length of the pulse and $1x10^7$ neutrons per pulse, the *instantaneous* strength of the neutron generator is $1x10^{12}$ neutrons per second. That is approximately ten times higher instantaneous strength than the strongest, currently available, off-the-shelf neutron generators. On the other hand, the lowest S/B values in Fig.29 belong to FA with unrealistically high burn-up, such as SFA with 2 or 3% IE and 60 GWd/tU burnup.

Another way to better define the required intensity of the neutron generator is presented in **Fig.30**, where it is presented as a function of desired S/B as well as the BU. Should we consider as our benchmark the fuel assembly with 4% IE, 45GWd/tU which has been cooled for 5 years, and a goal to achieve being S/B~0.5, then a required neutron generator would need to have the average strength of $5x10^8$ n/s and the instantaneous strength of $5x10^{10}$ n/s. This means that the already available off-the-shelf neutron generators should be sufficient for the full functionality of the proposed DDA instrument.

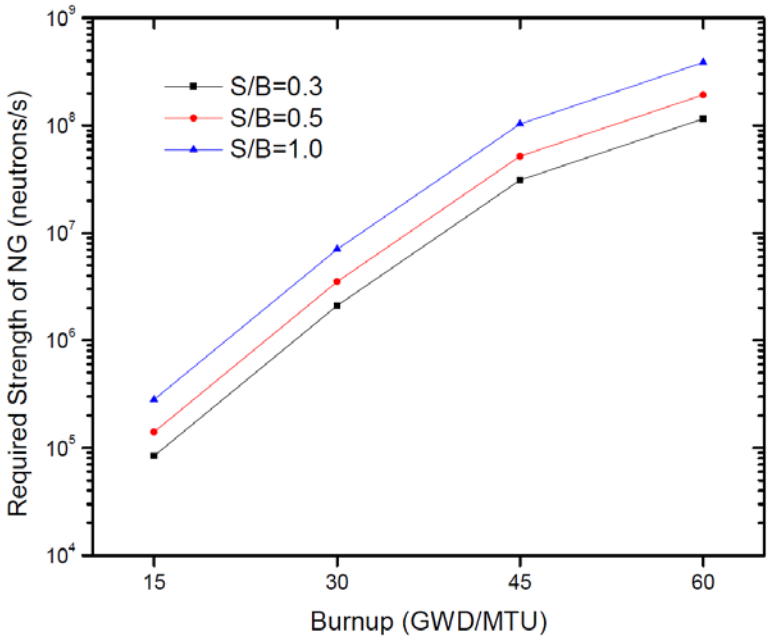

Fig.30 Strength of the neutron generator for certain signal-to-noise ratios as a function of the BU of SFA's with 4% IE and 5y CT. (reprinted from [11])

3.5.7. Variation in DDA Signal with IE, BU and CT

As already observed in Fig.19, the DDA signal at any time after the interrogating neutron pulse is generally a complex function of IE, BU and CT. To better understand the fundamental role of each individual of these three parameters we can plot the DDA signal for all 64 SFA's from the SFLI in the most simplistic way – as a function of only one of these parameters. **Fig. 31** thus illustrates how the DDA signal nonlinearly decreases with increasing BU, i.e. build-up of the neutron absorbers, while the **Fig. 32** shows that relationship between DDA signal and the IE is rather linear, since more fissile material to start

with translates almost directly into a greater DDA signal. **Fig. 33** then reflects the effect of the decay of several key isotopes leading to the DDA signal falling exponentially with increasing CT. In this case it is primarily the decay of ^{241}Pu to ^{241}Am ($T_{1/2}$=14 y) which transforms fissile material into a neutron absorber and the decay of ^{155}Eu to ^{155}Gd ($T_{1/2}$=4.7 y) which leads to a buildup of a strong neutron poison right inside the fuel rods.

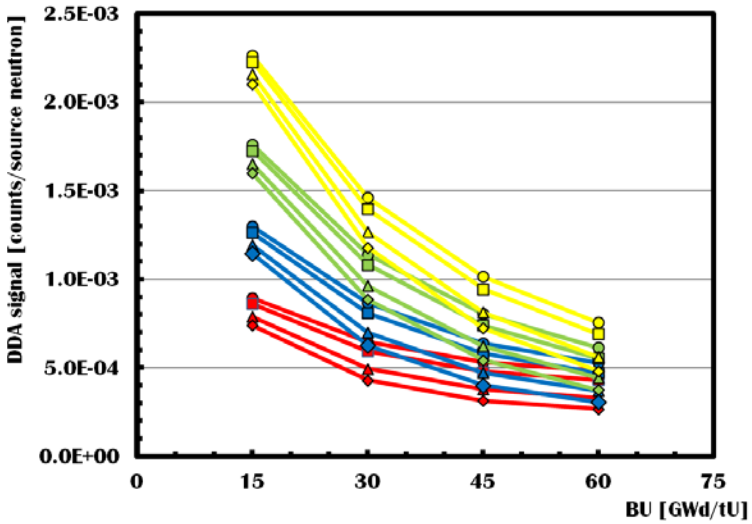

Fig.31 DDA signal count rate for 64 SFA's from SFLI as a function of BU.

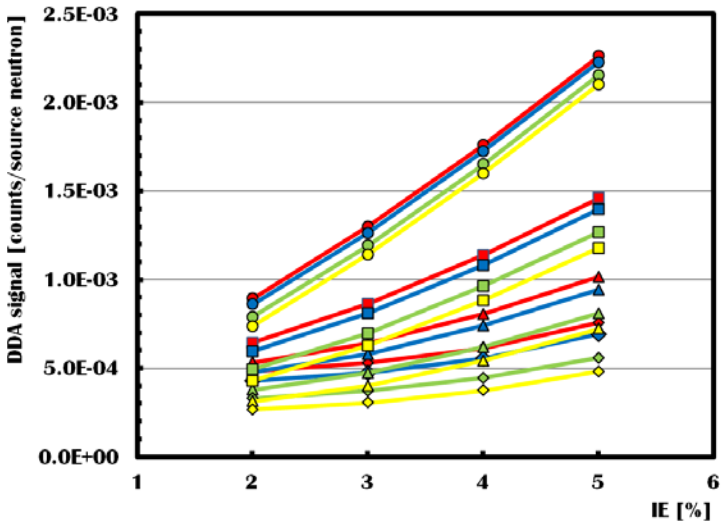

Fig.32 DDA signal count rate for 64 SFA's from SFLI as a function of IE.

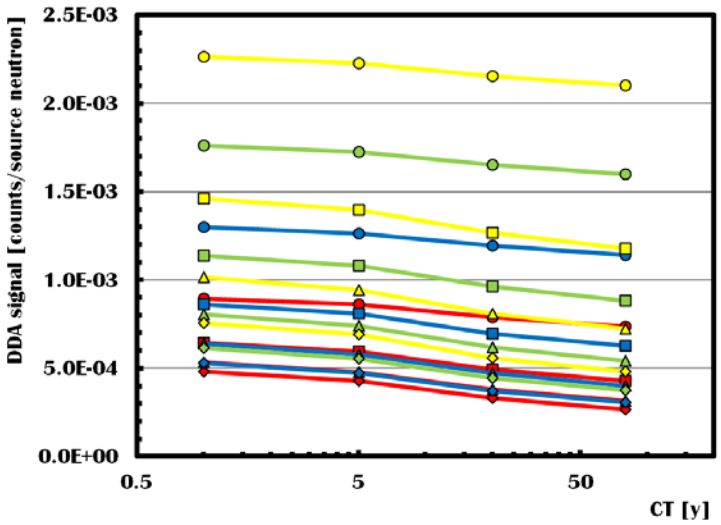

Fig.33 DDA signal count rate for 64 SFA's from SFLI as a function of CT.

3.5.8. Systematic Uncertainty in the Count Rate of the DDA Instrument

It is very difficult to estimate the systematic uncertainty of an instrument unless it can undergo vigorous experimental testing in near real-life conditions when sources of systematic uncertainty can be at least properly identified. Nevertheless, the authors of the previous report [11, p.28] expected that one of the sources of systematic uncertainty may be a displacement of the SFA in the DDA instrument during the interrogation. They have therefore performed a simulation study, where five different displacement positions were compared to the base case, i.e. a fuel assembly perfectly centered within the instrument. We reproduce their principle findings below, since we consider it as a useful benchmark comparison that can be easily expanded once the realistic tolerances for the DDA instrument are specified.

The **Fig.34** displays five extreme off-center positions in horizontal directions of the spent fuel assembly: (a) up-left, (b) left, (c) up-right, (d) right, and (e) up. The displacement is either by 5mm in one direction (e.g. "up") or combination of two displacements by 5 mm each in two directions (e.g. "up-left" is 5 mm "up" and 5 mm "left"). In Tab.3, the changes in the DDA count rate (sum of detected neutrons on all ^{3}He detectors with DDA design as in Fig 12) within a counting window 200-1000 μs for five positions

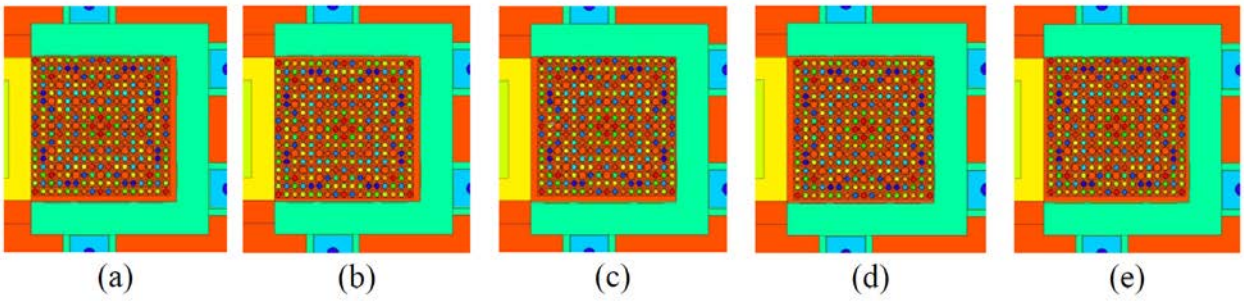

Fig.34 Five extreme off-center positions in horizontal directions of the spent fuel assembly: (a) up-left, (b) left, (c) up-right, (d) right, and (e) up (reprinted from [11])

indicated in Fig.34 are given. For the given displacement the count rate is expected to vary only by ~1%. Should the tolerance around the assembly increases, this uncertainty will also increase. In general, if the assembly leans toward the neutron generator, its count rate increases, and if the assembly leans away from the generator, the count rate decreases.

Tab.3 Systematic uncertainty in DDA count rate for off-center positions of spent fuel assembly

Case	4%, 15 GWd/tU, 5y		4%, 45 GWd/tU, 5y	
	Count Rate [counts/s]	Error [%]	Count Rate [counts/s]	Error [%]
Base	**3.08×10^5**	**-**	**9.84×10^5**	**-**
Up-Left	**3.11×10^5**	**1.0**	**9.94×10^5**	**1.0**
Left	**3.11×10^5**	**0.8**	**9.93×10^5**	**0.8**
Up-Right	**3.03×10^5**	**-1.8**	**9.78×10^5**	**-0.6**
Right	**3.03×10^5**	**-1.8**	**9.77×10^5**	**-0.8**
Up	**3.06×10^5**	**-0.6**	**9.87×10^5**	**0.3**

4. Determination of the Elemental Plutonium Content in an Assayed SFA

The most prominent objective of the NGSI research is to develop and test new or novel techniques to measure or determine mass of the elemental plutonium in a non-destructively assayed spent fuel assembly. Unfortunately, the DDA instrument investigated within this report cannot measure content of the elemental plutonium directly. However, the dynamic nature of the measurement technique allows to approach the problem from several different perspectives, and always retrieve a different piece of information, which when later put together as a jigsaw puzzle can complete the picture.

In principle, the DDA instrument offers two paths to the information about the plutonium content within the SFA. Depending on the actual measurement conditions and the amount, accuracy, and trustworthiness of any prior knowledge of the assayed SFA one or the other may turn out to be more beneficial and provide more accurate and/or complete answer.

The first method takes advantage of a direct correlation between the elemental plutonium and ^{244}Cm content in any spent fuel assembly and is described in detail in the next chapter 4.1. The second method uses the concept of the effective plutonium mass, and under various conditions can measure exactly that. The link between the $^{239}Pu_{eff}$ and the actual mass of the elemental plutonium is considered to be provided by the "Plutonium isotopic correlations" (PuIC) which is a concept based on results of burn up codes and is developed separately. The chapter 4.2 is thus limited only to the discussion of several different scenarios of direct measurement of the $^{239}Pu_{eff\_DDA}$.

4.1. ^{244}Cm Method

In a typical LEU spent fuel assembly with a reasonable cooling time (>1y) the dominant neutron background sources are two spontaneously fissioning isotopes of curium – ^{242}Cm and ^{244}Cm. For certain SFA's (increases with high IE and BU) the contribution of ^{242}Cm can be between 10-50%. However, due to its rather short half-life of 160 days, the ^{242}Cm becomes irrelevant within first couple of years, leaving ^{244}Cm (half-life of 18.1y) as virtually the sole source of neutron background in any of the LEU SFA with cooling times of 5y or greater. Interestingly enough, the amount of ^{244}Cm in any SFA is directly correlated with any plutonium isotope ($^{239\text{-}242}$Pu), making it thus a direct link to a total mass of the elemental plutonium. The main reason for the close tie between the ^{244}Cm and ^{elem}Pu is its mechanism of production schematically depicted below:

$$^{239}_{94}Pu \xrightarrow{4(n,\gamma)} {}^{243}_{94}Pu\,(4.956\,h) \xrightarrow{\beta^-} {}^{243}_{95}Am \xrightarrow{(n,\gamma)} {}^{244}_{95}Am(10.1\,h) \xrightarrow{\beta^-} {}^{244}_{96}Cm$$

The fact that the ^{244}Cm is produced via 4 neutron capture on ^{239}Pu means that it carries information on all five Pu isotopes. While the probability of a neutron capture reaction clearly depends on the individual reaction cross-section, it also depends on the overall neutron flux in the fuel assemblies. Moreover, seen as potential neutron absorbers, the plutonium isotopes are competing for neutrons with other neutron absorbers such as various fission products. Thus the relative amount of individual Pu isotopes capturing yet another neutron and ultimately leading to the creation of ^{244}Cm (by decay of ^{244}Am) reflects also

properties of the SFA, in other words IE, BU and CT tied together in the overall characteristic of the environment – its multiplication.

In the "real life" the measurement of the neutron background thus implicates the amount of the ^{244}Cm (and potentially ^{242}Cm) in the SFA modified by its multiplication. We can mimic such situation in MCNPX simulation simply by letting the present ^{244}Cm spontaneously fission and track the created neutrons. The **Fig.35** then displays how the background counts from spontaneous fission of ^{244}Cm are correlated with the content of this isotope in the SFA corrected for its multiplication.

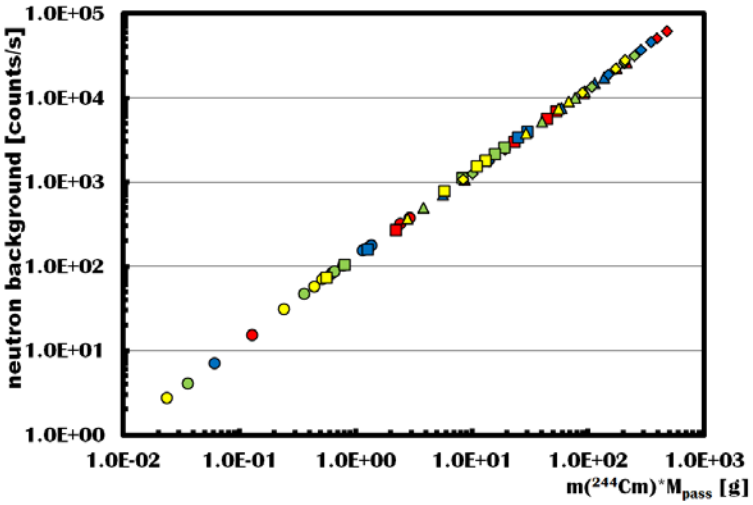

Fig. 35 Simulated neutron background rate from 64 SFA's from SFLI based on the spontaneous fission of ^{244}Cm is correlated with the ^{244}Cm content corrected for the effects of the FA's multiplication M_{pass}.

In other words, if we can measure the neutron background count rate and the multiplication of the assayed SFA, and we are sure that the CT of the SFA is at least 4-5 years, we can determine the mass of the present ^{244}Cm. The measurement of the background should be a rather straight forward task. The measurement of the multiplication of the SFA requires active interrogation of the SFA and (as discussed in detail in chapter 3.5.5) leads to the *active* multiplication M_{act}. However, as shown in Fig.23 the active multiplication is directly linked to the *passive* multiplication M_{pass} that is required to make the proper correction of background rate to determine mass of the ^{244}Cm.

Due to the mechanism of the ^{244}Cm production we can expect that the correlation with ^{elem}Pu will depend on the cooling time (CT). ^{244}Cm decays with half life of 18.1y, while half-lives of ^{239}Pu, ^{240}Pu and ^{242}Pu are counted in thousands of years (24100y, 6500y, and 373000y respectively). Only ^{241}Pu decays with a similar half-life (14y). Additionally, the DDA signal which is directly measured contains information related to ^{235}U. Relation between ^{235}U and fissile Pu isotopes is by no means easily quantifiable, but in general depends on BU, IE and CT which is reflected by the DDA count rate. We can therefore expect that the relation between ^{elem}Pu and ^{244}Cm is a function of DDA. Empirically we find out that the ratio of masses of ^{elem}Pu and ^{244}Cm follows a power law as in eq.(10):

$$m(^{elem}Pu)/m(^{244}Cm) \sim A\cdot(m(^{244}Cm)/DDA^{1/3})^{-B} \quad (10)$$

where A and B are empirical parameters depending on CT. **Fig.36** then displays the correlation of the ratio of ^{elem}Pu and ^{244}Cm masses for 64 SFA's of the SFLI. The data in the figure fall on one of the four different power dependencies according to their corresponding CT (1, 5, 20, and 80 years). **Fig.37** displays how much the individual data points differ from their corresponding power fits. According to this figure, should we know the CT of the assayed SFA's, the inherent inaccuracy of total ^{elem}Pu mass determination due to the unknown parameters of IE and BU is typically well below 5%.

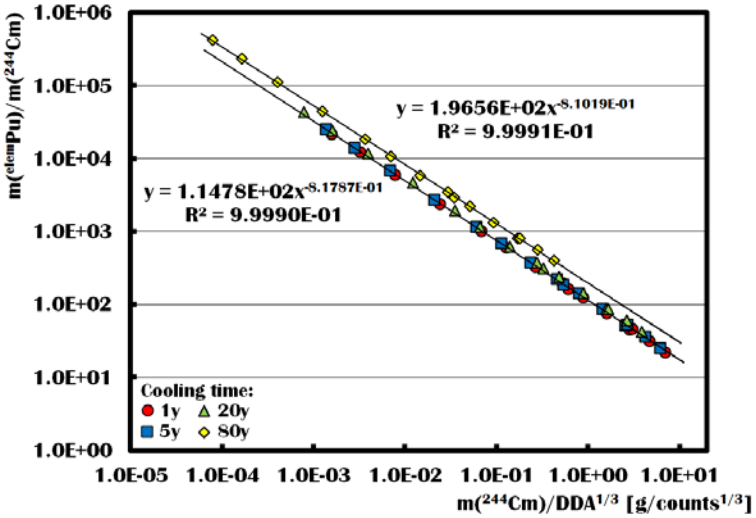

Fig.36 Power dependence of the ratio of masses of ^{elem}Pu and ^{244}Cm on the ratio of ^{244}Cm mass and 3rd root of the DDA counts. The lines represent power fits for data with 5 and 80 years of cooling time respectively.

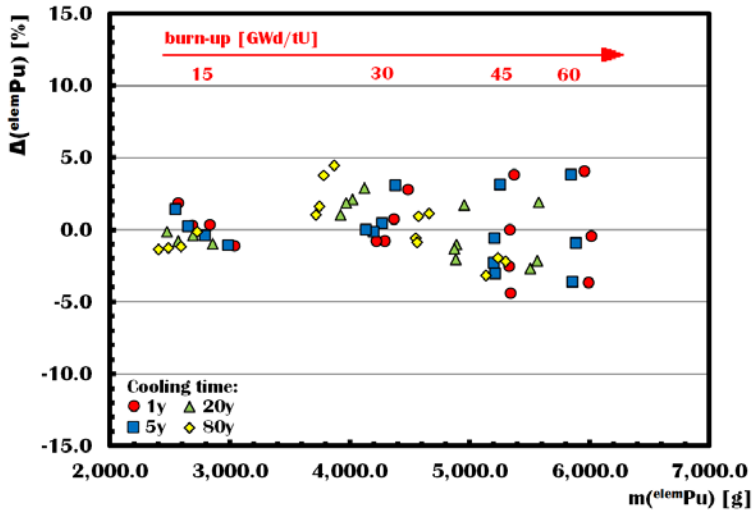

Fig. 37 Relative error in determination of the mass of ^{elem}Pu with ^{244}Cm method.

The significant advantage of this method is that it does not rely on the knowledge of any of the weighting parameters C_1, C_2 nor C_3. Moreover, it provides sufficient accuracy even if BU and IE of the assayed SFA is not known, although knowing these parameters may eventually lead to a further

improvement of the results. On the other hand, the method does not provide any information on the content of ^{235}U which may also be desirable to account for due to its fissile properties.

Worth mentioning is also the method's ability to determine ^{elem}Pu content independent of possible diversion. Should any of the pins with spent fuel be diverted and substituted with DU or ^{nat}U, the correlation between ^{244}Cm and ^{elem}Pu will still remain the same, since neither DU nor ^{nat}U pins contain any ^{244}Cm or ^{elem}Pu.

4.2. $^{239}Pu_{eff}$ Method

In general, the properties of the SFA in terms of its DDA response are determined by the three crucial parameters – IE, BU and CT (see Fig.19). Should all of these three parameters be known, we only have to verify that no nuclear material was diverted, and the determination of the effective mass of the fissile content in the FA is a straight forward process. However, as of now, the DDA instrument cannot independently measure all three of these parameters. For the real life application we may consider making use of continuity of knowledge about the fuel to be assayed making the task of determining $^{239}Pu_{eff}$ particularly easy. Nevertheless in order to challenge the potential of the DDA instrument we rather prefer to consider scenarios where only limited, if any, information about the SFA is available. It turns out that the dynamic analysis of the DDA response is a very powerful tool able to self-consistently provide enough information to determine $^{239}Pu_{eff}$ with reasonable precision (~ 5-10%).

The previous report on the DDA technique offered only a single scenario for determination of the effective mass of the fissile content in an assayed SFA. Unfortunately, the method relied on an independent knowledge (or determination) of BU and CT. In our opinion, the dynamic expansion of the analysis of the DDA signal offers several additional self-consistent scenarios to measure the effective mass of the fissile content. Depending on the conditions of the measurement, availability of trustworthy prior knowledge about the SFA and/or complimentary NDA technique one or the other method may prove to be more suitable than the other. Alternatively, the different approaches to measurement of $^{239}Pu_{eff}$ may serve as an important cross-check, and can provide very important information on the systematic uncertainty of the results.

4.2.1. Determination of $^{239}Pu_{eff}$ if IE is Known

The individual panels of Fig.19 reveal the complexity of the DDA response and how it depends on the amount of fissile mass present in a SFA in terms of the $^{239}Pu_{eff}$. They also reveal how the DDA signal changes with different levels of burn-up, initial enrichment and increasing cooling time. While all three crucial parameters play a significant role, it is the IE with by far the largest influence on the DDA response. Since our measure of $^{239}Pu_{eff\_DDA}$ is the counts detected by the DDA instrument, we can plot the effective fissile mass as function of the instruments response. The **Fig.38** then reveals that the effective fissile mass in general grows logarithmically with the number of detected neutrons but strongly scales with the IE for any given SFA.

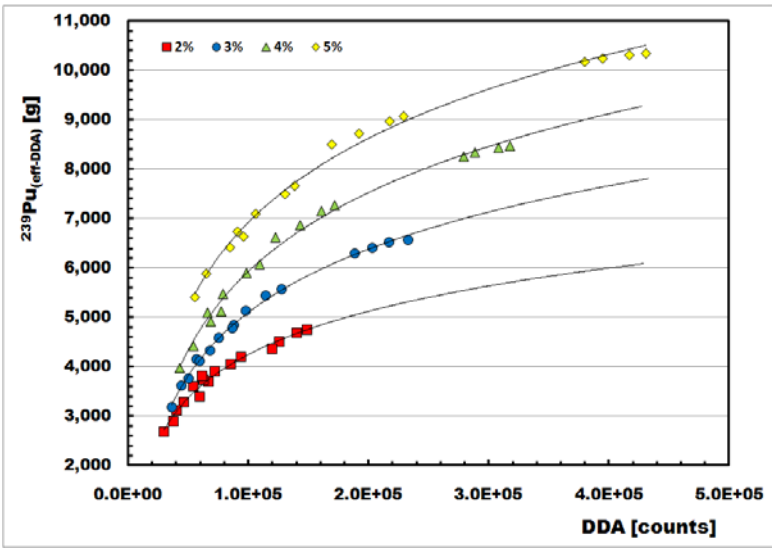

Fig.38 $^{239}Pu_{eff\_DDA}$ as the function of the DDA response reveals strong dependence on the IE and weak dependence on BU and CT.

Should we know the IE exactly, based on the MCNPX simulations (or calibration with multitude of known SFA's) we can introduce a correction according to the following formula:

$$\boldsymbol{cor} = (a\cdot\boldsymbol{IE}^2 - b\cdot\boldsymbol{IE} + c)\cdot\ln(\boldsymbol{DDA}) + d\cdot\boldsymbol{IE}^2 + e\cdot\boldsymbol{IE} - f) \tag{10}$$

where ***DDA*** is the measured response of the DDA instrument (after subtracting background), ***IE*** is the known (or otherwise determined) initial enrichment of the SFA, and ***a***, ***b***, ***c***, ***d***, ***e***, and ***f*** are empirical parameters depending on which particular logarithmic function we choose as our reference. In the present work we chose the logarithmic fit of the data points for IE=5% as our reference for DDA response defined as the sum of detected neutrons on all ^{3}He detectors in a time window from 200 to 1000μs, and described as:

$$^{239}\boldsymbol{Pu}_{\boldsymbol{eff\_DDA(IE=5\%)}} = 2.4540\cdot10^{3}\ln(\boldsymbol{DDA}) - 2.1333\cdot10^{4} \tag{11}$$

Under such conditions the values of parameters ***a*** to ***f*** are the following:

$$\boldsymbol{a} = 1.0817\cdot10^{2} \qquad \boldsymbol{b} = 1.1596\cdot10^{3} \qquad \boldsymbol{c} = 3.0854\cdot10^{3}$$
$$\boldsymbol{d} = -1.2803\cdot10^{3} \qquad \boldsymbol{e} = 1.2709\cdot10^{4} \qquad \boldsymbol{f} = -3.1434\cdot10^{4}$$

The actual mass of $^{239}Pu_{eff\_DDA}$ is then simply given by:

$$^{239}\boldsymbol{Pu}_{\boldsymbol{eff\_DDA}} = {}^{239}\boldsymbol{Pu}_{\boldsymbol{eff\_DDA(IE=5\%)}} - \boldsymbol{cor} \tag{12}$$

The **Fig.39** displays how well the correction defined by eq.(10) and (12) can aligned data for all 64 SFA's from SFLI along a simple logarithmic dependence given by eq.(11) (*left*), and how small the relative deviation of the individual SFA's from its analytic form is (*right*).

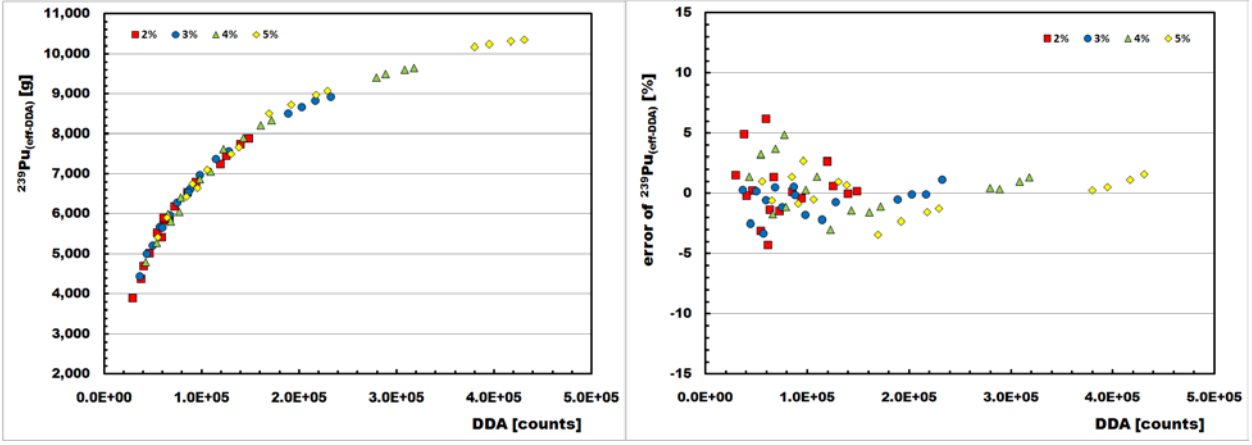

Fig.39 *Left* – $^{239}Pu_{eff\_DDA}$ as the function of the DDA response after correction for different IE. The refence being used in this figure is based on the data for SFA's with IE=5%. *Right* – relative variation of individual SFA cases from SFLI with respect to the reference curve as defined by the response of the DDA instrument to SFA's with IE=5%.

In general, we may consider knowing the IE exactly from a trusted documentation accompanying the spent fuel to be assayed, or determining it from a measurement by some other complementary NDA technique. However, the strength of the instrument (in our opinion) lies also in the fact that it can self-consistently determine (or verify) the IE by itself. According to Fig.27 the die-away time measured 100 to 200 μs after the interrogating pulse offers a possibility to determine the IE of the assayed FA. Of course such measurement will be burdened by a uncertainty which we estimate could reach +/-0.3% resulting in greater uncertainty of the $^{239}Pu_{eff\_DDA}$ determination. In order to precisely evaluate the impact of uncertainty of IE on the determination of $^{239}Pu_{eff\_DDA}$ more detailed analysis is necessary. But based on some preliminary considerations and the results in right panel of Fig.39 we estimate that the overall uncertainty of $^{239}Pu_{eff\_DDA}$ still would stay below 10%.

4.2.2. Determination of $^{239}Pu_{eff}$ by Evaluation of Neutron Absorber Effects

The authors of the previous report on the DDA technique [11] found out how important is the role of the neutron absorbers on the overall response of the instrument. Highlights of these findings were reproduced in chapter 3.5.4. of the current report. In Fig.21 we can see that should the neutron absorbers (i.e. their effect) be nullified, the DDA instrument response is a monotonic function of the effective fissile mass $^{239}Pu_{eff\_DDA}$. Inspired by this finding we simulated DDA response to fresh fuel assemblies with IE of 1%, 2%, 3%, 4% and 5% in order to establish a "base" DDA response as if no neutron absorbers were present. The Fig. 42 displays the DDA response of 64 SFA's together with 5 cases of fresh fuel assemblies (FFA) as the function of their active multiplication M_{act} in the time window A (0-50μs) and E (500-1000μs).

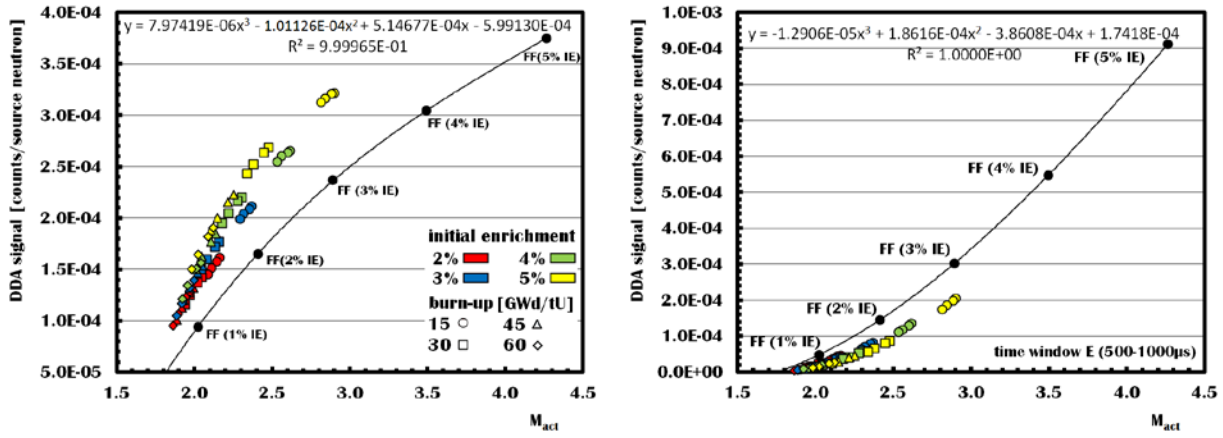

Fig. 42 DDA response of the instrument to the active interrogation of 64 SFA's and 5 FFA's from SFLI as the function of the active multiplication M_{act} in the time window A (*left*) and time window E (*right*).

The base-line DDA response is then defined by the 3rd degree polynomial fit through the FFA data points. The relative difference between the baseline and the actual DDA response for a given SFA and M_{act} is then attributed to the effect of neutron absorbers and is defined by the following prescription:

$$\boldsymbol{effNA} = [\boldsymbol{DDA}(SFA,M_{act})\text{-}\boldsymbol{DDA}(FFA,M_{act})]/\ \boldsymbol{DDA}(SFA,M_{act}) \qquad (13)$$

effNA will be called "*effective neutron absorber coefficient*" and is essentially a dimensionless constant. The fact that the DDA response for any SFA is for a given M_{act} in the very early times larger than the DDA response based on FFA's may seem rather counter intuitive. However it only reflects the fact that two FA's with same M_{act} may have very different fissile content. The dynamic evolution of the neutron flux may be than vastly different. For example, four data points from Fig.42 attributed to SFA's with 5% IE and BU=15 GWd/tU have approximately same active multiplication (M_{act}~2.85) as FFA with 3% IE. In both cases, the number of neutrons produced in the induced fissions due to the active interrogation will be the same, however, in case of the SFA's the neutron flux will develop rather rapidly leading to more neutrons per one from the source (i.e. higher DDA response) than in case of FFA with 3% IE. Then, due to the presence of various neutron absorbers as products of burnup, the neutron flux of the SFA's will be quenched significantly sooner, than in the case of the FFA. It can be shown that in later times the DDA response from the SFA's with same M_{act} as their FF counterparts is significantly smaller, such as displayed in the right panel of Fig.42. Therefore we attribute the difference between the FF base-line and the actual DDA response for SFA with a given M_{act} to the increased presence of neutron absorbers.

Based on the eq.(13) we may construct *effNA* for any arbitrary counting time window. However, it turns out that the *effNA* from the earliest time window provides for the best results. The Fig.43 displays the effective neutron absorber coefficient *effNA* as defined by eq.(13) and calculated for data from time window A as the function of M_{act} (*left*) and $^{239}Pu_{eff\_DDA}$ (*right*) for 64 SFA's from SFLI. While not identical, the structure of the data in plots of Fig.43 is very similar. It's most prominent feature is the lining of the data points according to the IE of individual SFA cases. This observation is not really very surprising, since we already showed in chapter 3.5.3 that IE is a parameter with most detrimental effect on the DDA response. On the other hand, the evaluation of effNA (with help of FFA's) provides yet another possibility to determine IE, complementing thus the die-away method described in chapter 3.5.5.

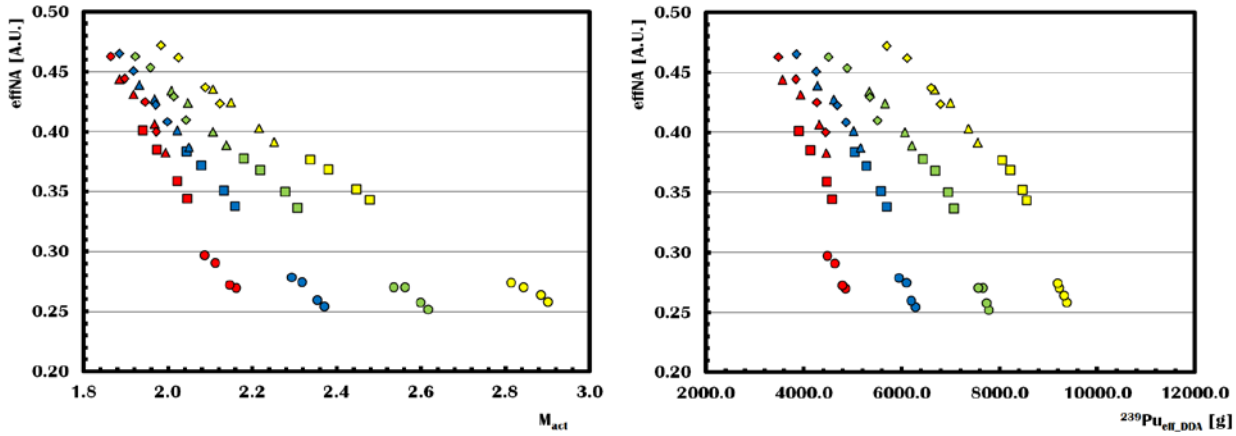

Fig.43 Effective neutron absorber coefficient *effNA* as the function of the active multiplication M_{act} (left) and effective fissile content $^{239}Pu_{eff\_DDA}$ (*right*) for 64 SFA's from SFLI.

In order to facilitate the effects of neutron absorbers on the overall DDA response we define the "*neutron absorber corrected DDA signal*" ***naCorDDA*** as follows:

$$\boldsymbol{naCorDDA} = \boldsymbol{DDA}(\mathrm{SFA},t) \cdot [1-\boldsymbol{effNA}(\mathrm{A})]^{\varepsilon(effNA,t)} \qquad (14)$$

where ***DDA*** is the uncorrected DDA response of an instrument for a given SFA measured in a specific time window, ***effNA*** is the effective neutron absorption coefficient determined from the data measured during time window A, and $\boldsymbol{\varepsilon}(effNA,t)$ is an empirical parameter which depends on the counting time window and the definition of *effNA* (e.g. parameter ε will be different if *effNA* is based on any other time window than A). The **Fig.44** and **Fig.45** display the effective fissile content $^{239}Pu_{eff\_DDA}$ as the function of the neutron absorber corrected DDA signal *naCorDDA* in all six different time windows A-F and the deviation of these values from the ideal fit represented by a 2nd or 3rd degree polynomial function. The value of $\boldsymbol{\varepsilon}$ used for calculating *naCorDDA* was chosen to minimize the scattering of $^{239}Pu_{eff\_DDA}$ from a simple function of *naCorDDA* and the actual values are summarized in **Tab.2**.

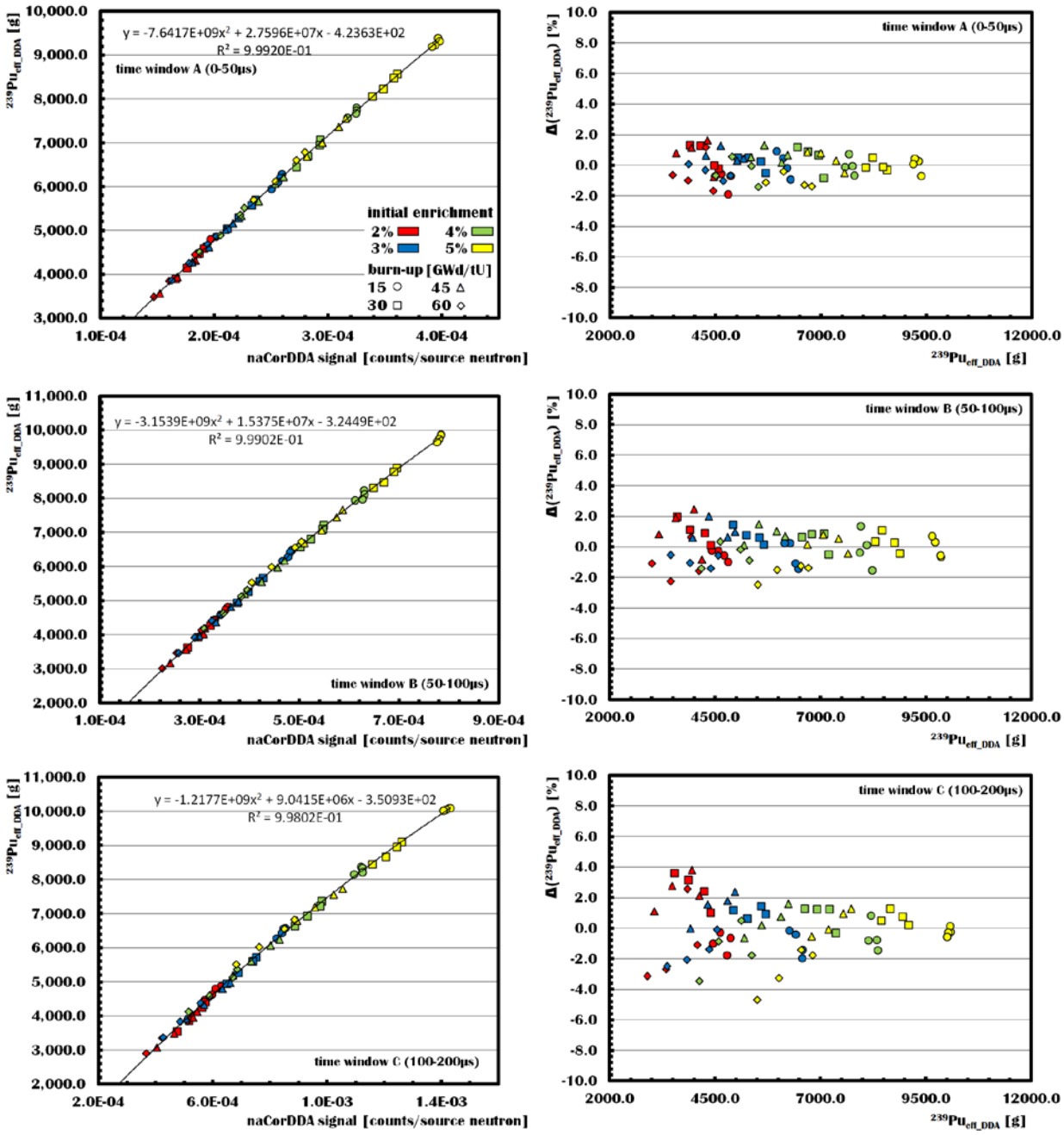

Fig.44 The effective fissile content $^{239}Pu_{eff\_DDA}$ as the function of the neutron absorber corrected DDA signal *naCorDDA* in three different time windows A-C and the deviation of these values from the ideal fit represented by a 2nd degree polynomial function.

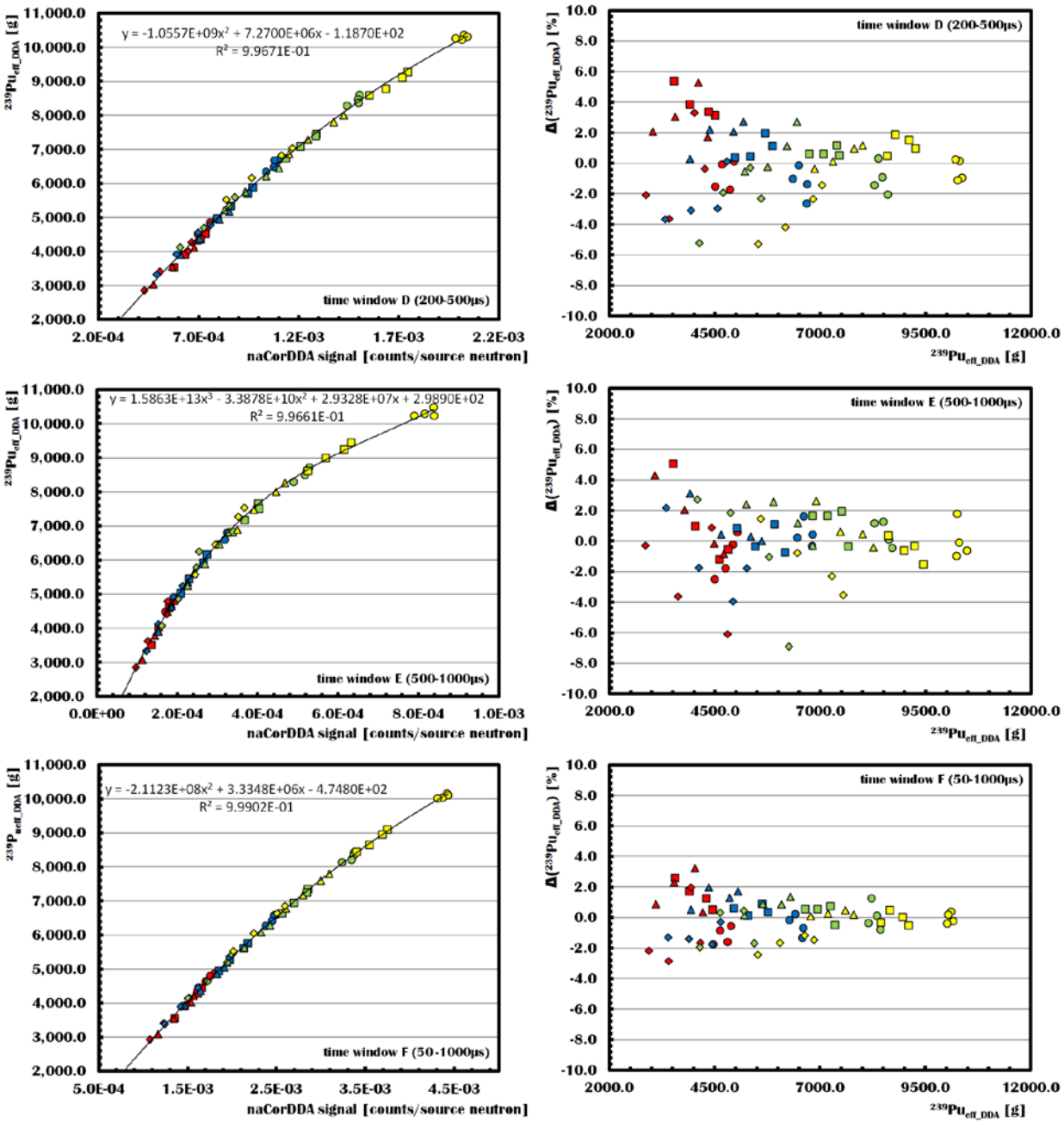

Fig.45 The effective fissile content $^{239}Pu_{eff\_DDA}$ as the function of the neutron absorber corrected DDA signal *naCorDDA* in three different time windows D-F and the deviation of these values from the ideal fit represented by a 2nd or 3rd degree polynomial function.

Tab.2 Values of empirical parameter ε for individual time windows.

Time window	ε	Time window	ε
0-50µs	-0.70	**200-500µs**	-3.41
50-100µs	-1.20	**500-1000µs**	-4.70
100-200µs	-2.03	**50-1000µs**	-2.24

The Fig.44 and 45 show that the evaluation of the neutron absorber effect with help of the DDA response measured for several FF assemblies leads to the determination of $^{239}Pu_{eff\_DDA}$ with very high precision. Depending on the time window of choice, the results for 64 SFA's deviate from an ideal simple dependency on *naCorDDA* by less than 2% in case of "the best" time window A or by less than 7% in case of "the worst" time window E.

In principle, different time windows could be used to establish FFA base-line leading to different set of *effNA* values. We have tested several other options as well, but unfortunately, not all combinations of one time window used for *effNA* and another for *naCorDDA* lead to converging results, and those which do are generally inferior to results presented in Fig.44 and 45. Perhaps a different correction term in *eq*.(14) may lead to more favorable results in such cases. However detailed systematic investigation of other empirical corrections exceeds the scope of this report. The point of this chapter was to demonstrate that the quantification of neutron absorbers is possible by comparison of DDA response to the active interrogation of SFA's and FFA's and that these results may be in turn used for correcting the complex dependency of $^{239}Pu_{eff\_DDA}$ on IE, BU and CT leading to a smooth dependence of the primary DDA signal on the effective fissile material content.

5. Detection of Diversion of the Nuclear Material from SFA

An important aspect of the safeguards analysis is the ability to detect removal or diversion of fuel pins from a spent fuel assembly. Such diversion of the fuel pins may be an indication of the intent of the reactor operator to extract the plutonium from the diverted pins for use in a nuclear weapon or illicit trade.

In general, there are two possible approaches to the detection of diversion of nuclear material. The approach based on a comparison of a signal from the assayed SFA with the signal from a well known reference will be called ***comparative diversion detection*** methods. Such method has been simulated and discussed in the previous DDA report [11], and has been extensively used in simulation studies of other NGSI NDA techniques as well. While in principle straight forward and potentially powerful method, this comparative method may suffer from practical limitations due to unavailability of an appropriate reference and/or possibly even with identification of a suitable reference if only too limited information about the assayed SFA is available.

On the other hand the second class of diversion detection methods is independent of any direct comparison to a compatible reference case. It relies on correlation on various properties of a SFA which are acquired during the burning in the nuclear reactor and which are to a great extend fixed unless unnatural physical (or chemical) manipulation of the SFA occurred. We will refer to these methods as ***self-consistent diversion detection*** methods. As will be shown in chapter 5.2 the self-consistent diversion detection methods do not currently provide such accuracy (i.e. level of discrimination) as the comparative diversion detection methods. However, due to their obvious advantage of independence on suitable reference, these methods may provide a possible cross-check or even a welcome diversion detection alternative.

To simulate the response of the DDA instrument to a potential diversion, nine diversion scenarios were created for assemblies used in SFLI, as depicted in **Fig. 46**. These diversion scenarios were applied to three original assemblies with 4% IE, 5y CT and burn-up of 15, 30, and 45 GWd/tU respectively.

In each of the nine diversion scenarios, the spent fuel pins were replaced with pins containing natural uranium (i.e. 0.7 wt% ^{235}U). The pins were substituted in one of three regions – inner, middle, and outer – in the 17 × 17 array of real fuel pins. In scenarios 1, 4, and 7, eight fuel pins were removed; in scenarios 2, 5, and 8 twenty-four pins were removed; and in scenarios 3, 6, and 9, forty pins were removed. In scenarios 1-3, 4-6, and 7-9, the pins were removed from the inner, middle, and outer regions of the 17 × 17 fuel pin array, respectively.

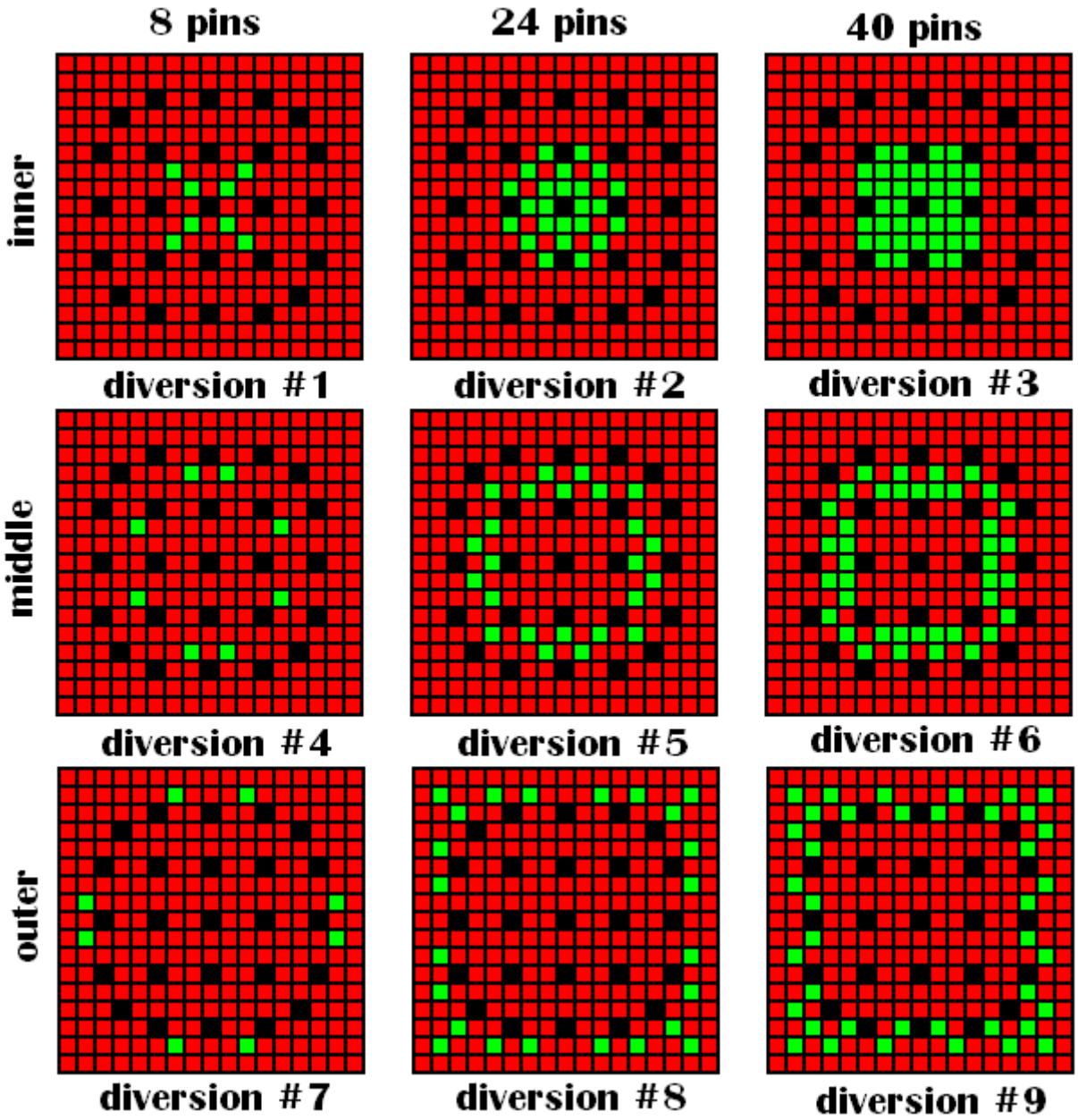

Fig. 46 Pin layout of nine diversion scenarios. Diverted pins (fuel pins replaced with natural uranium) are shown in green, with red and black representing undiverted spent fuel pins and water holes, respectively.

5.1. Comparative Diversion Detection

The main principle of a comparative diversion detection is a direct comparison of produced instrument response or any other measured quantity between a well known “reference case” and an unknown FA which is believed to have identical properties (unless diversion of nuclear material occurred)

as the reference case. Spatial sensitivity analysis performed in chapter 3.4 was in fact an example of such comparative diversion detection approach, although a diversion of solid block of pins may be considered as one of the least sophisticated, and thus possibly easier to detect, diversion scenario. In any case, the lesson learned from the chap. 3.4 has been that the comparison of the DDA response integrated over a single period of time and over all possible detectors may be often misleading. We have therefore suggested investigating the full dynamic evolution of the DDA response in form of a ratio of disturbed vs. undisturbed FA for back and front detectors separately and thus identifying the best time periods where possible diversion can be revealed. The **Fig.47** displays the time evolution of the relative change of the DDA signal from the front and back detectors separately for nine different fuel pin diversion scenarios in a FA with 4% IE, 5y CT and 15, 30 and 45 GWd/tU BU.

The results in Fig.47 resemble the trends in Fig.14 which depicts data for six different scenarios for substitution of 12 pins in a FA with identical IE and CT and 45 GWd/tU BU used in a spatial uniformity study. However, greater variability of results in Fig.47 allows for more detailed and expanded conclusions. In general, diversion of more pins leads to greater difference between modified and unmodified FA, but distribution of substituted pins can to a certain degree compensate for the diverted fissile mass. Especially the signal from the back detectors seems to be very similar for diversion scenarios number 2 and 9. In these two particular cases it seems that diversion of 24pins from the center of the SFA results in similar observable effect as diversion of 40 pins from the most outer layers of the SFA. This observation can be generalized, and we can state that the back detectors are more sensitivity to the removal of fissile material from the center of the SFA than from the outskirts of the SFA. Additionally, the sensitivity to diversion is not constant through the full time of the DDA measurement after the interrogating neutron pulse (i.e. the first millisecond). First highly sensitive time interval is approximately the first 200us, the second one is approximately between 300 and 600us, although in later times the statistical uncertainty becomes significant. It is interesting to observe how the apparent DDA response changes in each of these time intervals with increasing burn-up of the assayed SFA. In lightly burned cases, the modified FA produces smaller DDA response in both of the sensitive time domains. But in heavily burned SFA's and later time domains (after ~200us) the apparent DDA response can be significantly greater (by up to more than 15%) in a FA where regular fuel pins were substituted with ^{nat}U than in the unmodified SFA. This counterintuitive result is in the agreement with our observation already made in chapter 3.4, except now the effect is more pronounced. Our interpretation of the apparent increase of the DDA signal in later time domains when burned fuel pins are diverted is that the fresh natU pins do not contain any strong neutron poisons, and in fact the fissile content (0.7% of 235U) is comparable to the fissile content of the burned fuel pins. In other words, introduction of fuel pins which lack strong neutron absorbers leads to slower die-away of the neutron population in the SFA, thus the relative comparison between modified and unmodified SFA in later times when effects of strong neutron absorbers typically dominate the neutron flux dynamic evolution can lead to such counterintuitive result. On the other hand, in the early times after the interrogating pulse the neutron population spectrum did not yet reach its dynamic equilibrium, its mean energy is generally higher, and is thus less sensitive to the presence of neutron absorbers. The modified-to-unmodified DDA signal ratio is thus more correlated with actual ratio of fissile content actually present in each SFA.

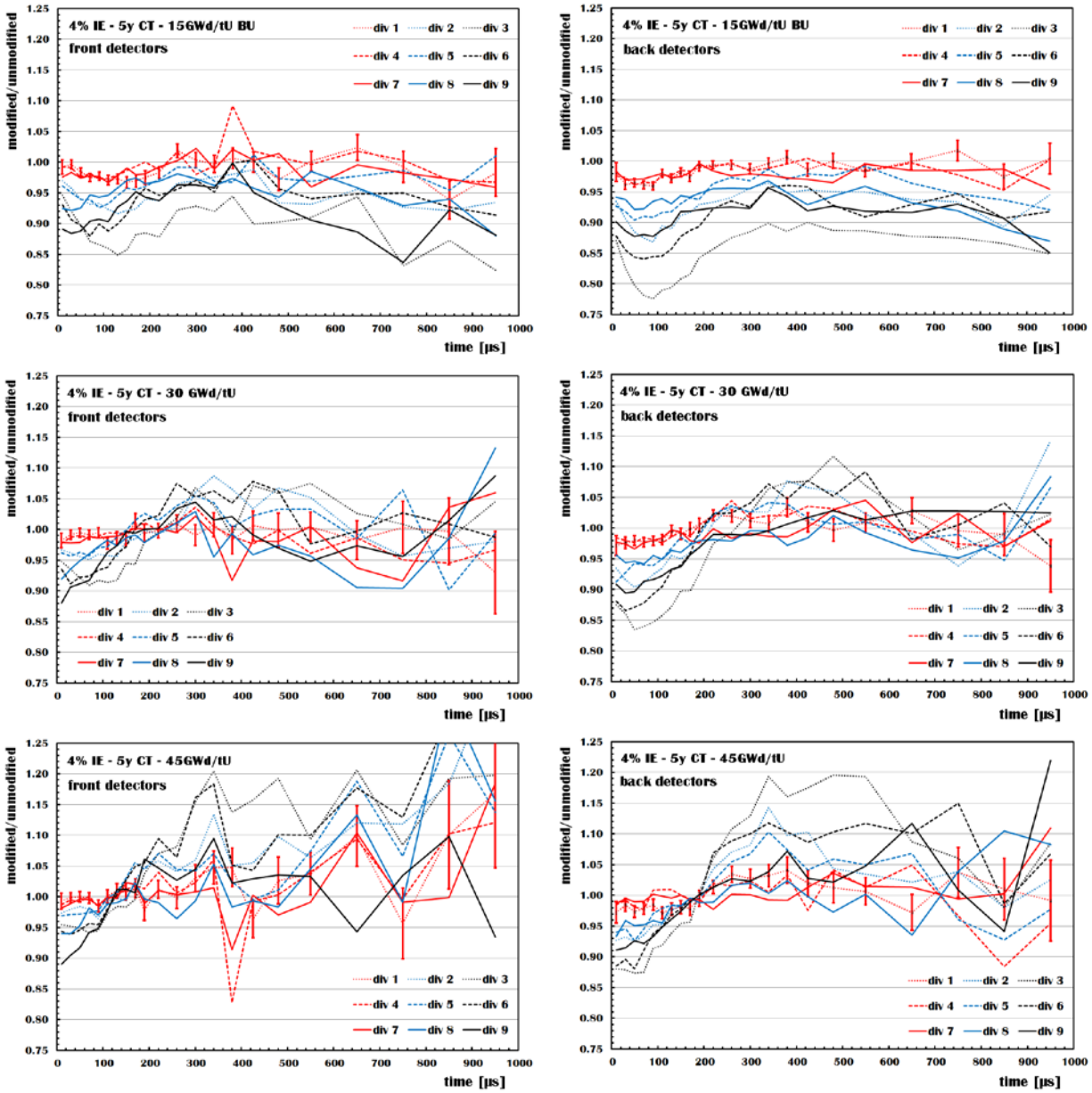

Fig.47 The time evolution of the relative change of the DDA signal from the front and back detectors separately for nine different fuel pin diversion scenarios in a FA with 4% IE, 5y CT and 15, 30 and 45 GWd/tU BU.

Unlike the surprising results in chapter 3.4, the difference between front and back detectors in case of the 27 currently investigated diversion scenarios does not seem to be that strikingly different. All assemblies, from lightly to most severally burned SFA's, seem to provide for somewhat lesser sensitivity of the front detectors to the diversion than the back detectors, although the sensitivity time domains are essentially the same. We can understand this with help of the results from the spatial uniformity studies. There we learned that the farther the place of the diversion is from the front detectors, the lesser their sensitivity. Comparing the places of diversion depicted in Fig.46 and Fig.12 we can clearly identify the

different geometrical distribution of substituted fuel pins. The symmetric and mostly spread out pins in Fig.46 will result in part of the diverted material not being “seen” by the front detectors, as was the case with SV3 and SV6 in Fig.14 a).

Fig. 48-50 provide another perspective to how the sensitivity to diversion changes in time for both front and back detectors. In these figures the DDA response has been integrated in the usual time windows A-F. When present, the error bars represent the statistical error, but in case of the most of the data the error bars are smaller than the points. In accordance with the discussion dedicated to the data in Fig.47 also in these plots it is clearly visible that the back detectors are more sensitive to the vast majority of diversion scenarios in most of the times. The only notable exception when front detectors perform significantly better than the back ones is in time window E in case of the highly burned fuel assembly with BU being 45 GWd/tU (lower left panel of Fig.50).

We can now conclude this chapter by stating that for every diversion scenario we can find a time domain where the active interrogation of modified fuel assembly will result in a statistically significant difference in the DDA response compared to the DDA response of an unmodified SFA. As expected, the smallest differences in DDA response were found for diversion scenarios with substitution of only 8 pins. In such cases, given the most ideal time domain the differences in DDA response were only about 2%. It is thus hard to imagine that such small diversion could be detectable with the current design of the DDA instrument, given realistic conditions and systematic uncertainties. Diversion of 24 pins leads to at least 5% effects on DDA response, and diversion of 40pins to at least 8% effect on the DDA signal, provided the best suitable time domain for data acquisition is chosen. In general, the back detectors provide higher sensitivity to diversion of nuclear material, which however changes with respect to the time domain of the data acquisition after the interrogating neutron pulse.

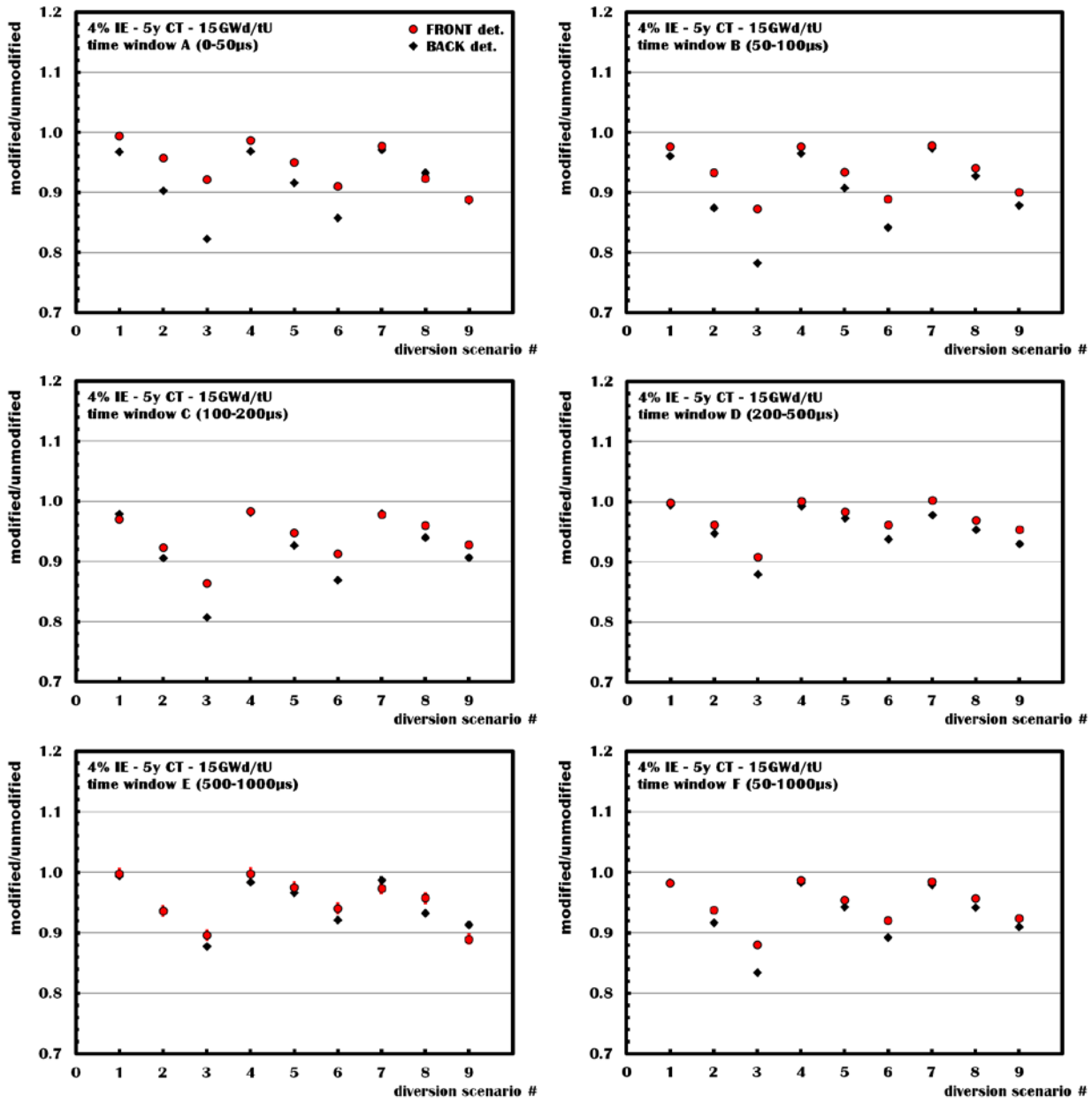

Fig.48 Relative difference in DDA count rate in six different time windows A-F for nine diversion scenarios for the SFA's with 4% IE, 5y CT and 15GWd/tU.

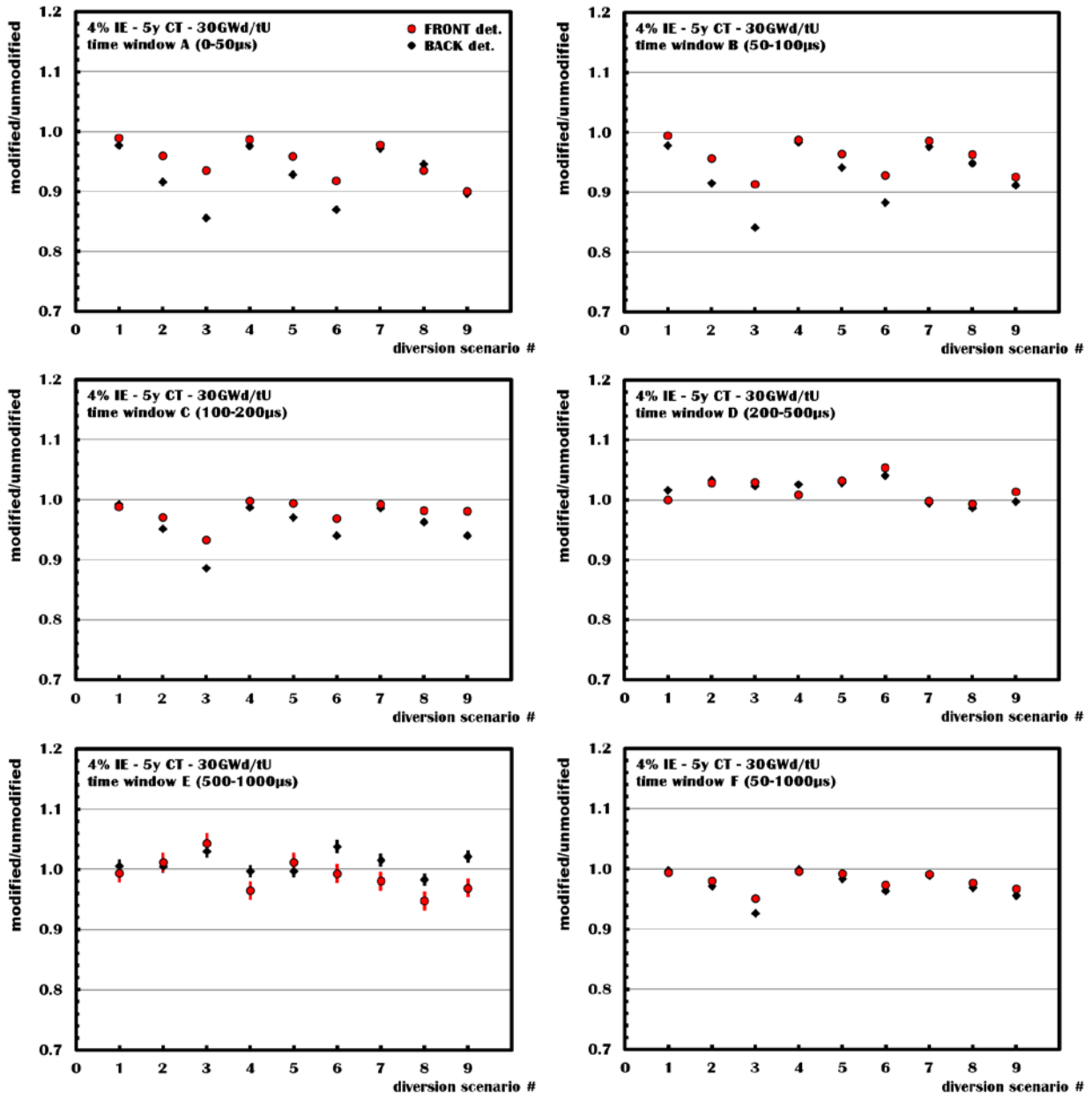

Fig.49 Relative difference in DDA count rate in six different time windows A-F for nine diversion scenarios for the SFA's with 4% IE, 5y CT and 30GWd/tU.

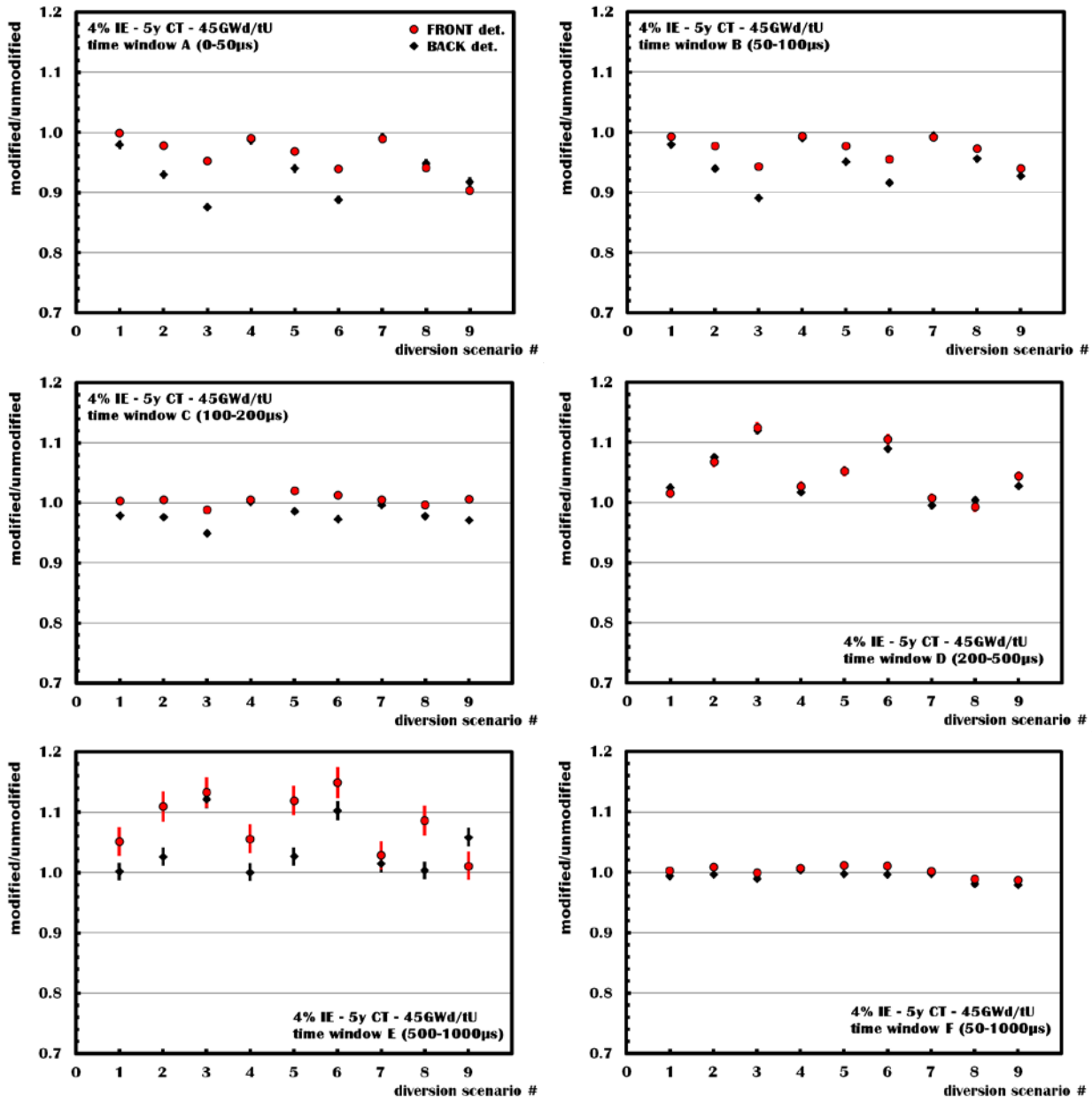

Fig.50 Relative difference in DDA count rate in six different time windows A-F for nine diversion scenarios for the SFA's with 4% IE, 5y CT and 45GWd/tU.

5.2. Self-Consistent Diversion Detection

The principles of self-consistent diversion detection techniques are naturally superior to those of the comparative diversion detection method, such as those described in the previous chapter. However, the self-consistent diversion detection concept within the scope of the proposed DDA instrument is a rather fresh idea still under investigation and development. On the other hand, its potential impact, in our opinion, justifies its introduction within this report, even though it still remains to be seen whether it can lead to any practical application.

The general concept of the method can be easily demonstrated by comparison of the data for 64 SFA's from SFLI and 27 SFA's from which certain substantial nuclear material was diverted and substituted with natural uranium. The **Fig.51** displays the effective fissile content $^{239}Pu_{eff\_DDA}$ as the function of the neutron absorber corrected DDA signal *naCorDDA* in the time windows B and the deviation of these values from the ideal fit represented by a 2nd degree polynomial function for 64 unmodified SFA's (as in Fig.44) and 27 SFA's modified as in Fig.46.

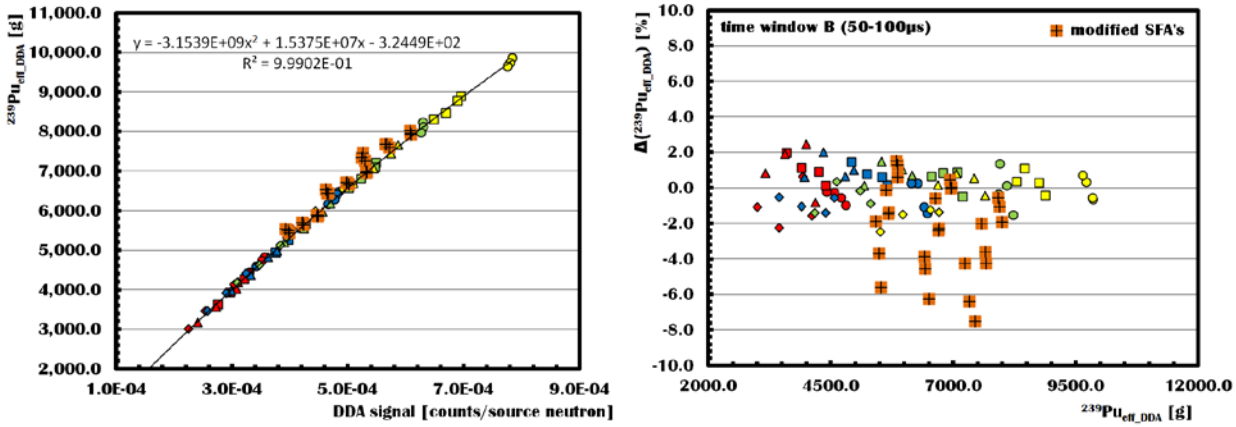

Fig.51 The effective fissile content $^{239}Pu_{eff\_DDA}$ as the function of the neutron absorber corrected DDA signal *naCorDDA* in the time windows B and the deviation of these values from the ideal fit represented by a 2nd degree polynomial function for 64 unmodified SFA's (as in Fig.44) and 27 SFA's modified as in Fig.46.

While the data for unmodified SFA's follow the trend established with the help of the neutron absorber correction (see chap. 4.2.2) and deviate from the ideal fit by less than 3%, some of the SFA's in which some burned nuclear fuel pins were substituted with ^{nat}U are off the trend by up to 8%. The imbalance of fissile material and products of "natural" burning in nuclear reactor causes a disparity between the response of the DDA instrument and the actual effective fissile content of the modified fuel assembly. Thus knowing the actual fissile content (perhaps from another independent method or instrument) and checking whether it properly correlates with the DDA response or not, we can identify at least some of the modified fuel assemblies. In the right panel of Fig.51 the band of data points for the modified SFA's with the lowest values of $^{239}Pu_{eff\_DDA}$ corresponds to the diversion scenarios involving FA with 4% IE, 5y CT and 45 GWd/tU BU, while the band of data points with the highest $^{239}Pu_{eff\_DDA}$ corresponds to the diversion scenarios involving FA with 4% IE, 5y CT and 15 GWd/tU BU. The modified SFA data points which differ the most from the polynomial fit are those which correspond to the diversion of 40 pins, while the diversion of only 8 pins is represented by data points almost perfectly following the trend set by the 64 unmodified SFA's.

But if we consider the DDA instrument to be a standalone device and know information on the fissile content is apriori known, then the $^{239}Pu_{eff\_DDA}$ is exactly the quantity we intent to determine, and the method based solely on Fig.51 cannot work – with a measured DDA signal, we would use the known trend in the left panel of Fig.51 to simply determine the $^{239}Pu_{eff\_DDA}$ ignorant of the fact that it is incorrect.

On the other hand, the complexity of the DDA instrument and the rich information extractable from the dynamic evolution of the signal allows for similar analyses of quantities measured by the DDA

instrument alone. The **Fig.52** displays how the data for unmodified 64 SFA's from SFLI compare to 27 diversion scenarios when correlation of die-away time measured by front and back detectors in time window C (100-200μs) is considered (*left*), and when B/F ratio is used to determine the active multiplication M_{act} (*right*).

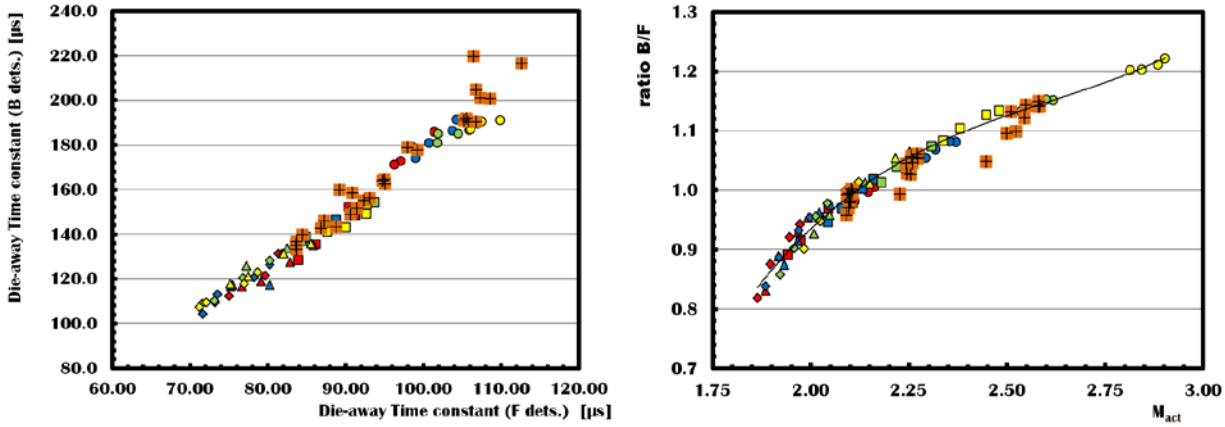

Fig.52 Comparison of data for unmodified 64 SFA's from SFLI compare to 27 diversion scenarios when correlation of die-away time measured by front and back detectors in time window C (100-200μs) is considered (*left*), and when B/F ratio in time window from 0 to 200μs is used to determine the active multiplication M_{act} (*right*)

In both of these plots the data for modified fuel assembly largely overlap with those for unmodified SFA's. But the few cases which are clearly of the trend established by regular FA's with unprecedented variation of IE, BU and CT illustrate well how a careful analysis of measured DDA signal may lead to a self-consistent diversion detection. Moreover, it should not be left unnoticed that the few points off the general trend in Fig.52 represent a whole class of possible diversions with substitution of about 15% of the burned fuel pins in rather lightly burned fuel assemblies. In general, lightly burned nuclear fuel is ideal for extraction of Pu with high content of ^{239}Pu isotope. Additionally, should DU be used as a substitution material, the disparity of compared quantities is generally larger, thus leading to a greater sensitivity of the method.

In conclusion, we are aware that the current sensitivity of the self-consistent diversion detection method laid out in this chapter cannot match the profound sensitivity of the comparative diversion detection method described in chap. 5.1. However, we believe that the potential for self-consistent diversion detection can only grow when DDA technique is integrated with another NDA technique based on different physics and/or measurement principles.

6. Conclusions

Since the underlying physical processes of the DDA instrument (i.e. emission of prompt fission neutrons) and the delayed neutron (DN) instrument (i.e. emission of delayed neutrons by fission products) are complementary and because the technical requirements are essentially compatible, the mechanical design of the instrument has been envisioned since the beginning to be used as a possible integrated DDA+DN instrument as well, although the DN results are not considered further in this report.

The DDA instrument is expected to produce a signal as strong as, or stronger than, the background produced by the fuel for the wide range of spent fuel in SFLI provided the driving deuterium-tritium fueled neutron generator can deliver $5x10^7$ n/s with a pulse rate of 100 Hz and pulse width of 10μs (i.e. instantaneous strength $5x10^{10}$ n/s). Such neutron generators are already available off-the-shelf.

Similar to all other techniques that measure fissile content ($^{239}Pu_{eff}$) in a given SFA, the correlation between the DDA signal and the $^{239}Pu_{eff}$ can be strongly influenced by the inventory of neutron absorbers. However the dynamic nature of the signal allows (under certain conditions) to either evaluate and correct for the effects of the absorbers directly or diminish their influence to a tolerable, correctable or negligible level. Within this report we explore several measurement and analytical scenarios leading either to the determination of the absolute amount of the fissile content in the terms of $^{239}Pu_{eff}$ or to the absolute amount of the elemental plutonium (^{tot}Pu) with the precision in order of a few %.

A fundamental design parameter of the DDA system is the time interval after the interrogating burst over which the neutrons are counted. The traditional approach in DDA technique calls for measurement in a constant time window typically after the thermalisation of the interrogating neutron field (after few hundreds of μs). In this report we present several novel approaches to the analysis of the DDA signal in various time intervals including times immediately after the interrogating burst and at different locations across the SFA, and demonstrate how such additional information can lead to the direct measurement of the SFA multiplication, amount of neutron absorbers and the absolute amount of the $^{239}Pu_{eff}$ and/or ^{tot}Pu.

We conclude our study with investigation of 27 standardized diversion scenarios adopted by the NGSI study. We have evaluated the sensitivity of the instrument and have demonstrated that a diversion of ~5% of the fuel mass from any region of the assembly could be detected, provided a base measurement was available for comparison. Additionally, we introduce several novel analytical approaches which allow for self-consistent and independent detection of several diversion scenarios even if no base measurement is available.

References:

[1] A. Scheinman, Next Generation Safeguards Initiative Inaugural Conference, September 11-12, 2008. Available website: http://nnsa.energy.gov/nuclear_nonproliferation/2147.htm

[2] S.J. Tobin, N.P. Sandoval, M.L. Fensin, S.Y. Lee, B.A. Ludewigt, H.O. Menlove, B.J. Quiter, A. Rajasingum, M.A. Schear, L.E. Smith, M.T. Swinhoe, S.J. Thompson, "*Determination of Plutonium Content in Spent Fuel with Nondestructive Assay*," Institute of Nuclear Materials Management 50th Annual Meeting, Tucson, AZ, July 12-16, 2009, Los Alamos National Laboratory document LA-UR-09-03748.

[3] M.L. Fensin, S.J. Tobin, N.P. Sandoval, M.T. Swinhoe, S.J. Thompson, "*A Monte Carlo linked Depletion Spent Fuel Library for Assessing Varied Nondestructive Assay Techniques for Nuclear Safeguards*," Advances in Nuclear Fuel Management IV (ANFM), Hilton Head Island, South Carolina, April 12-15, 2009.

[4] S.J. Tobin, S.F. Demuth, M.L. Fensin, J.S. Hendricks, H.O. Menlove, M.T. Swinhoe, "*Determination of Plutonium Content in Spent Fuel with NDA—Why an Integrated Approach?*" Annual Meeting of the Institute of Nuclear Materials Management, Nashville, TN, July 2008, Los Alamos National Laboratory document LA-UR-08-03763.

[5] H.O. Menlove, S.H. Menlove, S.J. Tobin, "*Verification of Plutonium Content in Spent Fuel Assemblies Using Neutron Self-Interrogation*," Institute of Nuclear Materials Management 50th Annual Meeting, Tucson, AZ, July 12-16, 2009, Los Alamos National Laboratory document LA-UR-09-03715.

[6] A.P. Simpson, M.J. Clapham, B. Swinson, "*Advanced Non-Destructive Assay System and Special Instrumentation Requirements for Spent Nuclear Fuel Recycling Facility*" Waste Management Conference, Phoenix, AZ, February 24-28, 2008.

[7] J.T. Caldwell, R.D. Hastings, G.C. Herrera, W.E. Kunz, et al., "*The Los Alamos Second-Generation System for Passive and Active Neutron Assays of Drum Size Containers*," Los Alamos National Laboratory report LA-10774-MS (1986).

[8] K.A. Jordan and T. Gozani, "*Pulsed Neutron Differential Die Away Analysis for Detection of Nuclear Materials*," *Nucl. Instr. Meth. Phys. Res.* **B** (261), 365-368 (2007).

[9] P. Blanc, S. J. Tobin, S. Croft, H. O. Menlove, "*Plutonium Mass Determination in Spent Fuel – Delayed Neutron Detection in an Integrated Delayed-Neutron and Differential Die-Away Instrument with 3He Detectors and DT Generator*", Los Alamos National Laboratory Report LA-UR-01912

[10] M.L. Fensin, S.J. Tobin, N.P. Sandoval, S.J. Thompson, M.T. Swinhoe, "*A Monte Carlo Linked Depletion Spent Fuel Library for Assessing Varied Nondestructive Assay Techniques for Nuclear Safeguards*," Los Alamos National Laboratory document LA-UR-09-01188 (2009).

[11] T.-H. Lee, S. J. Tobin, H. O. Menlove, and M. T. Swinhoe: *„Determining the Pu Mass in LEU Spent Fuel Assemblies: Focus on Differential Die-Away Technique"*, Los Alamos National Laboratory report LA-UR-11-00747

[12] D.T. Reilly, "*Passive Nondestructive Assay of Nuclear Materials*," Office of Nuclear Regulatory Research, NUREG/CR-5550, Los Alamos National Laboratory document LAUR-90-732 (1990).

[13] Chart of Nuclides, National Nuclear Data Center, Brookhaven National Laboratory website: http://www.nndc.bnl.gov/chart/.

[14] ENDF/B-VII from http://www.nndc.bnl.gov/